

คุณลักษณะและสมบัติการเป็นตัวเร่งปฏิกิริยาของตัวเร่งปฏิกิริยาโคบอลต์บนตัวรองรับไทเทเนียม



นางสาวทิพย์นภา วงศ์สาลี

สถาบันวิทยบริการ

จุฬาลงกรณ์มหาวิทยาลัย

วิทยานิพนธ์นี้เป็นส่วนหนึ่งของการศึกษาตามหลักสูตรปริญญาวิศวกรรมศาสตรมหาบัณฑิต

สาขาวิชาวิศวกรรมเคมี ภาควิชาวิศวกรรมเคมี


คณะวิศวกรรมศาสตร์ จุฬาลงกรณ์มหาวิทยาลัย

ปีการศึกษา 2548

ISBN 974-17-4046-8

ลิขสิทธิ์ของจุฬาลงกรณ์มหาวิทยาลัย

CHARACTERISTICS AND CATALYTIC PROPERTIES OF COBALT CATALYST
OVER TITANIA SUPPORTS



Miss Tipnapa Wongsalee

สถาบันวิทยบริการ
จุฬาลงกรณ์มหาวิทยาลัย

A Thesis Submitted in Partial Fulfillment of the Requirements
for the Degree of Master of Engineering Program in Chemical Engineering

Department of Chemical Engineering

Faculty of Engineering


Chulalongkorn University

Academic Year 2005

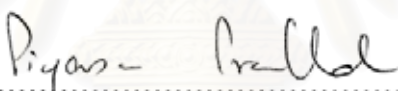
ISBN 974-17-4046-8

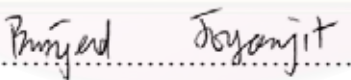
Thesis Title CHARACTERISTICS AND CATALYTIC PROPERTIES OF
 COBALT CATALYST OVER TITANIA SUPPORTS
By Miss Tipnapa Wongsalee
Field of Study Chemical Engineering
Thesis Advisor Bunjerd Jongsomjit, Ph.D.


Accepted by the Faculty of Engineering, Chulalongkorn University in Partial
Fulfillment of the Requirements for the Master's Degree



.....Dean of the Faculty of Engineering
(Professor Direk Lavansiri, Ph.D.)

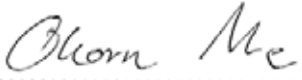
THESIS COMMITTEE


..... Chairman
(Professor Piyasan Praserttham, Dr.Ing.)


..... Thesis Advisor
(Bunjerd Jongsomjit, Ph.D.)


..... Member
(Joongjai Panpranot, Ph.D.)


..... Member
(Assistant Professor Artiwan Shotipruk, Ph.D.)


..... Member
(Okorn Mekasuwandumrong, D.Eng.)

ทิพย์นภา วงศ์สถี: คุณลักษณะและสมบัติการเป็นตัวเร่งปฏิกิริยาของตัวเร่งปฏิกิริยาโคบอลต์บนตัวรองรับไทเทเนีย (CHARACTERISTICS AND CATALYTIC PROPERTIES OF COBALT CATALYST OVER TITANIA SUPPORTS) อ. ที่ปรึกษา : ดร.บรรเจิด จงสมจิตร, 157 หน้า. ISBN 974-17-4046-8

วิทยานิพนธ์นี้ศึกษาผลของตัวรองรับไทเทเนียที่มีอัตราส่วนระหว่างเฟสรูไทล์ต่อเฟสแอนาเทสแตกต่างกันต่อคุณลักษณะและสมบัติในการเร่งปฏิกิริยาของตัวเร่งปฏิกิริยาโคบอลต์บนตัวรองรับไทเทเนียสำหรับปฏิกิริยาไฮโดรจิเนชันของคาร์บอนมอนอกไซด์ ตัวเร่งปฏิกิริยาโคบอลต์บนตัวรองรับไทเทเนียถูกเตรียมขึ้นด้วยตัวรองรับไทเทเนียที่ประกอบไปด้วยอัตราส่วนระหว่างเฟสรูไทล์ต่อเฟสแอนาเทสบนไทเทเนียหลายอัตราส่วน ในการพิสูจน์เอกลักษณ์ของตัวเร่งปฏิกิริยาทำการ ศึกษาโดยใช้ การวัดพื้นที่ผิว การกระเจิงรังสีเอ็กซ์ การส่องผ่านด้วยกล้องจุลทรรศน์อิเล็กตรอน/การวัดการกระจายตัวของโลหะ การส่องกราดด้วยกล้องจุลทรรศน์อิเล็กตรอน การรีดักชันแบบโปรแกรมอุณหภูมิ และการดูดซับด้วยไฮโดรเจน ปฏิกิริยาไฮโดรจิเนชันของคาร์บอนมอนอกไซด์ (มีอัตราส่วนของไฮโดรเจนต่อคาร์บอนมอนอกไซด์เท่ากับ 10/1) ถูกใช้เพื่อทดสอบความว่องไวของตัวเร่งปฏิกิริยาและการเลือกเกิดของผลิตภัณฑ์ ผลการศึกษาพบว่าทั้งความว่องไวของตัวเร่งปฏิกิริยาและการเลือกเกิดของผลิตภัณฑ์ปรับปรุงได้ โดยการเปลี่ยนแปลงอัตราส่วนระหว่างเฟสรูไทล์ต่อเฟสแอนาเทสบนตัวรองรับไทเทเนีย นอกจากนี้ทำการศึกษาพฤติกรรมการเป็นตัวเร่งปฏิกิริยาของตัวเร่งปฏิกิริยาโคบอลต์บนตัวรองรับไทเทเนียผสมซิลิกา สำหรับปฏิกิริยาการสังเคราะห์ฟิซเซอร์-โทรป ผลจากการทำปฏิกิริยาพบว่า การมีอยู่ของไทเทเนียในตัวรองรับแบบผสมส่งผลให้ความว่องไวของตัวเร่งปฏิกิริยาลดลงอย่างรวดเร็ว อย่างไรก็ตามสารประกอบไฮโดรคาร์บอนโซ่ยาว ได้แก่ คาร์บอน 2 อะตอม ถึง คาร์บอน 5 อะตอม เกิดมากขึ้นเมื่อเพิ่มปริมาณของไทเทเนียในตัวรองรับแบบผสม ผลจากการเติมตัวปรับปรุงเซอร์โคเนียบนไทเทเนียที่ประกอบไปด้วยเฟสต่างกัน ต่อคุณลักษณะและสมบัติในการเร่งปฏิกิริยาของตัวเร่งปฏิกิริยาโคบอลต์บนตัวรองรับไทเทเนียพบว่า ค่าความสามารถในการรีดิวซ์และความว่องไวของตัวเร่งปฏิกิริยาเพิ่มขึ้นสำหรับตัวรองรับไทเทเนียที่มีเฟสรูไทล์ 19 เปอร์เซ็นต์ อย่างไรก็ตามที่เปอร์เซ็นต์การเติมเซอร์โคเนียสูงขึ้น ไม่มีผลต่อการเลือกเกิดของผลิตภัณฑ์ ในทางตรงกันข้าม สำหรับตัวรองรับเฟสแอนาเทสบริสุทธิ์ ความว่องไวของตัวเร่งปฏิกิริยาลดลงเมื่อมีตัวปรับปรุงเซอร์โคเนีย อาจเป็นเพราะการเกิดสารประกอบระหว่างโคบอลต์กับตัวรองรับของตัวเร่งปฏิกิริยาโคบอลต์บนตัวรองรับไทเทเนีย

ภาควิชา.....วิศวกรรมเคมี..... ลายมือชื่อนิสิต.....ทิพย์นภา วงศ์สถี
สาขาวิชา.....วิศวกรรมเคมี..... ลายมือชื่ออาจารย์ที่ปรึกษา.....
ปีการศึกษา.....2548.....

##4670315921: MAJOR CHEMICAL ENGINEERING

KEY WORD: COBALT CATALYST/ TITANIA SUPPORT/ Co/TiO₂/
CHEMISORPTION/ CO HYDROGENATION/ TITANIA PHASE/ SILICA/
ZIRCONIA MODIFICATION

TIPNAPA WONGSALEE: CHARACTERISTICS AND CATALYTIC
PROPERTIES OF COBALT CATALYST OVER TITANIA SUPPORTS.
THESIS ADVISOR: BUNJERD JONGSOMJIT, Ph.D., 157 pp. ISBN: 974-17-
4046-8

A dependence of rutile to anatase ratios in titania on the characteristics and catalytic properties of Co/TiO₂ catalysts during CO hydrogenation was studied. The Co/TiO₂ catalysts were prepared using various titania supports consisting of various rutile to anatase ratios of titania. In order to identify the characteristics, all catalyst materials were characterized using BET surface area, XRD, SEM/EDX, TEM, TPR, and hydrogen chemisorption. CO hydrogenation (H₂/CO = 10/1) was also performed to determine the overall activity and selectivity. It was found that both activity and selectivity were altered by changing the rutile to anatase ratios in the titania support. In addition, the catalytic behaviors of mixed TiO₂-SiO₂-supported cobalt Fischer-Tropsch catalysts were also investigated. Based on the reaction study, it revealed that the presence of titania in the mixed supports resulted in decreased activities dramatically. However, longer chain hydrocarbons such as C₂-C₅ can be obtained substantially with increasing the amounts of titania in the mixed supports. The effect of zirconia-modified titania consisting of different phases on catalytic properties of Co/TiO₂ catalysts was found to enhance both reducibilities and the overall activities for the titania support consisting of 19% rutile. However, at high percent loading of zirconia tended to have no effect on selectivity of products. In contrast, for the pure anatase in titania support, the overall catalytic activity decreased upon Zr modification. This is probably due to the Co-support compound formation (Co-SCF) in titania-supported cobalt catalyst.

Department.....Chemical Engineering... Student's signature.....TIPNAPA WONGSALEE
Field of study...Chemical Engineering... Advisor's signature.....Bunjerd Jongsomjit
Academic year.....2005.....

ACKNOWLEDGEMENTS

The author would like to express her greatest gratitude and appreciation to her advisor, Dr. Bunjerd Jongsomjit for his invaluable guidance, providing value suggestions and his kind supervision throughout this study. In addition, she is also grateful to Professor Dr. Piyasan Praserttham, as the chairman, Dr. Artiwan Shotipruk and Dr. Okorn Mekasuvandamrong as the member. Special thanks and appreciation to Dr. Joongjai Panpranot for her kind supervision this thesis and as the member of the thesis committee.

The financial supports from the National Research Council of Thailand (NRCT), the Thailand Reserch Fund (TRF) and Thailand Japan Technology Transfer Project (TJTTP-JBIC) are also gratefully acknowledged. Furthermore, the author would like to extend her thankful to the National Metal and Materials Technology Center (MTECH) for the Raman spectroscopy analysis and Transmission Electron Microscope (TEM).

Many thanks for kind suggestions and useful help to Dr. Choowong Chaisuk, Dr. Okorn Mekasuvandamrong, Miss Soipatta Soisuwan, Miss Chitlada Sakdamnusun, Mr. Varutrit Jiraprawatthagool, Miss Juntana Wiwattanapongpan, Miss Kamonchanok Pansanga, Miss Onkanok Boonthumtirawuti, Miss Cheunkamol Kamolsawat and many friends in the petrochemical laboratory who always provide the encouragement and co-operate along the thesis study.

Most of all, the author would like to express her greatest gratitude to her parents and her family who always pay attention to her all the times for suggestions, support and encouragement.

CONTENTS

	page
ABSTRACT (IN THAI).....	iv
ABSTRACT (IN ENGLISH).....	v
ACKNOWLEDGMENTS.....	vi
CONTENTS.....	vii
LIST OF TABLES.....	x
LIST OF FIGURES.....	xii
CHAPTER	
I INTRODUCTION.....	1
II LITERATURE REVIEWS.....	4
2.1 Titania-supported cobalt catalysts.....	4
2.2 Effect of zirconia modified support of cobalt catalysts.....	7
2.3 Silica-supported cobalt catalysts.....	11
III THEORY.....	15
3.1 Fischer-Tropsch synthesis (FTS)	15
3.2 Cobalt.....	19
3.2.1 General.....	19
3.2.2 Physical properties.....	19
3.2.3 Cobalt oxides.....	22
3.3 Cobalt-based catalysts.....	23
3.4 Cobalt-support compound formation (Co-SCF).....	23
3.4.1 Co-Aluminate Formation.....	24
3.4.2 Co-Silicate Formation.....	24
3.4.3 Co-Titanate Formation.....	24
3.5 Titanium dioxide	25
3.5.1 Physical and chemical properties.....	25
3.6 Silicon dioxide	28
3.6.1 Occurrence and Classification	28
3.7 Zirconia	31
3.7.1 Physical and Chemical Properties	31
3.7 Promoters	32

CONTENTS (CONT.)

	page
IV EXPERIMENTS.....	34
4.1 Catalyst preparation.....	34
4.1.1 Chemicals.....	34
4.1.2 Preparation of various ratios of rutile:anatase in TiO ₂ support	35
4.1.3 Preparation of Zr-modified TiO ₂ support	35
4.1.4 Preparation of TiO ₂ -SiO ₂ mixed oxide support	35
4.1.5 Cobalt loading	35
4.1.6 Preparation of reference materials	36
4.1.7 Catalyst Nomenclature	36
4.2 Catalyst characterization.....	37
4.2.1 Atomic absorption spectroscopy (AAS).....	37
4.2.2 X-ray diffraction (XRD).....	37
4.2.3 (N ₂ physisorption) BET surface area.....	37
4.2.4 Temperature programmed reduction (TPR).....	38
4.2.5 Hydrogen chemisorption	39
4.2.6 Electron microscopy.....	39
4.2.7 Transmission Electron Microscope (TEM).....	40
4.2.8 Raman spectroscopy	40
4.3 Reaction study in CO hydrogenation.....	40
4.3.1 Materials.....	40
4.3.2 Apparatus.....	40
4.3.2.1 Reactor	41
4.3.2.2 Automation Temperature Controller.....	41
4.3.3.3 Electrical Furnace.....	41
4.3.3.4 Gas Controlling System.....	41
4.3.3.5 Gas Chromatography	41
4.3.3 Procedures.....	42
RESEARCH METHODOLOGY.....	45

CONTENTS (CONT.)

	page
V RESULTS AND DISCUSSION	46
5.1 Results.....	46
5.1.1 Various ratios of rutile to anatase phase of titania- supported Co catalysts.....	46
5.1.2 Various percent of zirconia modified titania-supported Co catalysts	69
5.1.3 Titania-Silica mixed oxide-supported Co catalysts	87
VI CONCLUSIONS AND RECOMMENDATIONS.....	110
6.1 Conclusions.....	110
6.2 Recommendations.....	111
REFERENCES.....	112
APPENDICES.....	117
APPENDIX A: CALCULATION FOR CATALYST PREPARATION.....	118
APPENDIX B: CALCULATION OF BET SURFACE AREA BY THE SINGLE POINT METHOD.....	120
APPENDIX C: CALCULATION FOR REDUCIBILITY.....	123
APPENDIX D: CALCULATION FOR TOTAL H ₂ CHEMISORPTION AND DISPERSION.....	125
APPENDIX E: CALIBRATION CURVES.....	126
APPENDIX F: CALCULATION OF CO CONVERSION, REACTION RATE AND SELECTIVITY.....	134
APPENDIX G: LIST OF PUBLICATIONS.....	136
VITAE.....	157

LIST OF TABLES

Table	page
3.1 Physical properties of cobalt	21
3.2 Crystallographic information on the different forms of titanium dioxide....	26
4.1 Chemicals used in the preparation of catalysts.....	34
4.2 Operating condition of the thermal conductivity detector for TPR.....	39
4.3 Operating condition for gas chromatograph.....	42
5.1 Content of Co from AAS and BET surface area measurement of various ratios of rutile to anatase phase of titania unsupported and supported Co catalysts.....	47
5.2 TPR and H ₂ chemisorption results for various ratios of rutile to anatase phase of titania-supported Co catalysts.....	48
5.3 Initial, final and maximum temperatures from TPR profiles of various ratios of rutile to anatase phase of titania-supported Co catalysts.....	50
5.4 The average diameters of cobalt metals sizes from TEM for various ratios of rutile to anatase phase of titania-supported Co catalysts.....	64
5.5 Reaction rate for CO hydrogenation on the various ratios of rutile to anatase phase of titania-supported Co catalysts.....	68
5.6 BET surface area measurement of various percent loading of zirconia modified titania unsupported and supported Co catalysts.....	70
5.7 TPR and H ₂ chemisorption results for the various percent loading of zirconia modified titania-supported Co catalysts.....	72
5.8 Initial, final and maximum temperatures from TPR profiles of various percent of zirconia modified titania-supported Co catalysts.....	74
5.9 The average diameters of cobalt metals sizes from TEM for various percent loading of zirconia modified titania-supported Co catalysts.....	83
5.10 Reaction rate for CO hydrogenation on the various percent loading of zirconia modified titania-supported Co catalysts.....	86
5.11 BET surface area measurement of Titania-Silica mixed oxide unsupported and supported Co catalysts.....	88
5.12 Initial, final and maximum temperatures from TPR profiles and H ₂ chemisorption results for Titania-Silica mixed oxide-supported Co catalysts	89

LIST OF TABLES

Table	page
5.13 The average diameters of cobalt metals sizes from TEM for various ratios of rutile to anatase phase of titania-supported Co catalysts.....	105
5.14 Reaction rate for CO hydrogenation on the Titania-Silica mixed oxide-supported Co catalysts.....	109
E.1 Conditions use in Shimadzu modal GC-8A and GC-14B.....	129



สถาบันวิทยบริการ
จุฬาลงกรณ์มหาวิทยาลัย

LIST OF FIGURES

Figure	page
3.1 Crystal structure of TiO ₂	26
3.2 The unit cells of the crystal systems	32
3.3 Crystal structure of cubic, tetragonal and monoclinic zirconia.....	32
4.1 Flow diagram of CO hydrogenation system.....	44
5.1 TPR profiles of various ratios of rutile to anatase phase of titania-supported Co catalysts.....	51
5.2 XRD patterns of various ratios of rutile to anatase phase of titania support samples.....	54
5.3 XRD patterns of various ratios of rutile to anatase phase of titania- supported Co catalysts.....	55
5.4 SEM micrograph and EDX mapping of Co/R0 catalyst granule.....	57
5.5 SEM micrograph and EDX mapping of Co/R3 catalyst granule.....	58
5.6 SEM micrograph and EDX mapping of Co/R19 catalyst granule.....	59
5.7 SEM micrograph and EDX mapping of Co/R40 catalyst granule.....	60
5.8 SEM micrograph and EDX mapping of Co/R95 catalyst granule.....	61
5.9 SEM micrograph and EDX mapping of Co/R99 catalyst granule.....	62
5.10 TEM micrographs of Co/R0, Co/R3 and Co/R19 catalysts.....	65
5.11 TEM micrographs of Co/R40, Co/R95 and Co/R99 catalysts.....	66
5.12 TPR profiles of various percent loading of zirconia modified titania -supported Co catalysts.....	73
5.13 XRD patterns of various percent loading of zirconia modified titania support.....	76
5.14 XRD patterns of various percent loading of zirconia modified titania -supported Co catalysts.....	77
5.15 SEM micrograph and EDX mapping of Co/R0Z1 catalyst granule.....	79
5.16 SEM micrograph and EDX mapping of Co/R0Z5 catalyst granule.....	80
5.17 SEM micrograph and EDX mapping of Co/R19Z1 catalyst granule.....	81
5.18 SEM micrograph and EDX mapping of Co/R19Z5 catalyst granule.....	82

LIST OF FIGURES

Figure	page
5.19 TEM micrographs of Co/R0Z1, Co/R0Z5, Co/R19Z1 and Co/R19Z5 catalysts.....	84
5.20 TPR profiles of Titania-Silica mixed oxide-supported Co catalysts.....	91
5.21 XRD patterns of Titania-Silica mixed oxide support samples.....	93
5.22 XRD patterns of Titania-Silica mixed oxide-supported Co catalysts.....	94
5.23 Raman spectra of Titania-Silica mixed oxide-supported Co catalysts.....	96
5.24 SEM micrographs and EDX mapping of Co_0/1 catalyst granule.....	98
5.25 SEM micrographs and EDX mapping of Co_2/8 catalyst granule.....	99
5.26 SEM micrographs and EDX mapping of Co_4/6 catalyst granule.....	100
5.27 SEM micrographs and EDX mapping of Co_6/4 catalyst granule.....	101
5.28 SEM micrographs and EDX mapping of Co_8/2 catalyst granule.....	102
5.29 SEM micrographs and EDX mapping of Co_1/0 catalyst granule.....	103
5.30 TEM micrographs of Co_0/1, Co_2/8 and Co_4/6 catalysts.....	106
5.31 TEM micrographs of Co_6/4, Co_8/2 and Co_1/0 catalysts.....	107
E.1 The chromatograms of catalyst sample from thermal conductivity detector, gas chromatography Shimadzu model 8A (Molecular sieve 5A column).....	127
E.2 The chromatograms of catalyst sample from flame ionization detector, gas chromatography Shimadzu modal 14B (VZ10 column).....	128
E.3 The calibration curve of CO.....	130
E.4 The calibration curve of methane.....	130
E.5 The calibration curve of ethane.....	131
E.6 The calibration curve of ethylene.....	131
E.7 The calibration curve of propane.....	132
E.8 The Calibration curve of propylene.....	132
E.9 The calibration curve of butane.....	133

CHAPTER I

INTRODUCTION

It is expected that in the near future the feedstock for the chemical industry will shift from crude oil to natural gas due to the limited reserves of crude oil and the increasing environmental constraints. To enable its chemical conversion, natural gas is first transformed into synthesis gas, which is a mixture of carbon monoxide and hydrogen. This synthesis gas is the basis for a number of large-scale industrial processes. Fischer-Tropsch synthesis (FTS) is one of the route for the chemical liquefaction of natural gas. As such, it allows the economic exploitation of remote natural gas resources and constitutes an alternative route for the production of clean transportation fuels and petrochemical feedstock in relation to the classic refining of crude oil.

FTS has a lively history of more than 80 years. Its name came from the work of Fisher and Tropsch and first described in the 1920s. It is known as a carbon monoxide (CO) hydrogenation which is added hydrogen to carbon monoxide. In general, the process is most widely used for synthesis of hydrocarbon waxes which are further cracked into gasoline and diesel fuel. The common FTS catalysts are based on iron (Fe), ruthenium (Ru), or cobalt (Co) as the active metal. The costs for Fe-based catalysts are low, but these catalysts suffer from a low wax selectivity, deactivation, and inhibition of the productivity by water at large syngas conversions. Despite the high activity of Ru-based catalysts, their utilization is limited to scientific studies because of the high price of ruthenium. However, Co-based catalysts are preferred due to their high activity for FTS based on natural gas, high selectivity to linear hydrocarbon and low activity for the competitive water-gas shift reaction (WGS). For Co catalysts, it is known that the reduced metal, rather than its oxides or carbides, is the most active phase in CO hydrogenation. However, under pretreatment and/or reaction conditions, the formation of Co and the support results in a lower activity of the catalysts due to a loss in active Co metal available for reaction.

Support effects in FTS catalysts have been investigated. One important focus in the development of this process is the improvement of the catalyst activity by

increasing the number of active Co metal sites that are stable under reaction conditions. Therefore, it is important to understand how the structural parameters of the catalyst influence the activity and stability of catalysts. To improve the number of active sites, the Co is most often present as dispersed clusters on a high surface area support such as Al₂O₃, TiO₂, SiO₂, and ZrO₂. Titania or TiO₂ is one of the most supports used for Co catalysts (Reuel and Bartholomew, 1984; Kraum and Baerns, 1999; Lin *et al.*, 2002; Jacobs *et al.*, 2002; Madikizela and Coville, 2002). However, it should be noted that titania itself has different crystalline phase such as anatase and rutile phase. The different crystalline phase composition of titania could play an important role on the catalytic performance of titania-supported Co catalysts (Jongsomjit *et al.*, 2005).

Moreover, to increase titania-supported cobalt catalyst activity, titania can be added in small amounts or mixed with some other oxides so as to improve surface characteristics (surface area and porosity), thermal stability and surface acidity of the composite catalysts and consequently their catalytic performances (Xingtao Gao and Israel E. Wachs, 1999; Mohamed Mokhtar Mohamed *et al.*, 2002; M.S. Rana *et al.*, 2003) and can be added many promoters such as Ru, Pt, Pd, B, Mn, Fe, Zn and Zr (E. IGLESIA *et al.*, 1994; D. Schanke *et al.*, 1995; JG. Price *et al.*, 1997; JL. Li *et al.*, 2000; N. Tsubaki *et al.*, 2001; NN. Madikizela *et al.*, 2002; DJ. Duvenhage *et al.*, 2002; JL. Li *et al.*, 2003; FM. Cano *et al.*, 2004; K. Nagaoka *et al.*, 2004; N. Nobuntu *et al.*, 2004). The use of these promoters as described above tends to lower the reduction temperature of Co, preserve the activity by preventing the formation of coke, increase the reducibility of Co, increase FT reaction rates, exhibit cluster and ligand effects, act as a source of hydrogen spillover, and enhances the dispersion.

This thesis focuses on investigation of characteristics and catalytic properties for titania-supported Co catalysts. Titania-based supports can be identified as titania supports consisting of various rutile/anatase phase ratios, titania supports contained promoters or modifiers, and titania supports mixed with other inorganic oxides. The study was scoped as follows:

1. Preparation of various ratio of rutile to anatase phase of titania by calcination pure anatase of titania (800-1000 °C, 10 °C /min, 4 h, in air).

2. Preparation of Zr-modified TiO₂ using the incipient wetness impregnation method.
3. Preparation of TiO₂-SiO₂ mixed oxides using solution mixing.
4. Preparation of various ratios of rutile to anatase phase of titania, TiO₂-SiO₂ mixed oxide and Zr-modified TiO₂ supported Co catalyst (20 wt% Co) using the incipient wetness impregnation method.
5. Characterization of the catalyst samples using atomic absorption spectroscopy (AAS), X-ray diffraction (XRD), BET surface area, temperature programmed reduction (TPR), hydrogen chemisorption, scanning electron microscopy (SEM), energy dispersive X-ray spectroscopy (EDX), transmission electron microscopy (TEM) and Raman spectroscopy.
6. Reaction study of the catalyst samples in CO hydrogenation at 220°C and 1 atm and a H₂/CO ratio of 10.

CHAPTER II

LITERATURE REVIEWS

There have been a number of researchers studying titania and silica-supported catalysts in Fischer-Tropsch synthesis. Many researchers have been found better knowledge about titania and silica especially supported cobalt catalyst and have been improved this by adding small amounts of metal such as zirconia. These reports are very useful and will use to develop works for the future.

2.1 Titania-supported cobalt catalysts

R. Zennaro *et al.* (2000) studied kinetics of Fischer-Tropsch synthesis on titania-supported cobalt. They have reported rates of CO hydrogenation on a well-characterized 11.7% Co/TiO₂ catalyst measured after 20h of reaction in a differential fixed-bed reactor at 20 atm, 180-240°C, and 5% conversion, over a range of reactant partial pressure, can be used to model precisely and accurately the kinetics of this reaction. In addition, turnover frequencies and rate constants determined from this study are in very good to excellence agreement with those obtained in previous studies of Co/TiO₂ and other cobalt-supported combination, when the data are normalized to the same conditions of temperature and partial pressure of the reactant. Based on this comparison it is concluded that CO conversion and the partial pressure of product water have little effect on specific rate per catalytic site. They also found that the data of this and other studies are fitted fairly well by a simple power law expression of the form,

$$-r_{CO} = kP_{H_2}^{0.74}P_{CO}^{-0.24}$$

where $k = 5.1 \times 10^{-3} \text{ s}^{-1}$ at 200°C, $P = 10 \text{ atm}$, and $H_2/CO = 2/1$. However, the data of this study are best fitted by the simple Langmuir-Hinshelwood (LH) rated form

$$-r_{CO} = aP_{H_2}^{0.74} / (1 + bP_{CO})^2$$

In comparison to fits of the same data by several other representative LH rate forms proposed in previous studies.

Y. Brik *et al.* (2001) studied characterization of titania-supported cobalt and cobalt-phosphorus and investigated performance in ethane oxidative dehydrogenation (ODH). They found that at low cobalt loading, the sample is essentially covered by octahedral Co^{2+} ions, whereas at concentrations superior to 3.7 wt% formation of the Co_3O_4 spinel is observed. The best performance in ethane ODH is achieved at 550°C with the sample containing 7.6 wt% Co. In addition, the reaction begins with a conversion of 33 % and selectivity around 75%, then it decreases to reach after 150 minutes on stream a stationary state at 22% of conversion and 60% selectivity. This loss of 30% of the initial activity may be associated with a decrease of the specific surface area and the concomitant formation of CoTiO_3 and Co_2TiO_4 . Moreover, addition phosphorus lead to a marked activity decrease, ascribed to the formation of cobalt-phosphorus compounds not active in the reaction.

J. Li *et al.* (2002) studied the effect of water vapor on the catalytic properties of a ruthenium promoted Co/TiO_2 catalyst during FTS operated, in a continuously stirred tank reactor (CSTR) by adding water into the feed gas at varying space velocity. They found that at higher space velocities ($\text{SV} = 4 \text{ NL g cat.}^{-1}\text{h}^{-1}$), the addition of water did not have significant effect on the CO conversion. At lower space velocity ($\text{SV} = 2 \text{ NL g cat.}^{-1}\text{h}^{-1}$), the addition of water decrease the CO conversion; however, the decrease was reversible with the catalyst quickly recovering the activity that it exhibited prior to water addition. Moreover, at high CO conversion (space velocity of $\text{SV} = 1 \text{ NL g cat.}^{-1}\text{h}^{-1}$) the addition of water resulted in a catalyst permanent deactivation. The methane selectivity was not influence by water addition, but the CO_2 selectivity was increased with water addition.

J. Li *et al.* (2002) investigated the effect of carbon monoxide pretreatment on the titania supported cobalt catalyst and compared with these of catalysts pretreated with hydrogen. They have reported that the pretreatment gas (reductant) had a remarkable effect on the performance a ruthenium promoted cobalt catalyst during Fischer-Tropch synthesis. The hydrogen reduced catalyst exhibited a higher initial synthesis gas conversion (72.5%) and reached steady state after 40h on stream. In

addition, the carbon monoxide catalyst reached steady state quickly, exhibited lower activity and good stability. Methane selectivity for the carbon monoxide reduced catalyst was 15-20% (carbon basis), higher than that on the hydrogen reduced catalyst (5-10%). Moreover, the effect of carbon monoxide treatment on the used catalyst also has been proposed they found that carbon monoxide regeneration increased the activity on the hydrogen reduced catalyst; however, it did not have a significant effect on the carbon monoxide reduced catalyst.

K. Nagaoka *et al.* (2003) investigated the influence of reduction temperature (973-1223 K) on the catalytic activity of the 0.5 wt% Co/TiO₂ for the CH₄/CO₂ reaction under 2.0 MPa mainly at a space velocity (SV) of 6000 ml g⁻¹ h⁻¹. They were found that (1) the catalytic activity and the coke deposition for the catalysts were strongly affected by the reduction temperature. (2) The Co/TiO₂ reduced below 1123 K showed rapid and complete deactivation at the beginning of the reaction. (3) On the other hand, the Co/TiO₂ reduced at and above 1123 K showed relatively stable activity at the same reaction condition. (4) However, the slow deactivation was prevented by the addition of a small amount of ruthenium (Ru/Co = 0.05) and it was found that strong resistance to coking for the Co/TiO₂ reduced at 1123 K was also retained after the addition of ruthenium.

B. Jongsomjit *et al.* (2005) studied Co-support compound formation in titania-supported cobalt catalyst. They have shown that Co-support compound formation (Co-SCF) in titania-supported cobalt catalyst can occur during standard reduction resulting in a lower reducibility of catalyst. The compound of cobalt and titania formed referred as “Co-titanate” was considered to be non-reducible at temperatures <800°C. The “Co-titanate” formed resulted in a decrease in the degree of reduction without any significant change in the reduction behaviors. It was found that the partial pressures of water vapor during reduction probably had only a slight effect on an increase in the “Co-titanate” formation. Due to its highly dispersed form, it can not be detected by XRD. However, Raman spectroscopy revealed that this highly dispersed “Co-titanate” formed was likely to be different from CoTiO₃ and present as a non-stoichiometric surface “Co-titanate” compound. The “Co-titanate” formed also resulted in decreased activities of catalyst without any changes in selectivity.

S. Storsæter *et al.* (2005) investigated the effect of water on the activity and selectivity of unpromoted and Re-promoted cobalt Fischer–Tropsch catalysts supported on Al₂O₃, SiO₂, and TiO₂ in a fixed-bed reactor at 483 K and 20 bar. Common for all the catalysts was an increase in C₅₊ selectivity and a decrease in the CH₄ selectivity at increased conversion or by external water addition. Promoting with Re increased the reaction rate [$g_{\text{HC}}/(g_{\text{cat}} \text{ h})$] for all catalysts and the C₅₊ selectivity for the SiO₂- and TiO₂-supported catalysts. They found that the Co/Al₂O₃ and CoRe/Al₂O₃ catalysts deactivate when water is added during Fischer–Tropsch synthesis. For the Co/SiO₂ and CoRe/SiO₂ catalysts the reaction rate increased with increasing conversion or upon water addition. However, at high concentrations of water the catalysts deactivate rapidly. An increased reaction rate was also observed for the Co/TiO₂ and CoRe/TiO₂ catalysts with increasing conversion or with the addition of small amounts of water. At higher partial pressures of water the reaction rate decreased. Water interacts with the catalysts in different ways, and the effect of water is discussed in terms of Co particle sizes, secondary reactions, adsorbed species on the catalyst surface, and diffusion in liquid-filled pores.

B. Jongsomjit *et al.* (2005) studied the dependence of crystalline phases in titania on the catalytic properties of Co/TiO₂ catalysts during CO hydrogenation. They suggested that the presence of rutile phase (19 mol%) in titania resulted in significant increases in the catalytic activities during CO hydrogenation. This is mostly due to an increase in stability of the titania support with the presence of rutile phase. They were proposed that the presence of rutile phase in titania stabilized the catalysts probably due to two reasons: (i) block the formation of Co species strongly interacted with the titania support or Co-SCF; and (ii) inhibition of the impact of water vapor produced during reduction.

2.2 Effect of zirconia modified support of cobalt catalysts

S. Ali *et al.* (1995) investigated the influence of Zr promotion of 20 wt% Co/SiO₂ on Fischer–Tropsch synthesis using catalysts prepared in different ways and having different loadings of Zr (up to 8.5 wt%). The catalysts were investigated using FTS (H₂/CO=2), H₂-D₂ exchange, and CO dissociation to provide insight into how Zr modifies the Co properties. They reported that Zr-promoted exhibited higher

overall rates of FTS compared to unpromoted Co/SiO₂. The sequentially impregnated Co/Zr/SiO₂ catalysts appeared to be the most active. However, the co-impregnation method of preparation appeared to result in higher cobalt dispersion. While Zr promotion did not appear to promote or inhibit H₂ activation, hydrogen spillover may have been partly responsible for enhancing the activity of the sequentially impregnated Zr/Co/SiO₂ catalysts. Zr also possibly created an active interface with Co that increased catalyst activity by facilitating Co dissociation. Although high levels of promotion tended to increase the selectivity for higher hydrocarbon, Zr appears to be primarily an excellent rate promoter for Co/SiO₂.

A. Feller *et al.* (1999) investigated the addition of zirconium oxide chloride to the catalyst formulation of Co/SiO₂. They found that it leads to a higher reducibility of cobalt, due to the formation of a cobalt–zirconium species, which can be reduced at lower temperatures than cobalt silicate. Furthermore, the metal particle size of cobalt is increased, but the size of cobalt clusters is reduced. For the reaction study, they reported that the CO-conversion of the promoted catalyst increases with increasing zirconium content. Moreover, the extent of secondary hydrogenation of olefins (e.g., ethene) passes a minimum, and the C₅₊-selectivity passes a maximum due to readsorption of small, reactive organic product compounds, which can be incorporated in larger product compounds.

F. Rohr *et al.* (2000) studied effect of adding zirconia to the alumina support on supported cobalt Fischer–Tropsch catalysts. They also showed that at 5 bar with H₂:CO ratio 9:1 zirconia addition to the support leads to a significant increase in both activity and selectivity to higher hydrocarbons as compared to the unmodified catalysts. This effect has been studied with SSITKA, and can be attributed to changes in the surface coverage of reactive intermediates, not to a change in the intrinsic activity. The SSITKA experiments also revealed unexpectedly an increase in the surface coverage of reactive intermediates with increasing temperature.

G. Jacobs *et al.* (2003) defined the reducibility of supported cobalt catalysts by used temperature programmed reduction (TPR) and hydrogen chemisorption combined with reoxidation measurements. Different supports (e.g. Al₂O₃, TiO₂, SiO₂, and ZrO₂ modified SiO₂ or Al₂O₃) and a variety of promoters, including noble metals

and metal cations, were examined. They found that significant support interactions on the reduction of cobalt oxide species were observed in the order $\text{Al}_2\text{O}_3 > \text{TiO}_2 > \text{SiO}_2$. Addition of Ru and Pt exhibited a similar catalytic effect by decreasing the reduction temperature of cobalt oxide species, and for Co species where a significant surface interaction with the support was present, while Re impacted mainly the reduction of Co species interacting with the support. For catalysts reduced at the same temperature, a slight decrease in cluster size was observed in H_2 chemisorption/pulse reoxidation with noble metal promotion, indicating that the promoter aided in reducing smaller Co species that interacted with the support. On the other hand, they have reported that addition of non-reducible metal oxides such as B, La, Zr, and K was found to cause the reduction temperature of Co species to shift to higher temperatures, resulting in a decrease in the percentage reduction. For both Al_2O_3 and SiO_2 , modifying the support with Zr was found to enhance the dispersion. Increasing the cobalt loading, and therefore the average Co cluster size, resulted in improvements to the percentage reduction. Finally, a slurry phase impregnation method led to improvements in the reduction profile of $\text{Co}/\text{Al}_2\text{O}_3$.

B. Jongsomjit *et al.* (2003) synthesized the zirconia (Zr)-modified alumina-supported Co catalysts by the sequential impregnation method. They have studied the impact of Zr loading on the reducibility of Co in the absence and presence of water vapor. They reported that Zr modification of the alumina support had a significant impact on the catalyst properties: the overall activity during FT synthesis increased significantly upon Zr modification due to an increase in reducibility during standard reduction. Furthermore, the increase in reducibility appeared to have been caused by a decrease in the amount of Co-SCF. They also suggested that Zr modification may have caused: (i) a stabilization of the alumina support by blocking Co “aluminate” formation and/or (ii) a minimization of the impact of water vapor in modifying the surface properties of alumina, thereby decreasing the ease of Co reaction with the alumina.

Y. Zhang *et al.* (2004) developed a new and simple method for preparing multi-functional nano-sized silica-silica or zirconia-silica bimodal pore catalyst support by direct introduction of silica or zirconia sols into silica gel. The pores of the obtained bimodal pore supports distributed distinctly as two kinds of main pores. On

the other hand, the increased BET surface area and decreased pore volume, compared to those of original silica gel, indicated that the obtained bimodal pore supports formed according to the designed route, and they was found that the zirconia-silica bimodal support improved catalyst activity significantly via not only spatial effect, the intrinsic property of the bimodal structure, but also chemically promotional effect of zirconia, when this kind of support was applied in the liquid-phase Fischer–Tropsch synthesis (FTS) as a cobalt-loading catalyst.

M. Shinoda *et al.* (2004) studied new bimodal pore catalysts for Fischer–Tropsch synthesis. They developed the method of introducing oxide sols into the large pore silica pellet, to form tailormade bimodal catalyst support. They found that the distinctly distributed two kinds of pores, the increased BET surface area and the decreased pore volume of the obtained bimodal support proved that the particles from the sol indeed entered the uniformly distributed intrinsic large pores of silica pellet to ensure bimodal structure. The Co/SiO₂ catalysts derived from silica bimodal supports were tested in slurry phase FTS. It showed higher activity and favorable selectivities, due to its improved dispersion of supported cobalt crystalline by bimodal structure, as proved by XRD and TEM, and fastened diffusion efficiency inside catalyst pellet with bimodal structure. Furthermore, besides the spatial effect from bimodal structure as shown in silica–silica bimodal catalyst, significantly enhanced activity was realized using ZrO₂-silica bimodal support, as ZrO₂ inside the large pores of SiO₂ not only formed small pores but also intrinsically promoted FT synthesis.

H. Xiong *et al.* (2005) prepared a series of zirconium-modified Co/Al₂O₃ catalysts and used XRD, XPS, TPR, H₂-TPD and oxygen titration for the characterization of the catalysts. The catalytic performance was performed in a fixed bed reactor for Fischer–Tropsch synthesis (FTS). The CoAl₂O₄ spinel phase was detected on the prepared catalysts and its content on the catalysts decreased with the increase of zirconium loading, indicating that Zr-added could inhibit CoAl₂O₄ formation. The addition of zirconium to the Co catalyst caused the increase of cobalt cluster size. Zr addition has been shown to improve the activity and C₅₊ selectivity of Co/Al₂O₃ catalyst for Fischer–Tropsch synthesis. This could be explained by the increase of active metal cobalt site and reducibility. The increase of zirconium loading

on Co/Zr/Al₂O₃ catalyst resulted in the increase of olefin/paraffin ratio in the products.

2.3 Silica-supported cobalt catalysts

A. Kogelbauer *et al.* (1995) studied the formation of cobalt silicates on Co/SiO₂ under hydrothermal conditions. Hydrothermal treatment at 220°C led to a catalyst with lower reducibility due to the formation of both reducible and nonreducible (at temperatures < 900°C) Co silicates. They also showed that silicate was formed in catalysts which had been used for FT synthesis. No significant change occurred upon hydrothermal treatment of calcined catalyst. The presence of air during the hydrothermal treatment inhibited the formation of silicate and they proposed that the formation of silicate was linked to the presence of metallic cobalt.

J. Choi (1995) investigated the reduction of cobalt catalysts supported on Al₂O₃, SiO₂ and TiO₂ and the effect of metal loading on the reduction. He reported that the activation energy of reduction increased in the following order: Co/SiO₂ > Co/Al₂O₃ > Co/TiO₂. For different metal loading, the catalyst with the higher loading is more readily reducible than with the lower metal loading.

R. Riva *et al.* (2000) studied the interaction of cobalt with two different kinds of support: silica and titania and their effect on the dispersion and reducibility by XPS, TPR, TPO, XRD and TEM. They also showed that the interaction is much stronger in the case of titania. The different reactivity of cobalt with silica and titania explains why reducing and reoxidizing treatments have opposite effects on the dispersion of cobalt depending on whether it is supported on SiO₂ or TiO₂. The low reactivity of cobalt with silica favors sintering effects. Conversely, due to the high reactivity of cobalt with titania, the coverage of TiO₂ by cobalt tends to increase after the same treatments.

S. Sun *et al.* (2000) studied the reaction performances and characterization of Fischer–Tropsch synthesis Co/SiO₂ catalysts prepared from mixed cobalt salts. Using a mixture of cobalt nitrate and cobalt acetate for impregnation resulted in highly

active cobalt silica catalyst. The supported cobalt acetate had stronger interaction with SiO_2 than cobalt nitrate and was difficult to be reduced. It is considered that the reduction of cobalt acetate species could be promoted by spillover hydrogen activated on the cobalt metal from cobalt nitrate. The N/A ratio had a great effect on catalyst reduction degree and metal particle size. High reduction degree and high cobalt metal dispersion are two important factors for FTS catalysts. The synthesis of highly dispersed cobalt catalysts required the initial formation of very small CoO or Co_3O_4 crystallites. The formation of small oxide clusters needs strong interactions between the support and the cobalt precursor. But too strong interaction between SiO_2 and small CoO_x clusters would suppress reduction of these CoO_x clusters; thus, assistance from other coexisting sites, such as cobalt-nitrate-derived metallic sites, was necessary. Using a suitable N/A ratio of precursors appeared to be a promising synthesis route of active cobalt silica catalysts.

M. Voß *et al.* (2002) investigated the structural, chemical and electronic properties of Co and Co/Mn catalysts supported on Al_2O_3 , SiO_2 and TiO_2 by a combination of different methods such as TEM, XRD, XPS, TPR and TPO. They reported that temperature-programmed reduction and oxidation reveal the formation of various oxides in dependence on temperature. In case of the alumina- and titania-supported cobalt catalysts, the formation of high-temperature compounds CoAl_2O_4 and CoTiO_3 , respectively. Moreover, these compounds are not reducible under the applied conditions, the degrees of reduction are only 18-20% ($\text{Co}/\text{Al}_2\text{O}_3$) and 77% (Co/TiO_2).

M.S. Rana *et al.* (2003) prepared high specific surface area and better textural properties TiO_2 - SiO_2 mixed oxide supports by urea hydrolysis precipitation and characterized by BET, XRD, pore volume, zero point charge (ZPC) and low temperature oxygen chemisorptions (LTOC). They reported that mixing of TiO_2 with SiO_2 alters the nature of weak interaction of active phases with the SiO_2 support, and overcome the poor dispersion on SiO_2 supported catalysts. TiO_2 counterpart in SiO_2 plays a role to provide high intrinsic activity and generate favorable morphology for MoS_2 phases and promote metal support interaction. HDS and HYD activities comparison on various supports for both functionalities relishes possible role of support, not only by increasing the number of sites but also changing the active sites

through subtle modifications of metal support interactions. The different loading of molybdenum does not change the nature of active sites for HDS and HYD functionalities, however at different concentration, the dispersion of active site is different and as a result the relative number of active site varies as a function of Mo loadings.

S. Hu *et al.* (2003) studied Binary TiO_2 - SiO_2 mixed oxides display interesting catalytic properties which have not been attributed to the pure TiO_2 and SiO_2 . Many authors have proposed that Brønsted acidity is generated upon interaction of the two oxides. They have demonstrated that high-purity crystalline and amorphous TiO_2 - SiO_2 mixed oxides do not possess Brønsted acidity, only Lewis acidity. The similarity in the composition of reaction products obtained with TiO_2 and TiO_2 - SiO_2 and the difference with reaction products obtained with Brønsted acids suggest that the reaction takes place on TiO_2 in both cases. The activity of TiO_2 - SiO_2 mixed oxides in the double bond isomerization of 1-butene could be accounted for simply by a high degree of dispersion of the TiO_2 nanoparticles. In this hypothesis, the role of SiO_2 could be that of enhancing the degree of dispersion of TiO_2 during the preparation process, and stabilizing the nanoparticles of TiO_2 against thermal sintering. They suggested that the pure TiO_2 sintering takes place at temperatures lower than those at which sintering of TiO_2 - SiO_2 mixed oxides takes place. This reduction in surface area of TiO_2 could be the cause of the low catalytic activity reported in previous studies.

Y. Zhang *et al.* (2005) developed a multi-functional bimodal pore catalyst support, alumina-silica bimodal pore support from a polymer complex solution and silica gel. The obtained bimodal pore support had two kinds of main pores; the pore volume was decreased and the specific surface area was enlarged, comparing with the original silica gel. This kind of bimodal pore support was applied in slurry phase Fischer-Tropsch synthesis, where cobalt was supported as active metal. Alumina-silica bimodal pore catalyst exhibited high catalytic activity and favorite selectivity, due to the spatial effects of bimodal pore structure and chemical effects of coexisting alumina, which formed the new small pores inside SiO_2 large pores. Alumina-silica bimodal pore catalyst showed higher activity than silica-silica bimodal pore catalyst with similar pore structure, proving that hetero-atom bond between alumina and silica was important to promote the performance of the dispersed cobalt. The various

catalysts were characterized by XRD, chemisorption, in situ DRIFT, TPR, and TPSR. They found that alumina in alumina–silica bimodal structure improved cobalt dispersion significantly while keeping the reduction degree almost the same. TOF of alumina–silica bimodal catalysts was the highest, supported by the largest bridge-type adsorbed CO peak in DRIFT observation of this catalyst, as bridge-type adsorbed CO was the active intermediate in FTS.

A. K. Dalai *et al.* (2005) investigated Fischer–Tropsch synthesis: water effects on Co supported on narrow and wide-pore silica. The effect of water on the performance of narrow and wide-pore silica-supported cobalt catalysts was investigated during Fischer–Tropsch synthesis in a continuously stirred tank reactor (CSTR). In these studies the added water replaced an equivalent amount of inert gas so that all other reaction conditions remained the same before, during and after water addition. A low cobalt loading of 12.4 wt% on wide-pore silica exhibited a beneficial effect on CO conversion with the addition of water up to 25 vol% of the total feed. In contrast, the addition of up to 20 vol% water to a 20 wt% Co on narrow- or wide-pore silica did not significantly alter the CO conversion. It appears that the CO conversion mainly increases when cobalt clusters are small enough to fit inside the silica pores.

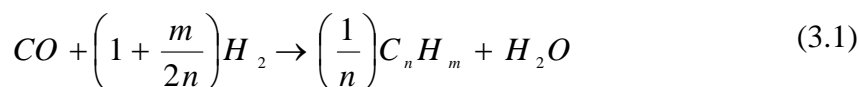
CHAPTER III

THEORY

In the previous chapter, reviews of recent research on titania-supported cobalt catalysts, titania supports mixed with other inorganic oxides, and titania supports contained promoters or modifiers for CO hydrogenation. They present knowledge and understanding of influencing parameters on the performance of Co-based catalysts for CO hydrogenation system. This chapter focuses on the fundamental theory of the Fischer-Tropsch Synthesis (FTS) which is well known as one type of carbon monoxide (CO) hydrogenation using Co-based catalysts. The chapter consists of five main sections. Basic details of Fischer-Tropsch Synthesis (FTS) are discussed in section 3.1. Cobalt properties are explained in section 3.2. Details of Co-based catalysts are described in section 3.3. Cobalt-support compound formation (Co-SCF) is discussed in section 3.4. Titanium dioxide which used as a support is detailed in section 3.5. Silicon dioxide which used as another support mixed with titanium dioxide is detailed in section 3.6. Zirconia which used as a promoter or modifier is detailed in section 3.7. Details of promoters are discussed in the last section 3.8.

3.1 Fischer-Tropsch synthesis (FTS)

Fischer-Tropsch synthesis (FTS) that discovered by Fischer and Tropsch over 80 years ago, as an alternate process, can convert the synthesis gas (H_2/CO) derived from carbon sources such as coal, peat, biomass and natural gas, into hydrocarbons and oxygenates. During the past decades, FTS has been developed continuously by many researchers, although the rise and fall in research intensity on this process has been highly related to the demands for liquid fuels and relative economics. This synthesis is basically the reductive polymerization (oligomerization) of carbon monoxide by hydrogen to form organic products containing mainly hydrocarbons and some oxygenated products in lesser amounts. The main reactions of FTS are:

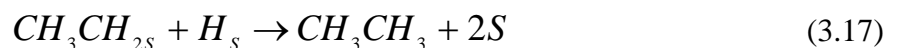
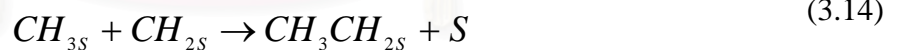


Equation (3.1) is the formation of hydrocarbons higher than C1, and the equation (3.2) is methanation. The water-gas shift reaction, which is undesirable for natural gas conversion, is shown in equation (3.3). The Boudouard reaction, which results in carbon deposition on the catalyst surface, is shown in equation (3.4).

The mechanism consists of surface steps in five categories: (1) the adsorption of reactants (H₂ and CO); (2) chain initiation; (3) chain propagation; (4) chain termination and desorption of products; (5) readsorption and secondary reaction of olefins. Depending upon the type of catalyst used, promoters, reaction conditions (pressure, temperature and H₂/CO ratios), and type of reactors, the distribution of the molecular weight of the hydrocarbon products can be noticeably varied.

Normally, catalysts used for this synthesis are group VIII metals. By nature, the hydrogenation activity increases in order of Fe < Co < Ni < Ru. Ru is the most active. Ni forms predominantly methane, while Co yields much higher ratios of paraffins to olefins and much less oxygenated products such as alcohols and aldehydes than Fe does. The reaction mechanism of FTS on Co, Fe and Ru catalysts has been reviewed by Bell (1991). A general and reasonably widely accepted mechanism for FTS on Group VIII metals from his review is shown below. This mechanism involves: (1) the adsorption and dissociation of CO (equation 3.5 and 3.6) and the dissociative adsorption of H₂ (equation 3.7) all in a quasi-equilibrium; (2) surface reactions of O and H_{atoms} to form water and of O atoms and CO to form CO₂ (equation 3.8 and 3.9); (3) reaction of adsorbed carbon and hydrogen atoms to form adsorbed CH_x species (reactions 3.10 and 3.12); (4) the hydrogenation of adsorbed methyl radicals to form methane (equation 3.13); (5) chain growth through the addition of methylene groups to methyl and ethyl radicals (equations 3.14 and 3.15);

and (6) the termination of an ethyl radical to form ethylene or hydrogenation to form ethane (equations 3.16 and 3.17).



With regards to the operating conditions, usually higher pressures will result in higher rates. There are basically three reactor types used for FTS: (1) fixed bed, (2) fluid bed, and (3) slurry bed. Because of the high exothermicity of the reaction (142 kJ mol⁻¹ of reacted carbon), all three reactor types are carefully designed for rapid

heat removal using a combination of various techniques including heat exchange, recycle, fluidized and slurry beds, and stage systems. The attributes, advantages and limitations of each of these reactors is different as summarized below.

Fixed-bed reactor: In a typical fixed bed reactor heat is removed by heat exchangers or by production steam. To facilitate temperature control while maximizing conversion and linear gas velocity, a portion of the tail gas is recycle, typically with a recycle: fresh volume ratio of about 2. Since the heat exchanger design favors lower temperatures of operation (220-250°C), predominantly higher hydrocarbons including gasoline, diesel fuel and waxes are produced. *Fluid-bed reactors:* Fluid beds are of generally two types, fixed and circulating. This reactor has better heat removal (near isothermal operation), higher reaction temperature (exit temperature of 340°C) and hence higher selectivities for lighter products, alkenes, branched products and aromatics, and higher throughput per volume of reactor relative to the fixed bed. With on-line catalyst removal and addition, process runs are much longer than for the fixed bed. Nevertheless, the fluid-bed reactor is a more complex system requiring an attrition-resistant catalyst and grater system maintenance. Moreover, process conditions and temperature must be adjusted to limit production of heavy hydrocarbons which would condense on the catalyst and defluidize the bed. *Slurry-bed reactor:* slurry-bed reactor, in which a finely divided catalyst is suspended in a heavy oil by gas bubbling up through the slurry, have been investigated fairly for FTS by Koelber, Sasol and Rheinpreussen-Koppers. This reactor type has the advantages of (1) capability of operating at low H₂:CO ratios without problems with carbon deposition, (2) very efficient heat transfer and uniform temperature, (3) high catalyst efficiency/performance, and (4) simple construction. Although some of the operating problems in using a slurry bed reactor FTS are daunting, such as high slurry viscosities, particle settling, catalyst liquid-separation and possible gas-liquid mass transport limitations. Slurry-bed reactors are better than fixed-bed reactors for FTS since they can remove heat from this exothermic synthesis, allowing better temperature control.

The current main goal in using FTS is to obtain high molecular weight, straight chain hydrocarbons. However, methane and other light hydrocarbons are always present as less desirable products from the synthesis. According to the

Anderson-Schulz-Flory (ASF) product distribution, typically 10 to 20% of products from the synthesis are usually light hydrocarbon (C_1 - C_4) these light alkanes have low boiling points and exist in the gas phase at room temperature, which is inconvenient for transportation. Many attempts have been made to minimize these byproducts and increase the yield of long chain liquid hydrocarbons by improving chain growth probability. It would be more efficient to be able to convert these less desirable products into more useful forms, rather than re-reforming them into syngas and recycling them.

3.2 Cobalt (Young 1960; Othmer, 1991)

3.2.1 General

Cobalt, a transition series metallic element having atomic number 27, is similar to silver in appearance.

Cobalt and cobalt compounds have expanded from use colorants in glasses and ground coat frits for pottery to drying agents in paints and lacquers, animal and human nutrients, electroplating materials, high temperature alloys, hard facing alloys, high speed tools, magnetic alloys, alloys used for prosthetics, and used in radiology. Cobalt is also as a catalyst for hydrocarbon refining from crude oil for the synthesis of heating fuel.

3.2.2 Physical Properties

The electronic structure of cobalt is $[Ar] 3d^7 4s^2$. At room temperature the crystalline structure of the α (or ϵ) form, is close-packed hexagonal (cph) and lattice parameters are $a = 0.2501$ nm and $c = 0.4066$ nm. Above approximately $417^\circ C$, a face-centered cubic (fcc) allotrope, the γ (or β) form, having a lattice parameter $a = 0.3544$ nm, becomes the stable crystalline form. Physical properties of cobalt are listed in Table 3.1.

The scale formed on unalloyed cobalt during exposure to air or oxygen at high temperature is double-layered. In the range of 300 to 900°C, the scale consists of a thin layer of mixed cobalt oxide, Co_3O_4 , on the outside and cobalt (II) oxide, CoO , layer next to metal. Cobalt (III) oxide, Co_2O_3 , may be formed at temperatures below 300 °C. Above 900°C, Co_3O_4 decomposes and both layers, although of different appearance, are composed of CoO only. Scales formed below 600°C and above 750°C appear to be stable to cracking on cooling, whereas those produced at 600-750°C crack and flake off the surface.

Cobalt forms numerous compounds and complexes of industrial importance. Cobalt, atomic weight 58.933, is one of the three members of the first transition series of Group 9 (VIIB). There are thirteen known isotopes, but only three are significant: ^{59}Co is the only stable and naturally occurring isotope; ^{60}Co has a half-life of 5.3 years and is a common source of γ -radioactivity; and ^{57}Co has a 270-d half-life and provides the γ -source for Mössbauer spectroscopy.

Cobalt exists in the +2 or +3 valence states for the major of its compounds and complexes. A multitude of complexes of the cobalt (III) ion exists, but few stable simple salts are known. Octahedral stereochemistries are the most common for cobalt (II) ion as well as for cobalt (III). Cobalt (II) forms numerous simple compounds and complexes, most of which are octahedral or tetrahedral in nature; cobalt (II) forms more tetrahedral complex than other transition-metal ions. Because of the small stability difference between octahedral and tetrahedral complexes of cobalt (II), both can be found in equilibrium for a number of complexes. Typically, octahedral cobalt (II) salts and complexes are pink to brownish red; most of the tetrahedral Co (II) species are blue.

Table 3.1 Physical properties of cobalt (Othmer, 1991)

Property	Value
atomic number	27
atomic weight	58.93
transformation temperature, °C	417
heat of transformation, J/g ^a	251
melting point, °C	1493
latent heat of fusion, ΔH_{fus} J/g ^a	395
boiling point, °C	3100
latent heat of vaporization at bp, ΔH_{vap} kJ/g ^a	6276
specific heat, J/(g·°C) ^a	
15-100°C	0.442
molten metal	0.560
coefficient of thermalexpansion, °C ⁻¹	
cph at room temperature	12.5
fcc at 417°C	14.2
thermal conductivity at 25 °C, W/(m·K)	69.16
thermal neutron absorption, Bohr atom	34.8
resistivity, at 20 °C ^b , 10 ⁻⁸ Ω·m	6.24
Curie temperature, °C	1121
saturation induction, 4πI _s , T ^c	1.870
permeability, μ	
initial	68
max	245
residual induction, T ^c	0.490
coercive force, A/m	708
Young's modulus, Gpac	211
Poisson's ratio	0.32

Table 3.1 Physical properties of cobalt (cont.)

Property	Value		
Hardness ^f , diamond pyramid, of %Co	99.9	99.98 ^e	
At 20 °C	225	253	
At 300 °C	141	145	
At 600 °C	62	43	
At 900 °C	22	17	
strength of 99.99 %cobalt, MPa ^g	as cast	annealed	sintered
tensile	237	588	679
tensile yield	138	193	302
compressive	841	808	
compressive yield	291	387	

^a To convert J to cal, divided by 4.184.

^b conductivity = 27.6 % of International Annealed Copper Standard.

^c To convert T to gauss, multiply by 10⁴.

^d To convert GPa to psi , multiply by 145,000.

^e Zone refined.

^f Vickers.

^g To convert MPa to psi , multiply by 145.

3.2.3 Cobalt Oxides

Cobalt has three well-known oxides:

Cobalt (II) oxide, CoO, is an olive green, cubic crystalline material. Cobalt (II) oxide is the final product formed when the carbonate or the other oxides are calcined to a sufficiently high temperature, preferably in a neutral or slightly reducing atmosphere. Pure cobalt (II) oxide is a difficult substance to prepare, since it readily takes up oxygen even at room temperature to re-form a higher oxide. Above about 850°C, cobalt (II) oxide form is the stable oxide. The product of commerce is usually dark gray and contains 75-78 wt % cobalt. Cobalt (II) oxide is soluble in

water, ammonia solution, and organic solvents, but dissolves in strong mineral acids. It is used in glass decorating and coloring and is a precursor for the production of cobalt chemical.

Cobalt (III) oxide, Co_2O_3 , is formed when cobalt compounds are heated at a low temperature in the presence of an excess of air. Some authorities told that cobalt (III) oxide exists only in the hydrate form. The lower hydrate may be made as a black powder by oxidizing neutral cobalt solutions with substances like sodium hypochlorite. Co_2O_3 or $\text{Co}_2\text{O}_3 \cdot \text{H}_2\text{O}$ is completely converted to Co_3O_4 at temperatures above 265°C . Co_3O_4 will absorb oxygen in a sufficient quantity to correspond to the higher oxide Co_2O_3 .

Cobalt oxide, Co_3O_4 , is formed when cobalt compounds, such as the carbonate or the hydrated sesquioxide, are heated in air at temperatures above approximately 265°C and not exceeding 800°C .

3.3 Co-based Catalysts

Supported cobalt (CO) catalysts are the preferred catalysts for the synthesis of heavy hydrocarbons from natural gas based syngas (CO and H_2) because of their high Fischer-Tropsch (FT) activity, high selectivity for linear hydrocarbons and low activity for the water-gas shift reaction. It is known that reduced cobalt metal, rather than its oxides or carbides, is the most active phase for CO hydrogenation in such catalysts. Investigations have been done to determine the nature of cobalt species on various supports such as alumina, silica, titania, magnesia, carbon, and zeolites. The influence of various types of cobalt precursors used was also investigated. It was found that the used of organic precursors such as CO (III) acetyl acetate resulting in an increase of CO conversion compared to that of cobalt nitrate.

3.4 Cobalt-Support Compound Formation (Co-SCF)

Compound formation between cobalt metal and the support can occur under pretreatment and/or reaction conditions, leading to catalyst deactivation. The compound formation of cobalt metal with support materials, however, is difficult to

predict because of the lack of sufficient thermodynamic data. Co-support compound formation can be detected evidentially.

3.4.1 Co-Aluminate Formation

Interaction of cobalt with its alumina support has been observed by many authors using various techniques including TPR, XRD, EXAFS, and XPS (ESCA). The migration of cobalt ions into alumina lattice sites of octahedral or tetrahedral symmetry is limited to the first few layers of the support under normal calcination conditions. The reaction of Co with $\gamma\text{-Al}_2\text{O}_3$ can form a surface spinel in Co/ $\gamma\text{-Al}_2\text{O}_3$ catalysts. The surface spinel structure can not be observed by X-ray diffraction because it does not have long range, three dimensional order. It has been suggested that cobalt ions occupying surface octahedral site of $\gamma\text{-Al}_2\text{O}_3$ are reducible while cobalt ions occupying tetrahedral sites are non-reducible, at least at temperatures $\leq 900^\circ\text{C}$. At lower calcination temperatures, filling of the octahedral sites is more favorable. Filling of the tetrahedral site of $\gamma\text{-Al}_2\text{O}_3$ may be enhanced by an increase in calcination temperature.

3.4.2 Co-Silicate Formation

The formation of cobalt silicates on Co/SiO₂ under hydrothermal conditions has been extensively studied by Kogelbauer *et al.* (1995). Hydrothermal treatment at 200°C led to a catalyst with lower reducibility due to the formation of both reducible and non-reducible (at temperatures $\leq 900^\circ\text{C}$) cobalt silicates. It was found that hydrothermal treatment of the reduced catalyst or hydrothermal treatment of the calcination catalyst in the presence of hydrogen produces cobalt silicates, while hydrothermal treatment of the calcined catalyst in air does not result in their formation. Hydrothermal treatment of the calcined catalyst in inert gas also has little effect.

3.4.3 Co-Titanate Formation

Cobalt-support compound formation in titania supported Cobalt catalysts

was investigated by Jongsomjit *et al.* (2003). It is known that the formation of Cobalt and oxide supports during standard reduction is facilitated by the presence of water vapor and resulted in a less active catalyst. The reduction peaks of cobalt oxides during TPR were shifted to higher temperature as the amount of water vapor increased suggesting an increase in the formation of more difficult to reduced Co-support species. However, the Co-SCF in titania support is in highly dispersed form that could not be detected by XRD due probably to the migration of cobalt into the titania matrix. The Co- SCF in titania is non-reducible at temperatures $< 800^{\circ}\text{C}$ during TPR.

3.5 Titanium dioxide (Othmer, 1991; Fujishima *et al.*, 1999)

3.5.1 Physical and Chemical Properties

Titanium dioxide occurs in nature in three crystalline forms: anatase which tends to be more stable at low temperature, brookite, which is usually found only in minerals and rutile, which tends to be more stable at higher temperatures and thus is sometimes found in igneous rock. These crystals are essentially pure titanium dioxide but contain small amounts of impurities, such as iron, chromium or vanadium, which darken them. Crystallographic information on the different forms of titanium dioxide is summarized in Table 3.2.

Although anatase and rutile are both tetragonal, they are not isomorphous (Figure 3.1). Anatase occurs usually in near-regular octahedral, and rutile forms slender prismatic crystal, which are frequently twinned. Rutile is the thermally stable form and is one of the two most important ores of titanium.

The three allotropic forms of titanium (IV) oxide have been prepared artificially but only rutile, the thermally stable form, has been obtained in the form of transparent large single crystal. The transformation from anatase to rutile is accompanied by the evolution of ca. 12.6 kJ/mol (3.01 kcal/mol), but the rate of transformation is greatly affected by temperature and by the presence of other substance which may either catalyze or inhibit the reaction. The lowest temperature at which conversion of anatase to rutile takes place at a measurable rate is ca. 700°C , but

this is not a transition temperature. The change is not reversible; ΔG for the change from anatase to rutile is always negative.

Table 3.2 Crystallographic information on the different forms of titanium dioxide (Othmer, 1991)

Properties	Anatase	Brookite	Rutile
Crystal structure	Tetragonal	Orthorhombic	Tetragonal
Optical	Uniaxial, negative	Biaxial, positive	Uniaxial, negative
Density, g/cm ³	3.9	4.0	4.23
Hardness, Mohs scale	5 ^{1/2} – 6	5 ^{1/2} – 6	7 – 7 ^{1/2}
Unit cell	D _{4d} ¹⁹ .4TiO ₂	D _{2h} ¹⁵ .8TiO ₂	D _{4h} ¹² .3TiO ₂
Dimension, nm			
a	0.3758	0.9166	0.4584
b	-	0.5436	-
c	0.9514	0.5135	2.953

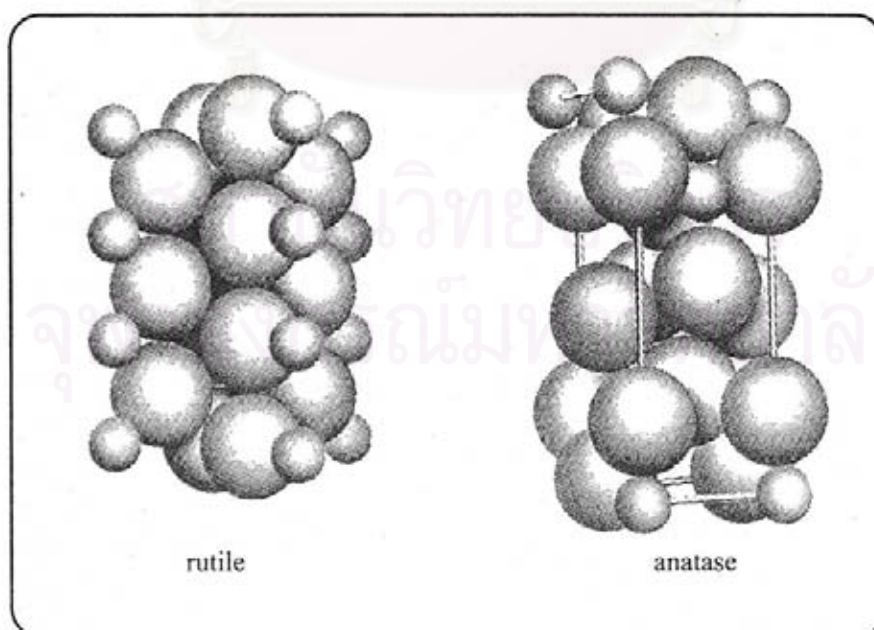


Figure 3.1 Crystal structure of TiO₂. (Fujishima *et al.*, 1999)

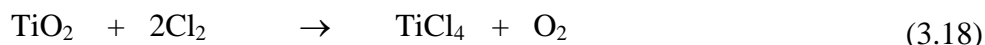
Brookite has been produced by heating amorphous titanium (IV) oxide, prepared from an alkyl titanates of sodium titanate with sodium or potassium hydroxide in an autoclave at 200 to 600°C for several days. The important commercial forms of titanium (IV) oxide are anatase and rutile, and these can readily be distinguished by X-ray diffraction spectrometry.

Since both anatase and rutile are tetragonal, they are both anisotropic, and their physical properties, e.g. refractive index, vary according to the direction relative to the crystal axes. In most applications of these substances, the distinction between crystallographic direction is lost because of the random orientation of large numbers of small particles, and it is mean value of the property that is significant.

Measurement of physical properties, in which the crystallographic directions are taken into account, may be made of both natural and synthetic rutile, natural anatase crystals, and natural brookite crystals. Measurements of the refractive index of titanium (IV) oxide must be made by using a crystal that is suitably orientated with respect to the crystallographic axis as a prism in a spectrometer. Crystals of suitable size of all three modifications occur naturally and have been studied. However, rutile is the only form that can be obtained in large artificial crystals from melts. The refractive index of rutile is 2.75. The dielectric constant of rutile varies with direction in the crystal and with any variation from the stoichiometric formula, TiO_2 ; an average value for rutile in powder form is 114. The dielectric constant of anatase powder is 48.

Titanium (IV) oxide is thermally stable (mp 1855°C) and very resistant to chemical attack. When it is heated strongly under vacuum, there is a slight loss of oxygen corresponding to a change in composition to $\text{TiO}_{1.97}$. The product is dark blue but reverts to the original white color when it is heated in air.

Hydrogen and carbon monoxide reduce it only partially at high temperatures, yielding lower oxides or mixtures of carbide and lower oxides. At ca. 2000°C and under vacuum, carbon reduces it to titanium carbide. Reduction by metal, e.g., Na, K, Ca, and Mg, is not complete. Chlorination is only possible if a reducing agent is present; the position of equilibrium in the system is



3.6 Silicon dioxide

3.6.1 Occurrence and Classification

Silicon dioxide or silica occurs almost everywhere on earth. It is one of the most important and abundant oxides on earth, constituting about 60% weight of the earth's crust as silica itself or in combination with other metal oxides in silicates. It commonly is found as sand in the vast ocean and river shores, their beds, deserts, rocks, and minerals.

Silicon dioxide exists in several structural forms: polymorphic crystalline silica, synthetic quartz crystals, amorphous silica, and vitreous silica. This classification is not complete as there are other forms of silica synthesized for specialized application. Various forms of silica are mentioned briefly below.

Crystalline Silica: Three principal polymorphic forms exist at atmospheric pressure. These are quartz, tridymite, and cristobalite. *Quartz* is stable below 870°C. It transforms to tridymite format about 870°C. Tridymite is stable up to 1,470°C and transforms to cristobalite at 1,470°C. High cristobalite melts around 1,723°C. Other than these three polymorphs, there are also three high pressure phases of crystalline silica: keatite, coesite, and stishovite. Quartz occurs in granite, sand, crystals, and sandstone. Quartz also has several crystalline varieties such as purple amethyst, colorless rock crystal, and yellow citrine. Flint, agate, and chert, etc. are other forms of quartz. Quartz is an excellent insulator. It does not break under temperature changes because of its low coefficient of expansion. Fused quartz transmits ultraviolet light. Quartz exhibits two slightly varying atomic arrangements. One is the beta or high quartz that consists of linked tetrahedral-forming helixes in which the hexagonal unit cell contains three SiO₂ units and in which Si-O bond distance is 1.62Å. The density of high quartz at 600°C is 2.53g/cm³. The other form, know as the low, or alpha quartz, has a density of 2.65g/cm³ at 0°C. Here the Si-O bond distance differs slightly, measured as 1.567 and 1.617Å. Low quartz is the most common form of silica. Thermal inversion of quartz occurs around 573°C in which

one form converts to the other form by slight displacement of atoms in their structural arrangements. The presence of impurities can affect the inversion temperature. Quartz also is optically active; individual crystals are either levorotatory or dextrorotatory. *Tridymite* is found in volcanic rocks and has been identified in many stony meteorites. Tridymite also exists in various forms. It has six different modifications that undergo thermal inversions from one to another. Its density at 200°C is about 2.22g/cm³. The hexagonal unit cell contains four SiO₂ units. The Si-O bond distance is 1.52Å. *Cristobalite* is the third crystalline silica form that has three-layer sequences of SiO₄. The oxygen atoms of the tetrahedral SiO₄ have cubic close-packed structure. Cristobalite is found in some volcanic rocks.

Amorphous silica: The term amorphous silica refers to aggregate of small particles with high specific surface area. They lack crystal structure and do not form a sharp x-ray diffraction pattern. They are known in several forms such as colloidal silica, precipitated silica, silica gels, and fumed silica. The surface of such amorphous silica may contain silanol (SiOH) groups or can be anhydrous. Amorphous silica in nature may originate from aquatic organisms, secreted as amorphous solid in the form of shells, plates, or skeletons. Amorphous silica also is found in volcanic ash or in precipitated material from the hot supersaturated waters of hot springs. Amorphous silica can be hydrated up to about 14% or made anhydrous. They usually contain siloxane (-Si-C-Si-) or silanol (-Si-O-H) bonds. At the surface there may be silane (-Si-H) or organic silicon (-Si-O-R or -Si-O-H) bonds. Hydrated amorphous silica is made by polymerization of silicic acid in water in slightly acidic solution at a low temperature. At ambient temperature, such hydrated silica is stable and does not lose water below 60°C. Amorphous silica is broadly categorized into vitreous silica or glass, silica M and microamorphous silica. Vitreous silica is made by fusing quartz. Silica M is prepared by irradiation amorphous or crystalline silica with high speed neutrons. It is a dense form of amorphous silica and is thermally unstable. When heated at 930°C for several hours, silica M converts to quartz. Microamorphous silica is made of particles with diameters less than 1 µm. They have very high surface areas, usually greater than 3m²/g. These microamorphous silica are an aggregation of colloidal ultimate particles that broadly include sols, gels powder, and porous glass. An important class of microamorphous silica constitutes what is known as microparticulate silica. These are the silicas precipitated from aqueous solution such

as sol and gel or that are formed at higher temperatures by condensation from vapor phase, such as pyrogenic silica. Pyrogenic silica is made by vaporizing sand at 2,000°C and then cooling the vapors, or oxidizing silicon tetrachloride vapors at high temperatures. It has a SiO₂ content above 99.7% and density of 2.16g/cm³. The ultimate particle size is in the range 1 to 100 nm. When heated at 105°C, the weight loss is between 0.5 to 2.5%. There is no additional loss in the weight when the material is further heated at 1,200°C. Silica sol is a stable dispersion of fine particles, while gel has a three dimensional continuous structure. SiO₂ content in sol range between 10-50%, while that in dry silica gels is between 96.5 to 99.6%. Density of dry gels is 2.22g/cm³ and sols 2.20 to 2.30g/cm³. Weight loss in sols at 105°C is between 50-80%. Silica gel is a rigid, continuous three-dimensional network of spherical colloidal particles. If the pores are filled with water it is known as hydrogel. The surface of silica gel consists of silanol (Si-O-H) groups or siloxane (Si-O-Si) groups. It also may have an organic surface. Silica gels are precipitated from water. When dried below 150°C, silanol surfaces are developed. When heated at 300 to 1000°C, the silanol surfaces dehydrate to form siloxane surface. Silica gels are made by many ways. One method involves mixing sodium silicate with a strong mineral acid. This final gel properties, such as, density, hardness, surface area, and pore volume depend on silica concentration, temperature, pH, gellingtime, and rate of drying. Hydrolysis of silicon tetrachloride, ethyl silicate and other silicon compounds also produces gels. These gels are dense, having very small pore size, and are of high purity.

Vitreous Silica: Vitreous silica is a glass form of silica composed of SiO₂. It may be transparent, translucent, or opaque. It has a number of abnormal and anomalous properties in thermal expansion, viscosity, bulk density, compressibility, and elasticity. These properties depend on thermal history and preparation method. Vitreous silica exhibits high resistance to chemical attack. At ambient temperature, it is not attacked by any chemical except hydrofluoric acid. Transparent vitreous silica is made by electric melting of natural quartz minerals such as sand in vacuum. It also may be made by fusing quartz in flame or by vapor phase hydrolysis or oxidation of pure silicon compounds by heating electrically or using a flame or plasma. Translucent form is made by fusion of high purity quartz sand crystals.

3.7 Zirconia

3.7.1 Physical and Chemical Properties

Zirconia exhibits three polymorphs, the monoclinic, tetragonal, and cubic phases. Figure 3.2 shows the typical systems: cubic, tetragonal and monoclinic ones. Crystal structure of cubic, tetragonal and monoclinic zirconia are shown in Figure 3.3 The monoclinic is stable up to $\sim 1170^{\circ}\text{C}$, at which temperature it transforms into the tetragonal phase, which is stable up to 2370°C (Cormak and Parker, 1990). The stabilization of the tetragonal phase below 1100°C is important in the use of zirconia as a catalyst in some reaction. Above 2370°C , the cubic phase is stable and it exists up to the melting point of 2680°C . Due to the martensitic nature of the transformations, neither the high temperature tetragonal nor cubic phase can be quenched in rapid cooling to room temperature. However, at low temperature, a metastable tetragonal zirconia phase is usually observed when zirconia is prepared by certain methods, for example by precipitation from aqueous salt solution or by thermal decomposition of zirconium salts. This is not the expected behavior according to the phase diagram of zirconia (i.e., monoclinic phase is the stable phase at low temperatures). The presence of the tetragonal phase at low temperatures can be attributed to several factors such as chemical effects, (the presence of anionic impurities) (Srinivasan et al., 1990 and Tani et al., 1982) structural similarities between the tetragonal phase and the precursor amorphous phase (Osendi et al., 1985; Tani, 1982 and Livage, 1968) as well as particle size effects based on the lower surface energy in the tetragonal phase compared to the monoclinic phase (Garvie, 1978; Osendi et al., 1985 and Tani 1982). The transformation of the metastable tetragonal form into the monoclinic form is generally complete by $650\text{-}700^{\circ}\text{C}$.

Crystal system	Unit cell shape
Cubic	$a = b = c, \alpha = \beta = \gamma = 90^{\circ}$
Tetragonal	$a = b \neq c, \alpha = \beta = \gamma = 90^{\circ}$
Monoclinic	$a \neq b \neq c, \alpha = \gamma = 90^{\circ}, \beta \neq 90^{\circ}$

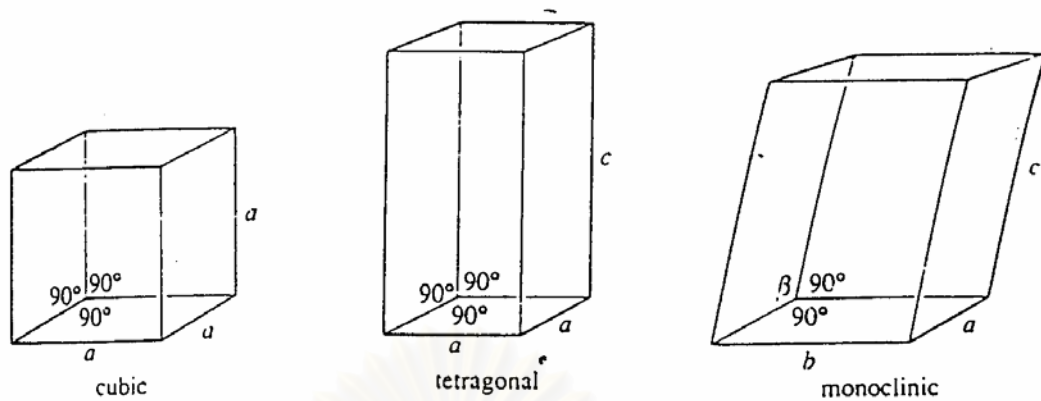


Figure 3.2 The unit cells of the crystal systems. (West, 1997)

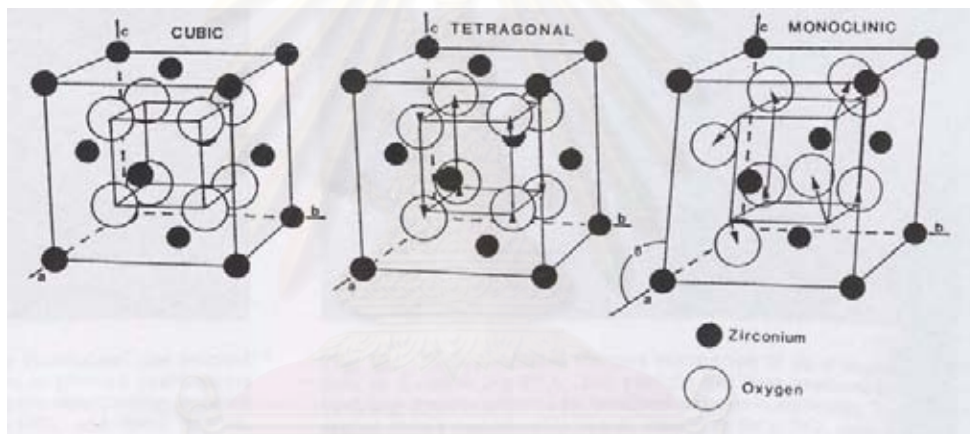


Figure 3.3 Crystal structure of cubic, tetragonal and monoclinic zirconia. (Heuer, 1987)

3.8 Promoters (Farrauto and Bartholomew, 1997; Jongsomjit *et al.*, 2001).

There are two kinds of promoters such as textural and chemical promoters. Textural promoters are used to facilitate the dispersion of metal phase during preparation and/or reaction conditions. Chemical promoters are used to enhance the activity and/or selectivity of catalysts. Generally, noble, alkali and alkaline earth metals are considered to be chemical promoters, which play important roles on catalyst performance to date.

The effects of promoters such as Ru, Re, Rh, Pt and Pd on Co catalysts were studied. They reported that these metal promoters can increase the reducibility and dispersion of Co, preserve the activity by preventing the formation of coke, exhibit cluster and ligand effect and act as a source for hydrogen spillover.



สถาบันวิทยบริการ
จุฬาลงกรณ์มหาวิทยาลัย

CHAPTER IV

EXPERIMENTAL

This chapter consists of experimental systems and procedures used in this work which is divided into three parts including catalyst preparation, catalyst characterization and reaction study in CO hydrogenation.

The first part (section 4.1) is described catalyst preparation such as titania supports consisting of various rutile/anatase phase ratios, titania supports contained promoters or modifiers, titania supports mixed with other inorganic oxides, titania supported Co catalyst, reference materials (Co_3O_4), and catalyst nomenclature. The second part (section 4.2) is explained catalyst characterization by various techniques include of AAS, XRD, BET surface area, TPR, hydrogen chemisorption, Electron microscopy, TEM and Raman spectroscopy. Finally, the last part (section 4.3) is illustrated catalyst activity measurement in CO hydrogenation.

4.1 Catalyst preparation

4.1.1 Chemicals

The details of chemicals used in this experiment are shown in Table 4.1.

Table 4.1 Chemicals used in the preparation of catalysts.

Chemical	Grade	Supplier
Titania (TiO_2) support	Japan	Department of Material
JRC-TIO-1 (pure anatase)	Reference	Science, Shimane University
JRC-TIO-4 (81% anatase)	Catalyst	University Catalysts and Chemicals Ind. Co., Ltd.
Silica gel (Cariact P-10)	Reference	Fuji Silasia Chemical Ltd.
Zirconia (IV) propoxide, 70 wt.% solution in 1-propanol	Analytical	Aldrich
Cobalt (II) nitrate hexahydrate	Analytical	Aldrich

4.1.2 Preparation of various ratios of rutile:anatase in TiO₂ support

The various ratios of rutile:anatase in titania support will be prepared by calcination of TiO₂ supports: JRC-TIO-1 (pure anatase) in air at temperatures between 800-1000°C at the rate of 10 °C/min and held at that temperature for 4 hours. The ratios of rutile:anatase will be determined by XRD according to the method described by Jung et al., 1999 as follows:

$$\% \text{ Rutile} = \frac{1}{[(A/R)0.884 + 1]} \times 100 \quad (4.1)$$

Where, A and R are the peak area for major anatase ($2\theta = 25^\circ$) and rutile phase ($2\theta = 28^\circ$), respectively.

4.1.3 Preparation of Zr-modified TiO₂ support

A Zr-modified TiO₂ supports will be prepared by impregnation method at Zr/TiO₂ ratios of 0.5/99.5, 1/99, and 5/95 weight ratios. The support will be dried at 110 °C for 12 hours and calcined in air at 500 °C for 4 hours. Details of calculation of preparation are given in Appendix A.

4.1.4 Preparation of TiO₂-SiO₂ mixed oxide support

Mixed TiO₂-SiO₂ supported will be prepared by the solution mixing. The desired amounts of TiO₂-SiO₂ will be impregnated by physical force and were stirred in toluene with a magnetic stirrer. The mixture will be separated and washed 5 times with 20 ml of toluene, followed by drying in vacuum at room temperature to obtain the catalyst support precursor mixed TiO₂-SiO₂ oxides.

4.1.5 Cobalt loading

The Co/TiO₂ (20 wt% of Co) catalysts will be prepared by the incipient wetness impregnation of the supports with aqueous solution of cobalt nitrate. The catalyst will be dried at 110 °C for 12 hours and calcined in air at 500 °C for 4 hours. Details of calculation of preparation are given in Appendix A.

4.1.6 Preparation of reference materials

Co_3O_4 were calcined in air at 500°C for 4 hours.

4.1.7 Catalyst Nomenclature

The nomenclature used for the catalyst samples in this study is following:

- **Rn:** titania support containing **n%** of rutile phase (R)
- **Co/Rn:** titania support containing **n%** of rutile phase (R)-supported cobalt
- **x/y:** TiO_2 - SiO_2 mixed oxide support containing **x%** of titania and **y%** of silica
- **Co_x/y:** TiO_2 - SiO_2 mixed oxide support containing **x%** of titania and **y%** of silica-supported cobalt
- **RnZm:** Zr-modified TiO_2 support containing **n%** of rutile phase (R) of titania and **m%** of zirconia
- **Co/RnZm:** Zr-modified TiO_2 support containing **n%** of rutile phase (R) of titania and **m%** of zirconia-supported cobalt

4.2 Catalyst characterization

Various characterization techniques were used in this studied in order to clarify the catalyst structure and morphology, surface composition of various titania-supported cobalt catalyst.

4.2.1 Atomic absorption spectroscopy (AAS)

AAS was performed to determine the composition of elements in the bulk of catalysts. The composition content of catalysts were collect using Varian, Spectra A8000 at the Department of Science Service Ministry of Science Technology and Environment.

4.2.2 X-ray diffraction (XRD)

The X-ray diffraction (XRD) patterns of powder will be performed using a X-ray diffractometer SIEMENS D5000 connected with a computer with Diffract ZT version 3.3 program for fully control of the XRD analyzer. The experiments will be carried out by using Ni-filtered CuK_α radiation. Scans were performed over the 2θ ranges from 10° to 80° . The crystallite size is estimated from line broadening according to the Scherrer equation and $\alpha\text{-Al}_2\text{O}_3$ was used as standard.

4.2.3 N_2 physisorption (BET surface area)

BET apparatus for the single point method

The reaction apparatus of BET surface area measurement consisted of two feed lines for helium and nitrogen. The flow rate of the gas is adjusted by means of fine-metering valve on the gas chromatograph. The sample cell is made from pyrex glass.

The mixture gases of helium and nitrogen flowed through the system at the nitrogen relative of 0.3. The catalyst sample (ca. 0.3 to 0.5 g) will be placed in the

sample cell, which will be then heated up to 160 °C and held at this temperature for 2 h. After the catalyst sample is cooled down to room temperature, nitrogen uptakes will be measured as follows:

Step (1) Adsorption step: The sample that set in the sample cell will be dipped into liquid nitrogen. Nitrogen gas that flowed through the system will be adsorbed on the surface of the sample until equilibrium is reached.

Step (2) Desorption step: The sample cell with nitrogen gas-adsorption catalyst sample will be dipped into the water at room temperature. The adsorbed nitrogen gas will be desorbed from the surface of the sample. This step will be completed when the indicator line is in the position of base line.

Step (3) Calibration step: 1 ml of nitrogen gas at atmospheric pressure will be injected through the calibration port of the gas chromatograph and the area will be measured. The area below curve will be considered as a calibration peak.

Calculation of BET surface area of the catalyst samples are given in Appendix B.

4.2.4 Temperature programmed reduction (TPR)

TPR was used to determine the reducibility of catalysts. The catalyst sample 50 mg used in the operation and temperature ramping from 35°C to 800°C at 10°C/min. The carrier gas is 5 %H₂ in Ar. During reduction, a cold trap will be placed to before the detector to remove water produced. A thermal conductivity detector (TCD) was measure the amount of hydrogen consumption. The operating condition of the TCD is shown in Table 4.2. The calibration of hydrogen consumption was used cobalt oxide (Co₃O₄) at the same condition. Details of calculation for reducibility of the catalyst samples are given in Appendix C.

Table 4.2 Operating condition of the thermal conductivity detector for TPR.

Model	GOW-MAC
Detector type	TCD
Carrier gas	5 %H ₂ in Ar
Carrier gas flow rate (ml/min)	30
Detector temperature (°C)	80
Detector current (mA)	80

4.2.5 Hydrogen chemisorption

Static H₂ chemisorption at 100°C on the reduced catalysts (re-reduced at 350°C) was used to determine the number of reduce surface cobalt metal atoms and percentage overall cobalt dispersion. H₂ chemisorption was carried out following the procedure described by Reuel and Bartholomew (1984) using a Micromeritics Pulse Chemisorb 2700 instrument at the Analysis Center of Department of Chemical Engineering, Faculty of Engineering, Chulalongkorn University. Prior to chemisorption, the catalysts were reduced at 350°C for 10 hours. Details of calculation of the total hydrogen chemisorption and dispersion are given in Appendix D.

4.2.6 Electron microscopy

Scanning electron microscopy (SEM) and Energy dispersive X-ray spectroscopy (EDX) was used to determine the catalyst granule morphology and elemental distribution of the catalyst particles using a JEOL JSM-35CF scanning electron microscope. The SEM was operated using the back scattering electron (BSE) mode at 20 kV. After the SEM micrographs were taken, EDX was performed to determine the elemental concentration distribution on the catalyst granules using Link Isis 300 software at the Scientific and Technological Research Equipment Centre, Chulalongkorn University (STREC).

4.2.7 Transmission Electron Microscope (TEM)

The cobalt oxide particle size and distribution of cobalt on titania support will be observed using JEOL-JEM 200CX transmission electron microscope operated at 100 kv at National Metal and Materials Technology Center (MTEC), Klong Luang, Pathumthani.

4.2.8 Raman spectroscopy

Raman spectroscopy was used to determine the surface composition of catalyst samples. The Raman spectra of the samples were corrected by projecting a continuous wave laser of argon ion (Ar⁺), 514.5 nm through the samples. A scanning range between 200 and 1000 cm⁻¹. The data were analyzed using Raman microscope (Renishaw Raman Microscope System 2000) which detector is CCD chip at National Metal and Materials Technology Center (MTEC), Klong Luang, Pathumthani.

4.3 Reaction study in CO hydrogenation

4.3.1 Material

The reactant gas used for the reaction study was the carbon monoxide in hydrogen feed stream as supplied by Thai Industrial Gas Limited (TIG). The gas mixture contained 9.73 vol % CO in H₂. The total flow rate was 30 ml/min with the H₂/CO ratio of 10/1. Ultra high purity hydrogen and high purity argon manufactured by Thai Industrial Gas Limited (TIG) were used for reduction and balanced flow rate

4.3.2 Apparatus

Flow diagram of CO hydrogenation system is shown in Figure 4.1. The system consists of a reactor, an automatic temperature controller, an electrical furnace and a gas controlling system.

4.3.2.1 Reactor

The reactor was made from a stainless steel tube (O.D. 3/8"). Two sampling points were provided above and below the catalyst bed. Catalyst was placed between two quartz wool layers.

4.3.2.2 Automation Temperature Controller

This unit consisted of a magnetic switch connected to a variable voltage transformer and a solid state relay temperature controller model no. SS2425DZ connected to a thermocouple. Reactor temperature was measured at the bottom of the catalyst bed in the reactor. The temperature control set point is adjustable within the range of 0-800°C at the maximum voltage output of 220 volt.

4.3.2.3 Electrical Furnace

The furnace supplied heat to the reactor for CO hydrogenation. The reactor could be operated from temperature up to 800°C at the maximum voltage of 220 volt.

4.3.2.4 Gas Controlling System

Reactant for the system was each equipped with a pressure regulator and an on-off valve and the gas flow rates were adjusted by using metering valves.

4.3.2.5 Gas Chromatograph

The composition of hydrocarbons in the product stream was analyzed by a Shimadzu GC-14B (VZ-10) gas chromatograph equipped with a flame ionization detector. A Shimadzu GC-8A (molecular sieve 5A) gas chromatograph equipped with a thermal conductivity detector was used to analyze CO and H₂ in the feed and product streams. The operating conditions for each instrument are shown in the Table 4.3.

Table 4.3 Operating condition for gas chromatograph

Gas Chromatograph	SHIMADZU GC-8A	SHIMADZU GC-14B
Detector	TCD	FID
Column	Molecular sieve 5A	VZ10
– Column material	SUS	-
– Length	2 m	-
– Outer diameter	4 mm	-
– Inner diameter	3 mm	-
– Mesh range	60/80	60/80
– Maximum temperature	350°C	80°C
Carrier gas	He (99.999%)	N ₂ (99.999%)
Carrier gas flow (ml/min)	30 ml./min	30 ml./min
Column temperature		
- initial (°C)	60	70
- final (°C)	60	70
Injector temperature (°C)	100	100
Detector temperature (°C)	100	150
Current (mA)	80	-
Analysed gas	Ar, CO, H ₂	Hydrocarbon C ₁ -C ₄

4.3.3 Procedures

CO hydrogenation was performed using 0.2 g of catalyst was packed in the middle of the stainless steel microreactor, which located in the electrical furnace. The total flow rate was 30 ml/min with the H₂/CO ratio of 10/1. The catalyst sample was re-reduced *in situ* in flowing H₂ at 350°C for 10 h prior to CO hydrogenation. CO hydrogenation was carried out at 220°C and 1 atm total pressure. The product streams were analyzed by gas chromatography (GC). In all cases, steady-state was reached within 5 h.

The effluent gases were sampled to analyse the concentration of hydrocarbon (C1-C4) using GC-14B equipped with a VZ10 column, whereas carbon monoxide concentration was analyzed by GC-8A equipped with a Molecular sieve 5A column. The example of chromatogram of catalyst sample from GC-8A and GC-14B and the calibration curve of reactant (CO) and products (light hydrocarbon such as methane (CH₄), ethane (C₂H₆), propane (C₃H₈), etc.) are shown in Appendix E. Details of the calculation of the catalytic activity to convert carbon monoxide, reaction rate and the selectivity towards hydrocarbon (C1-C4) are given in Appendix F.



สถาบันวิทยบริการ
จุฬาลงกรณ์มหาวิทยาลัย

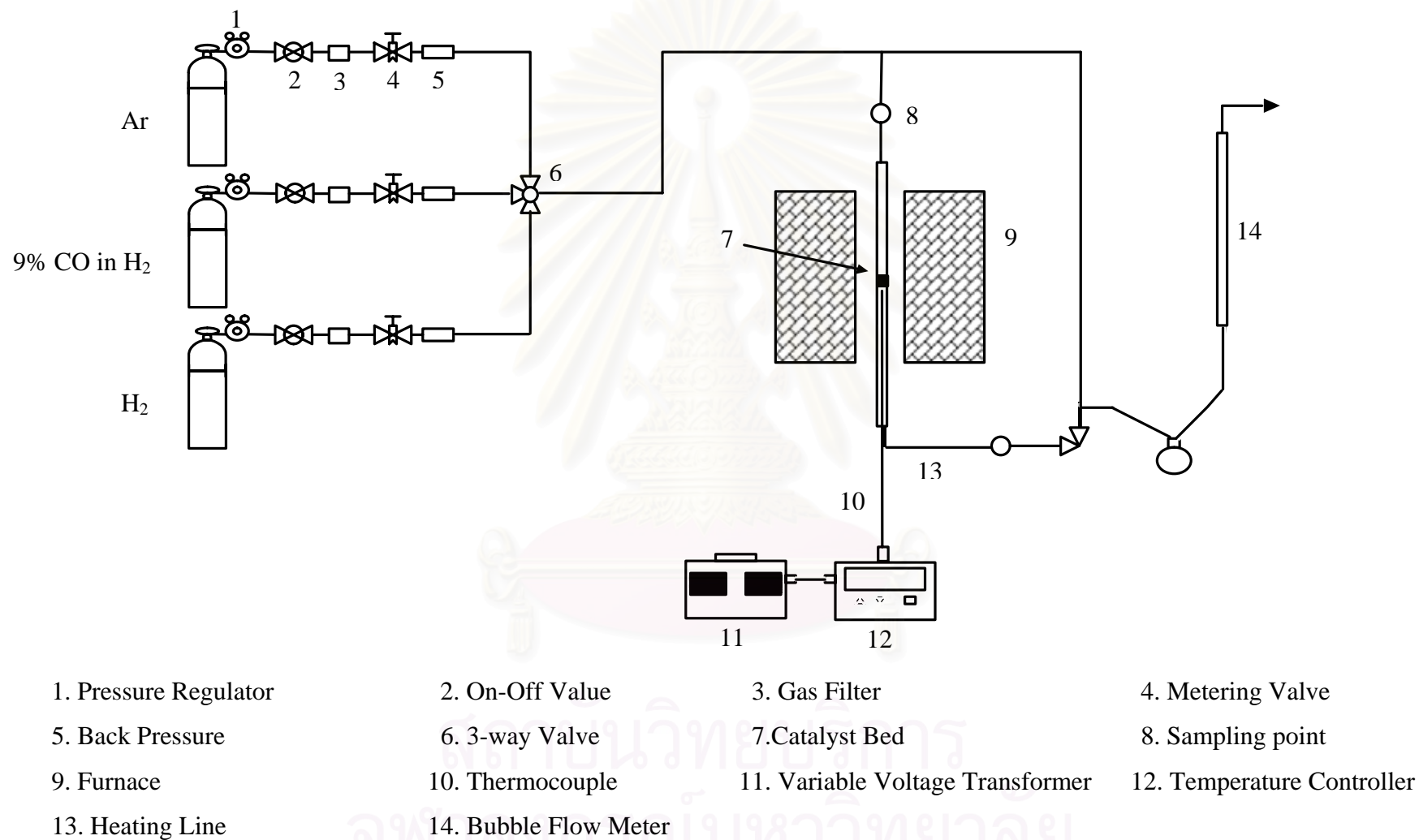
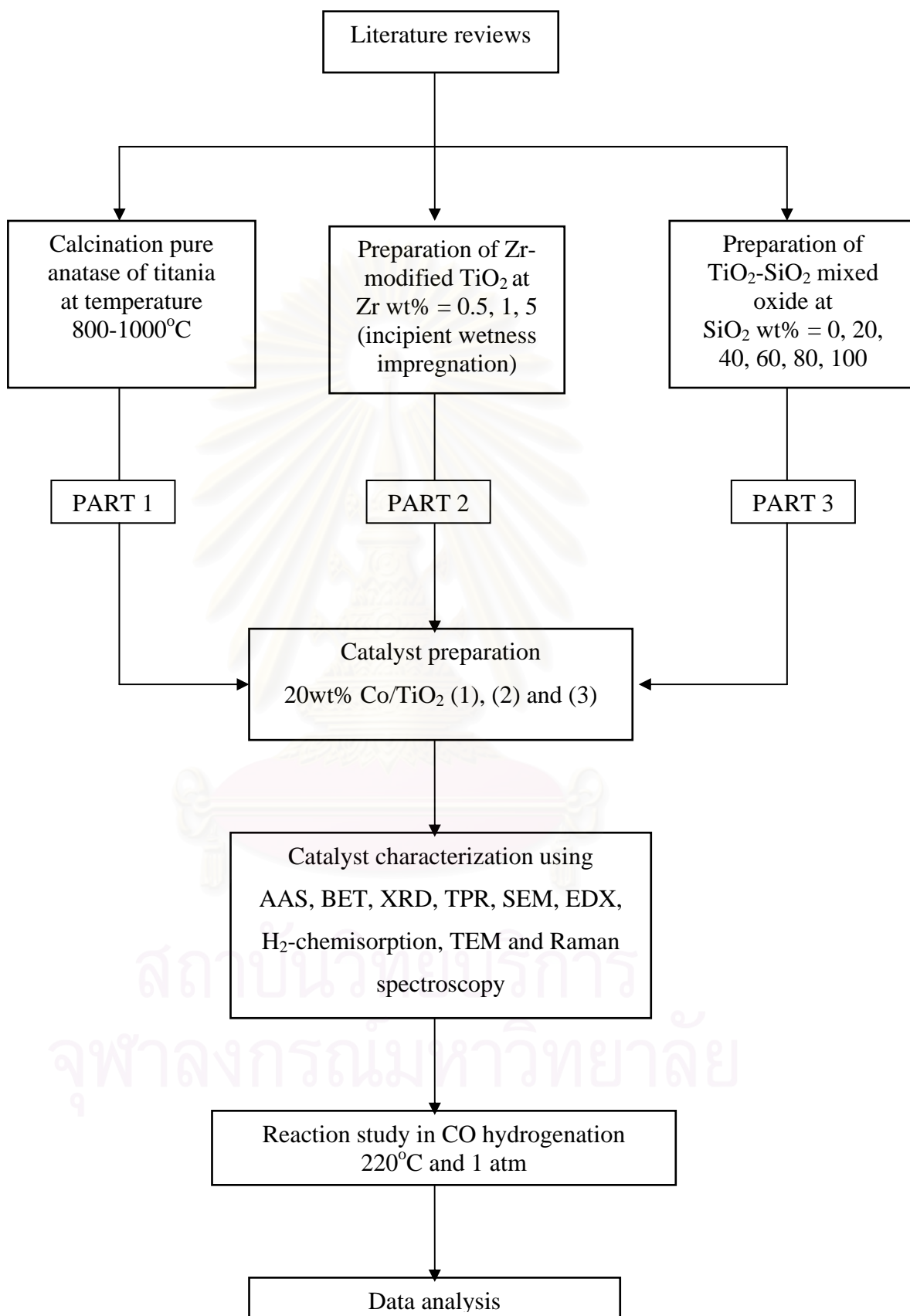


Figure 4.1 Flow diagram of CO hydrogenation system

RESEARCH METHODOLOGY

CHAPTER V

RESULTS AND DISCUSSION

The results and discussion in this chapter are divided into three sections. Section 5.1 is described characteristics and catalytic properties of Co/TiO₂ for various rutile:anatase ratios. Section 5.2 is explained effect of zirconia-modified titania consisting of different phases on catalytic properties of Co/TiO₂ catalysts. A catalytic behaviors of mixed TiO₂-SiO₂-supported cobalt Fischer-Tropsch catalysts for CO hydrogenation is illustrated in section 5.3.

5.1 Results

5.1.1 Various ratios of rutile to anatase phase of titania-supported Co catalysts

Titania itself has different crystalline phases such as anatase, brookite and rutile phase. As mentioned, in general titania used contains mainly two phases; anatase and rutile phases. Phase transformation of titania depends on the preparation of titania such as sol-gel or solvothermal methods and also calcination temperatures. The differences in compositions of crystalline phases could result in changes on physical and chemical properties of titania, then consequently for the dispersion of cobalt. In order to give a better understanding of those, different characterization techniques were used to investigate the cobalt dispersion on titania consisting various ratios of rutile:anatase.

5.1.1.1 Crystalline phases of titania

After calcination of the pure anatase titania under calcination temperatures ranging between 800 and 1000°C for 4 h, the amounts of rutile phase formed during calcination depended on the temperature used. The high space velocity of the air flow at 16,000 h⁻¹ was applied during the calcination process in order to minimize the rapid sintering due to the phase transformation of titania. It was found

that after calcination of the pure anatase sample, the amounts of rutile phase obtained ranged between 3 and 99%. The titania supports containing rutile phase of ca. 0%, 3%, 19%, 40%, 96%, and 99% were named as R0, R3, R19, R40, R96, and R99, respectively. The ratios of rutile to anatase determined by XRD according to the method described by Jung et al., 1999.

5.1.1.2 Atomic absorption spectroscopy (AAS)

AAS was performed to determine the composition of elements in the bulk of catalysts. The Co content of various ratios of rutile to anatase phase of titania-supported cobalt catalysts are shown in Table 5.1. It revealed that catalyst samples have 16.6 wt% cobalt.

Table 5.1 Content of Co from AAS and BET surface area measurement of various ratios of rutile to anatase phase of titania unsupported and supported Co catalysts.

Supports	BET surface area (m ² /g) ^a	Catalyst samples	Co (wt %) ^b	BET surface area (m ² /g) ^a
R0	70	Co/R0	16.6	52
R3	65	Co/R3	16.6	48
R19	49	Co/R19	16.6	34
R40	43	Co/R40	16.6	28
R96	39	Co/R96	16.6	21
R99	38	Co/R99	16.6	20

^a Measurement error is $\pm 5\%$.

^b Measurement error is $\pm 2\%$.

5.1.1.3 BET surface area

BET surface areas of various ratios of rutile to anatase phase of titania unsupported and supported Co catalysts are also shown in Table 5.1. BET surface areas of titania containing various rutile anatase ratios essentially decreased from 70 m²/g for the R0 sample (pure anatase titania) to 38 m²/g for the R99 sample (99% rutile titania). After loading 20 %wt Co, the BET surface areas of cobalt supported on titania were lower than the BET surface area of the unsupported titania. BET surface areas of various ratios of rutile to anatase phase of titania-supported Co catalysts were found in the range of 20-52 m²/g. The significant decrease in surface area of the original support material suggests that cobalt was deposited significantly in the pores of TiO₂.

Table 5.2 TPR and H₂ chemisorption results for various ratios of rutile to anatase phase of titania-supported Co catalysts.

Catalyst samples	Reducibility (%) during TPR at 35-800°C ^{a,b}	Total H ₂ chemisorption (μmol H ₂ /g _{cat}) ^c	Overall Co metal dispersion (%)
Co/R0	92	0.93	0.07
Co/R3	44	1.55	0.11
Co/R19	78	2.44	0.17
Co/R40	39	1.66	0.12
Co/R96	33	1.71	0.12
Co/R99	26	0.69	0.05

^a The reduced samples were recalined at the original calcination conditions prior to performing TPR.

^b Measurement error is ± 5%.

^c Error = ± 5% of measurement of H₂ chemisorption.

5.1.1.4 Temperature programmed reduction (TPR)

TPR was performed in order to identify the reduction behaviors and reducibility of catalysts. TPR profiles for all samples are shown in Figure 5.1. TPR of the titania support samples used was also conducted at the same TPR conditions used for the catalyst samples and no hydrogen consumption was detected. This indicated that the titania supports used themselves were not reducible at these TPR conditions. Apparently, TPR profiles of all calcined samples were similar exhibiting only one strong reduction peak as shown in Figure 5.1. And from these profiles the initial, final and maximum temperatures for each catalyst sample are given in Table 5.3. This peak can be assigned to the overlap of two-step reduction of Co_3O_4 to CoO and then to Co^0 (Kraum and Baern, 1999; Jongsomjit *et al.*, 2001). Upon the TPR conditions, the two reduction peaks based on the two-step reduction may or may not be observed. The only one reduction peak during TPR for all catalyst samples indicated that no residual cobalt nitrates precursor remains on the samples upon the calcination condition used in this study.

It was found that the TPR peak located at ca. 370-695°C (max. at 550°C) was observed for the Co/R0 sample. However, this reduction peak was dramatically shifted about 25-200°C lower when ca. 3-99% of rutile phase. Besides reduction behaviors obtained from TPR results, reducibilities of samples can be measured based on the peak areas below TPR curve (calibrated using Ag_2O), which are related to the amounts of hydrogen consumed during TPR (Kogelbaue *et al.*, 1995; Zhang *et al.*, 1999). The reducibilities during TPR at temperature 35-800°C of the various ratios of rutile to anatase phase of titania-supported Co catalysts are shown in Table 5.2. The reducibilities were ranged between 26 to 92% which decreased when the percent of rutile phase of titania increased. The reducibilities decreased when the calcined samples were reduced and performed TPR indicating a loss in reducibility of cobalt oxide species after reduction (Jongsomjit *et al.*, 2004).

From results, this suggested that the presence of rutile phase in titania can facilitate the reduction process of cobalt oxide species on the titania support leading to reduction at a lower temperature. Since TPR is more of a bulk

technique, it should be noted that the number of reduced Co metal obtained from the TPR measurement might not be well representative of the number of reduced Co metal surface atoms available for catalyzing CO hydrogenation. The results were consistent with Jongsomjit *et al.* (Jongsomjit *et al.*, 2005). They studied the dependence of crystalline phases in titania on catalytic properties during CO hydrogenation of Co/TiO₂ catalysts. They reported that pure anatase phase in titania-supported Co catalyst has a stronger interaction between cobalt and titania support due to the shift of a reduction peak to a higher temperature. For the mix phase in titania-supported Co catalyst, they found that there was no significant shift of the reduction temperature upon the hydrothermal treatment during reduction indicating a lesser degree of cobalt-support interaction compared to another one. They suggested that the presence of rutile phase in titania support result in an increase in stability of the titania support. An increase in stability could be the cause for a difficulty of cobalt to interact with it. Moreover, they indicated that the loss in reducibilities can be probably attributed to a nonreducible (at temperatures < 800°C) “Co-titanate” species formed during standard reduction.

Table 5.3 Initial, final and maximum temperatures from TPR profiles of various ratios of rutile to anatase phase of titania-supported Co catalysts.

Catalyst samples	Temperature (°C)		
	Initial	Final	Maximum
Co/R0	370	695	550
Co/R3	270	540	385
Co/R19	320	735	530
Co/R40	285	480	375
Co/R96	275	475	355
Co/R99	275	475	355

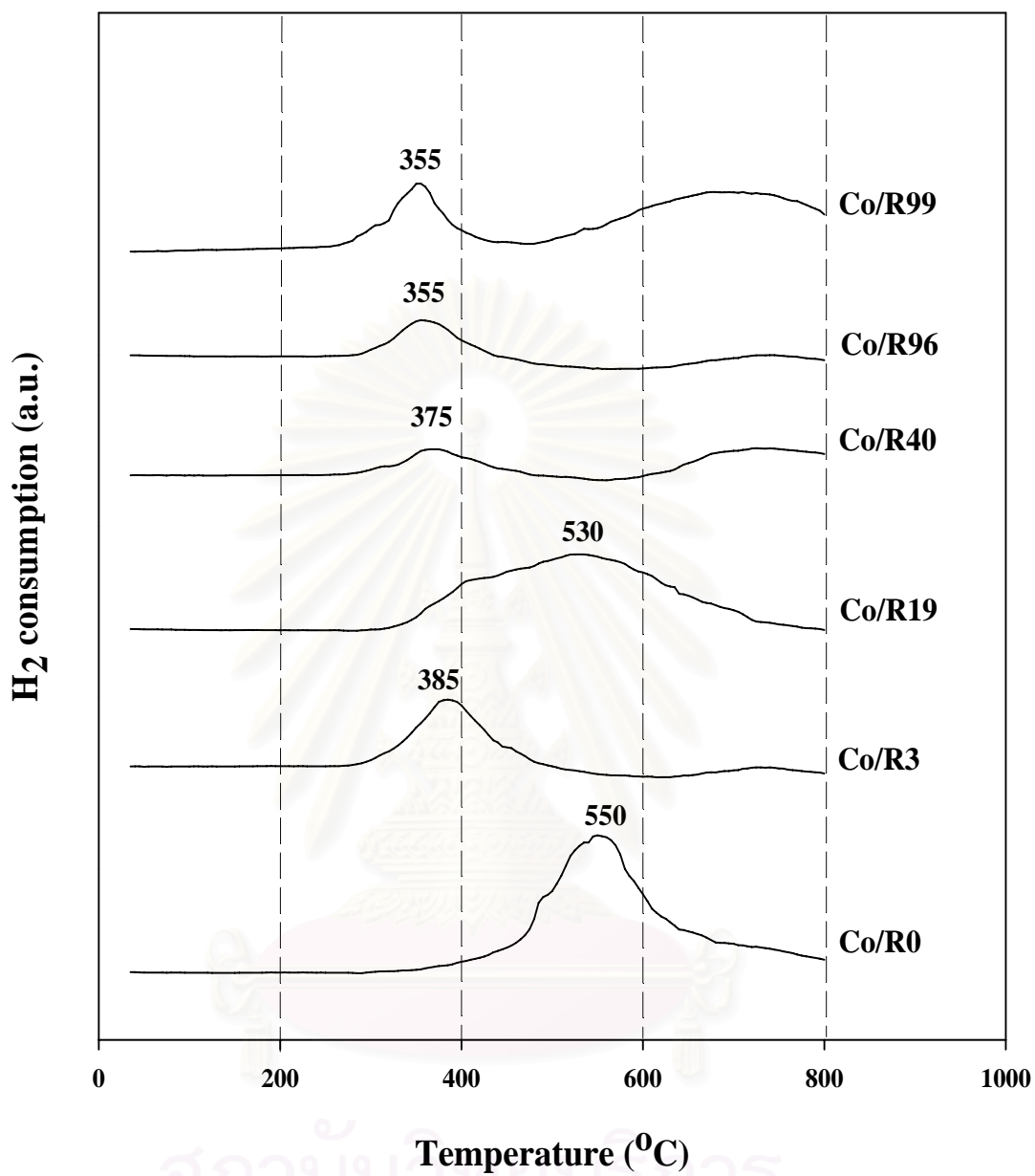


Figure 5.1 TPR profiles of various ratios of rutile to anatase phase of titania-supported Co catalysts.

5.1.1.5 H₂ chemisorption

Static H₂ chemisorption on the reduced cobalt catalyst samples was used to determine the number of reduced Co metal surface atoms. This is usually related to the overall activity of the catalyst during CO hydrogenation. H₂ chemisorption was used to determine the number of reduce surface cobalt metal atoms and percentage overall cobalt dispersion. The results of H₂ chemisorption for various ratios of rutile to anatase phase of titania-supported Co catalysts are given in Table 5.2. The amounts of H₂ adsorbed increased with the presence of rutile phase in titania up to a maximum at 19% of rutile phase (Co/R19) before decreasing when greater amounts of the rutile phase were present. Since H₂ chemisorption is a surface technique that the reduced Co metal surface atoms can be measured directly. The amounts of H₂ adsorbed on Co/TiO₂ obtained were lower compared to those for Co/Al₂O₃ and Co/SiO₂ at similar loading (Jongsomjit *et al.*, 2001; Panpranot *et al.*, 2002).

Moreover, the overall Co metal dispersion in the catalyst samples are also shown. The Co metal dispersion of the catalyst samples are given the same result as H₂ chemisorption. However, based on the H₂ chemisorption results, different ratios of rutile to anatase phase in titania exhibited different amounts of H₂ chemisorbed on the catalyst samples.

5.1.1.6 X-ray diffraction (XRD)

The bulk crystalline phases of samples were determined using XRD. XRD patterns of titania samples calcined at various temperatures between 800 and 1000 °C are shown in Figure 5.2. For the pure anatase titania (R0), XRD peaks of the anatase phase of titania at 25° (major), 37°, 48°, 55°, 56°, 62°, 71°, and 75° were evident. After calcination of pure anatase titania sample, it was observed that besides the XRD peaks of pure anatase titania as shown above XRD peaks at 28° (major), 36°, 42°, and 57° were gradually seen. These peaks were assigned to the rutile phase essentially formed after calcination of the pure anatase titania. Apparently, the major peak at 28° of rutile phase gradually increased with increasing the calcinations temperatures indicating higher content of rutile phase in titania was obtained. It was shown that the transformation from anatase to rutile phase (R99) was almost complete at temperature of ca. 1000°C resulting in the disappearance of XRD peaks for the anatase phase of titania. After various titania supports were obtained, the preparation of Co/TiO₂ via various rutile to anatase ratios of titania was consequently conducted in order to investigate the effect of various ratios of rutile to anatase in titania supports on characteristics, especially the cobalt dispersion of Co/TiO₂.

A 20 wt% of cobalt supported on titania consisting of various ratios of rutile to anatase phase was prepared by the conventional incipient wetness impregnation method. The XRD patterns for all calcined samples (Co/TiO₂) are shown in Fig. 5.3. After calcination, all calcined samples exhibited XRD peaks, which were identical with those for the corresponding titania supports. This indicated that there was no further phase transformation from anatase to rutile occurred after calcination (at temperature ca. 500 °C for 4 h) of the samples. Besides the XRD peaks of the corresponding titania supports detected, all calcined samples also exhibited weak XRD peaks at 31°, 36°, and 65°, which were assigned to the presence of Co₃O₄. However, at high content of rutile phase, the XRD peaks of Co₃O₄ were gradually diminished due to the hindrance of strong intensity of XRD peaks for the rutile phase of titania. Based on the XRD results, it was clear that Co₃O₄ species was definitely present in a highly dispersed form.

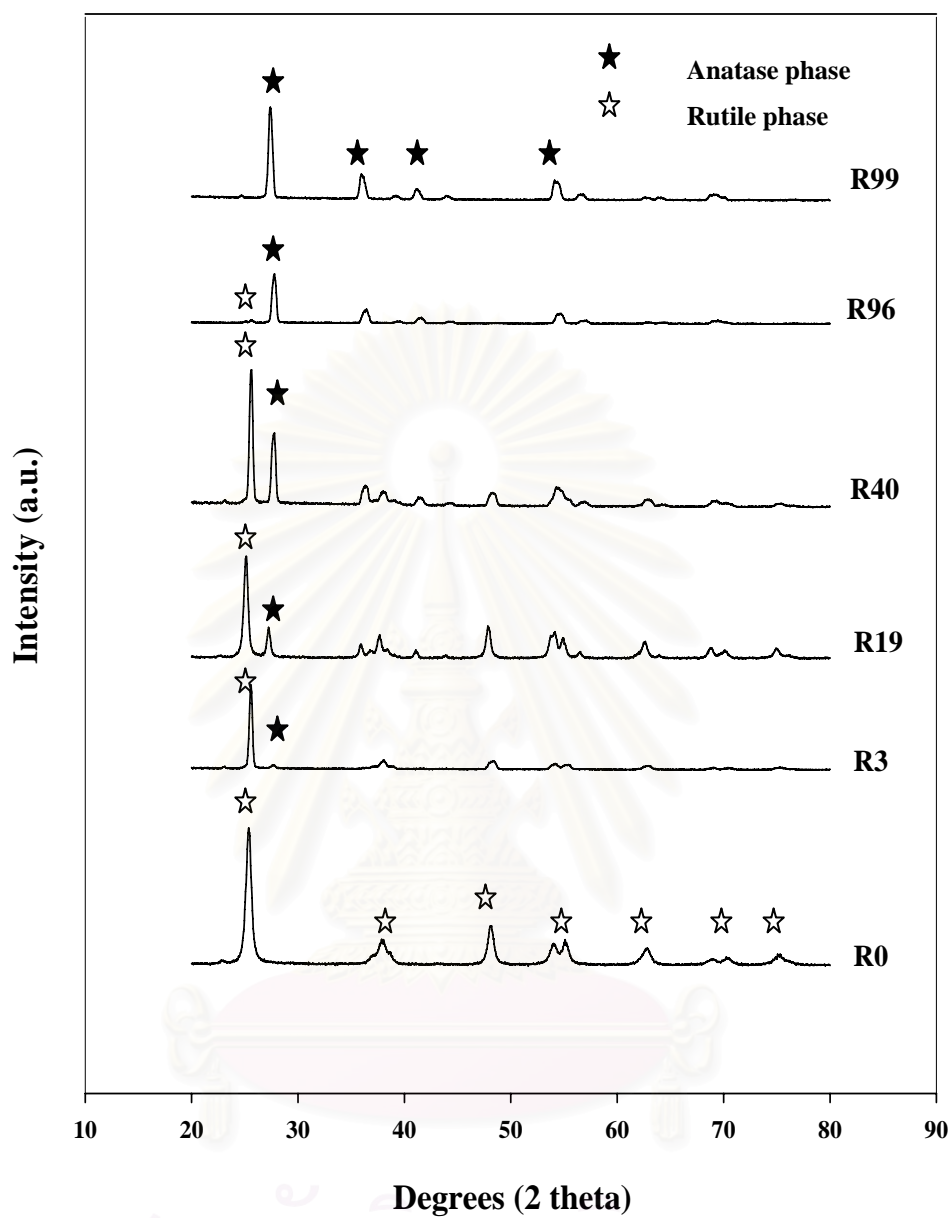


Figure 5.2 XRD patterns of various ratios of rutile to anatase phase of titania support samples.

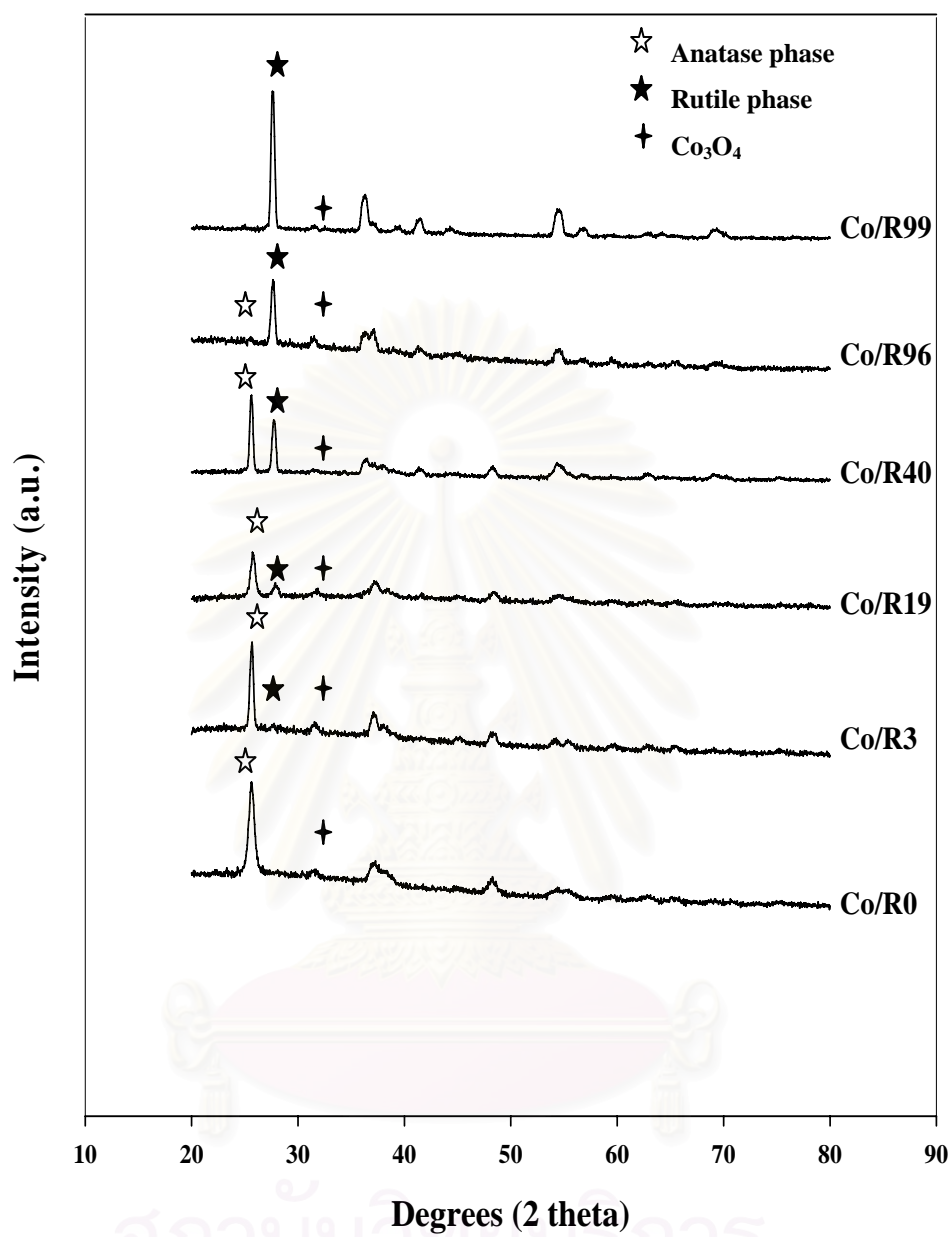


Figure 5.3 XRD patterns of various ratios of rutile to anatase phase of titania-supported Co catalysts.

5.1.1.7 Electron microscopy

SEM and EDX were also conducted in order to study the morphologies and elemental distribution of the catalyst samples, respectively. The typical SEM micrograph along with the EDX mapping (for Co, Ti, and O) are illustrated in Figure 5.4 - 5.9 for the all various ratios of rutile to anatase phase of titania-supported Co catalysts samples (Co/R0, Co/R3, Co/R19, Co/R40, Co/R96 and Co/R99). The external surface of catalyst granule is shown in all figures and the light or white patches (the term “patches” is used to refer the entities rich in cobalt supported on the catalyst granules) on the catalyst granule surface represent high concentration of cobalt oxides species on the surface. It can be seen that the cobalt oxide species were well dispersed and distributed (shown on mapping) all over the catalyst granule in all samples regardless of the ratio of rutile to anatase in the titania.

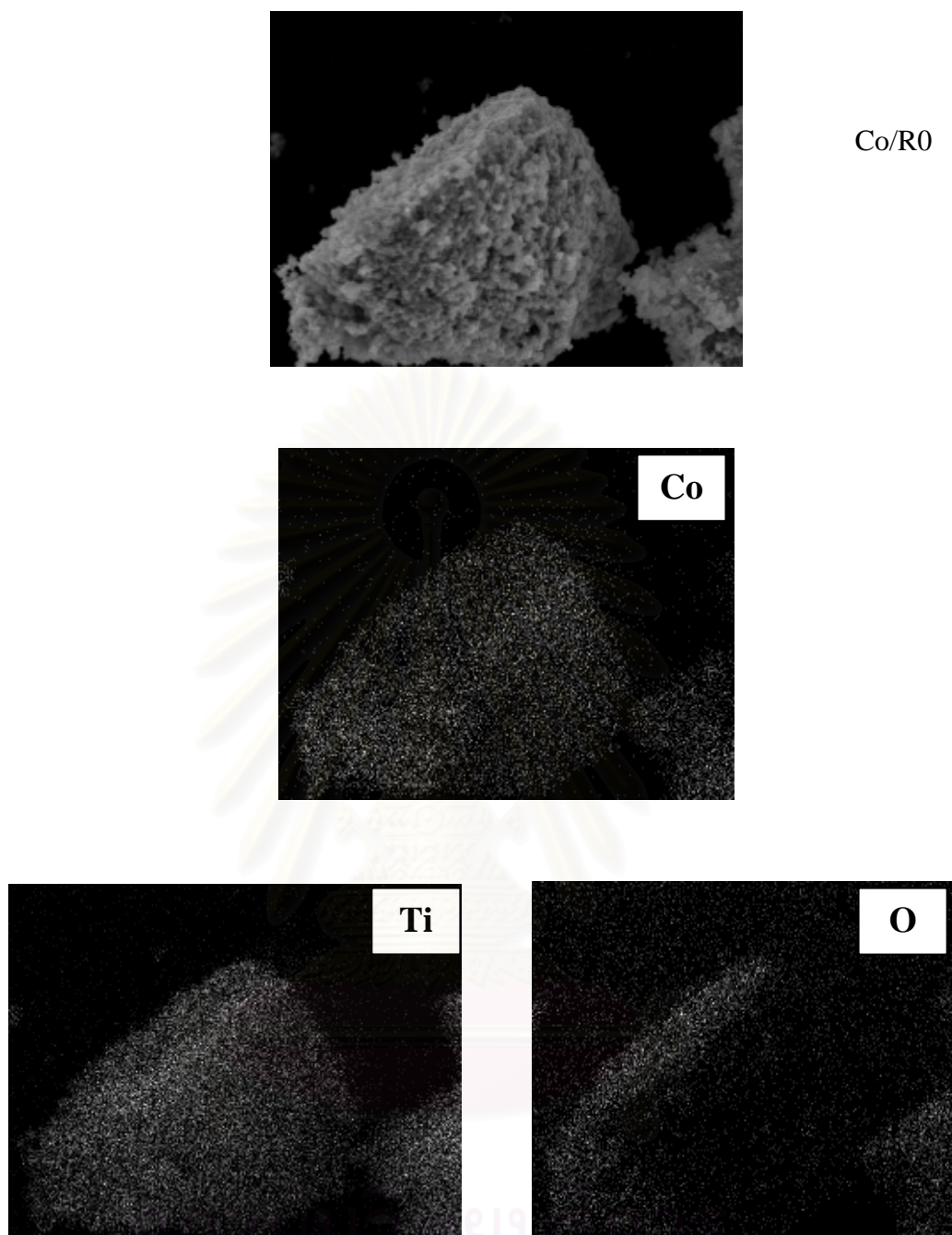


Figure 5.4 SEM micrograph and EDX mapping of Co/R0 catalyst granule.

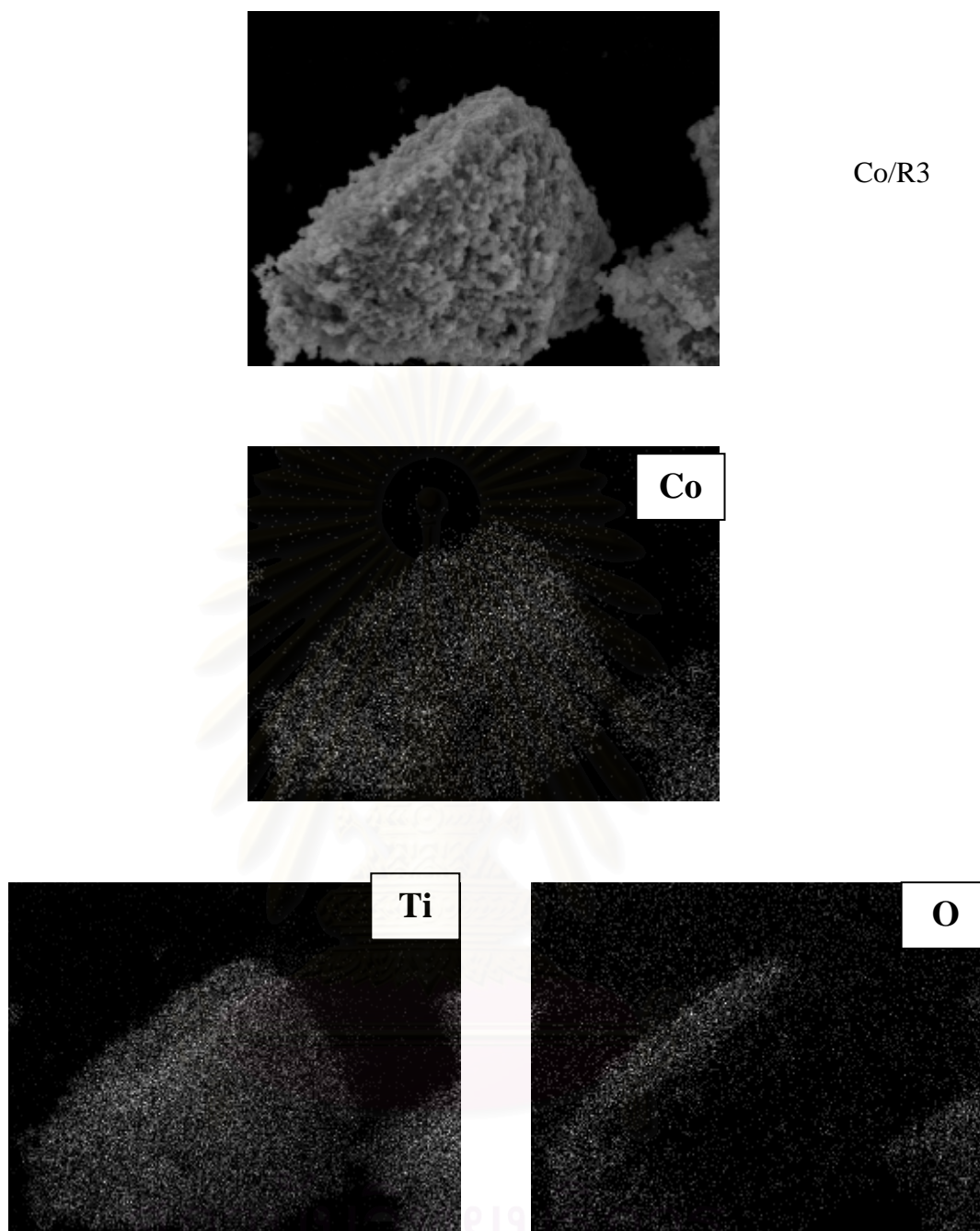
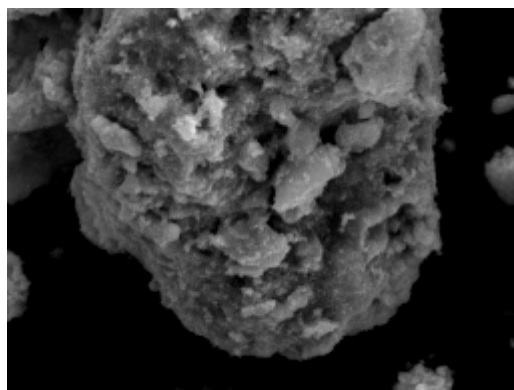


Figure 5.5 SEM micrograph and EDX mapping of Co/R3 catalyst granule.



Co/R19

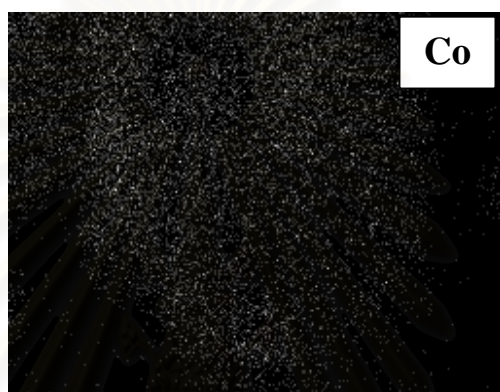


Figure 5.6 SEM micrograph and EDX mapping of Co/R19 catalyst granule.

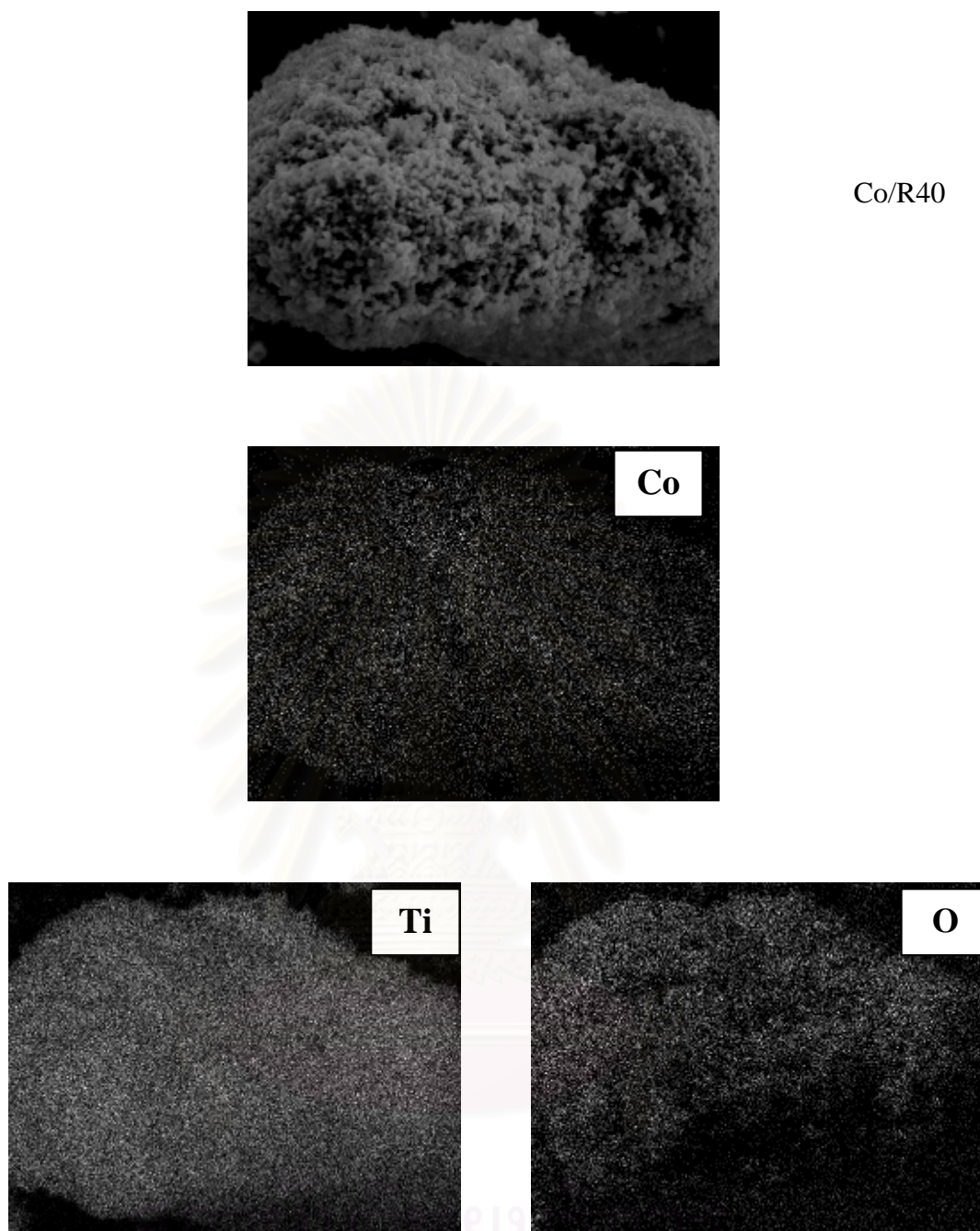


Figure 5.7 SEM micrograph and EDX mapping of Co/R40 catalyst granule.

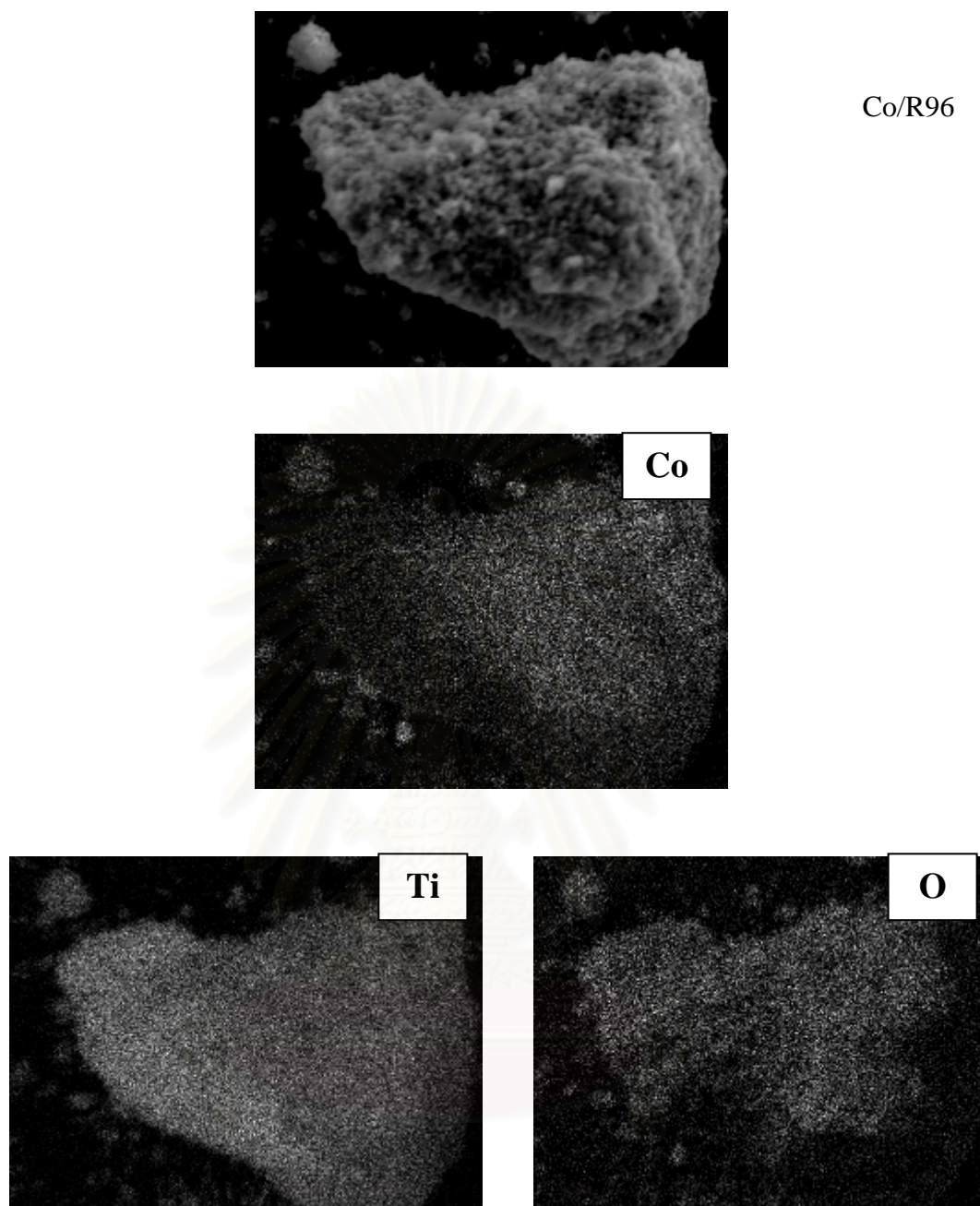


Figure 5.8 SEM micrograph and EDX mapping of Co/R96 catalyst granule.

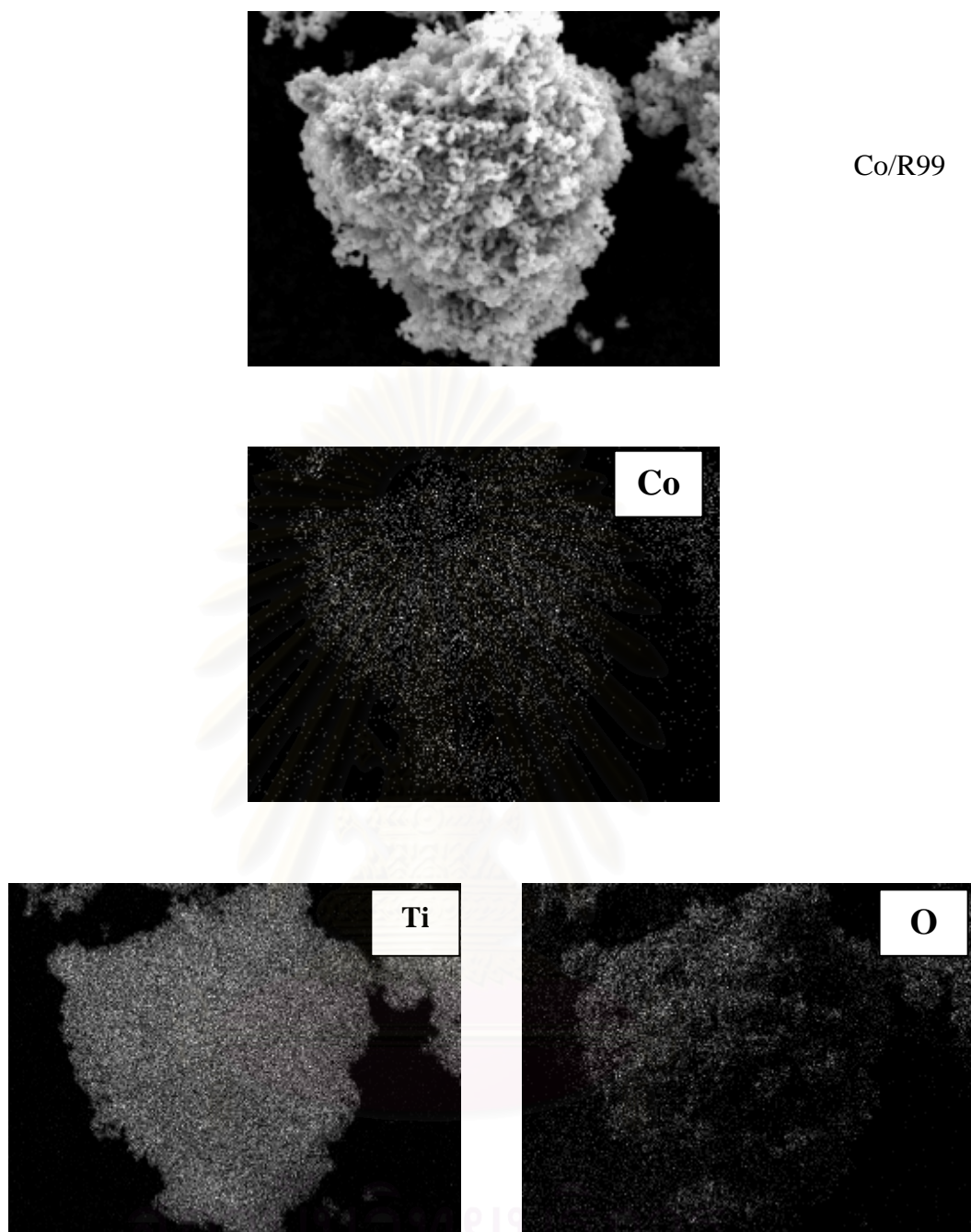


Figure 5.9 SEM micrograph and EDX mapping of Co/R99 catalyst granule.

5.1.1.8 Transmission Electron Microscopy (TEM)

TEM micrographs were taken for all the catalysts in order to physically measure the size of cobalt oxide particles and/or cobalt clusters. The TEM micrographs for all samples are shown in Figure 5.10 and 5.11, respectively. The dark spots represented cobalt oxide species present after calcination of samples dispersing on titania consisting of various ratios of rutile to anatase. It can be observed that cobalt oxide species were highly dispersed on the titania supports for Co/R0, Co/R3, and Co/R19 samples resulting in an appearance of smaller cobalt oxide patches present. However, the degree of dispersion for cobalt oxide species essentially decreased with increasing the rutile phase in titania from 40 to 99% as seen for Co/R40, Co/R96, and Co/R99 samples resulting in the observation of larger cobalt oxide patches. The average cobalt particle/cluster sizes from TEM are given in Table 5.4. It was found that the average cobalt particle/cluster diameters of cobalt oxide particles were ranged between 10.5 to 25 nm for Co/R0, Co/R3 and Co/R19 and between 119 to 148 for Co/R40, Co/R96, and Co/R99. This indicated that the diameter of cobalt oxide particles increased with increasing amount of rutile phase in titania, especially for the rutile rich titania.

It is suggested that the presence of the rutile phase in titania from 0 (pure anatase phase) to 19% exhibited the highly dispersed forms of cobalt oxide species for the calcined samples. From H₂ chemisorption result for all samples, it was found that the number of the reduced cobalt metal surface atoms increased with the presence of rutile phase in titania up to a maximum at 19% of rutile phase (Co/R19) before decreasing with the greater amounts of rutile phase. Considering the number of cobalt metal atoms for Co/R0 (pure anatase titania), the number was apparently low even though highly dispersed cobalt oxides species. This was suggested that highly dispersed forms of cobalt oxide species be not only the factor that insures larger number of reduced cobalt metal surface atoms in Co/TiO₂. On the other hand, it can be observed that the number of reduced cobalt metal surface atoms for Co/R40 and Co/R96 (with the low degree of dispersion of cobalt oxide species as seen by TEM) was larger than that for Co/R0. This was due to the presence of rutile phase in Co/R40 and Co/R96. It should be mentioned that the largest number of reduced cobalt metal

surface atoms for the Co/R19 sample was attributed to both highly dispersed cobalt oxide species and the presence of rutile phase in titania atoms. Thus, both highly dispersed cobalt oxide species along with the presence of rutile phase in titania could play an important role on the number of reduced cobalt metal surface atoms for Co/TiO₂.

Table 5.4 The average diameters of cobalt metals sizes from TEM for various ratios of rutile to anatase phase of titania-supported Co catalysts.

Catalyst samples	The average diameters of cobalt metals sizes (nm)
Co/R0	10.5
Co/R3	20
Co/R19	25
Co/R40	119
Co/R96	144
Co/R99	148

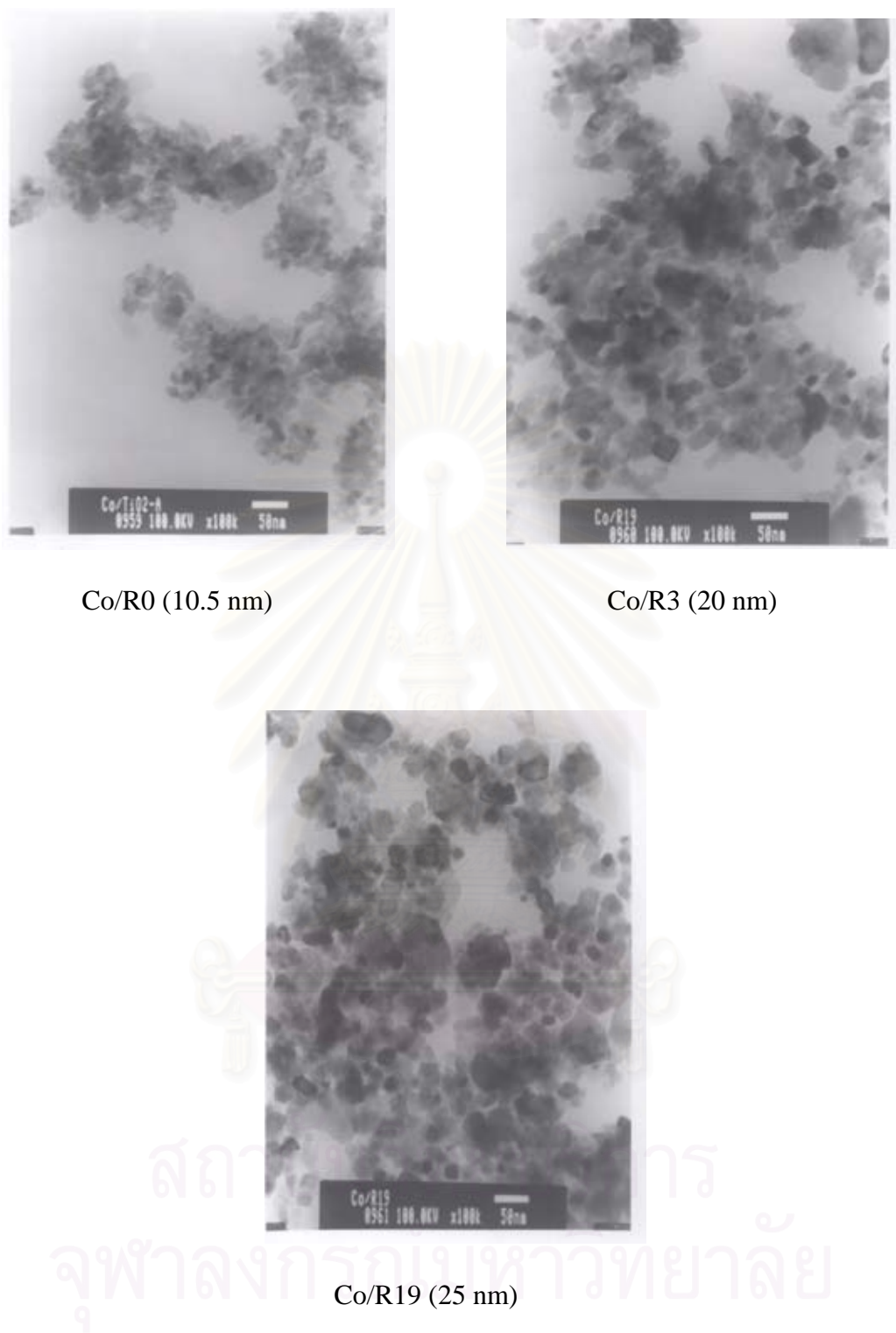
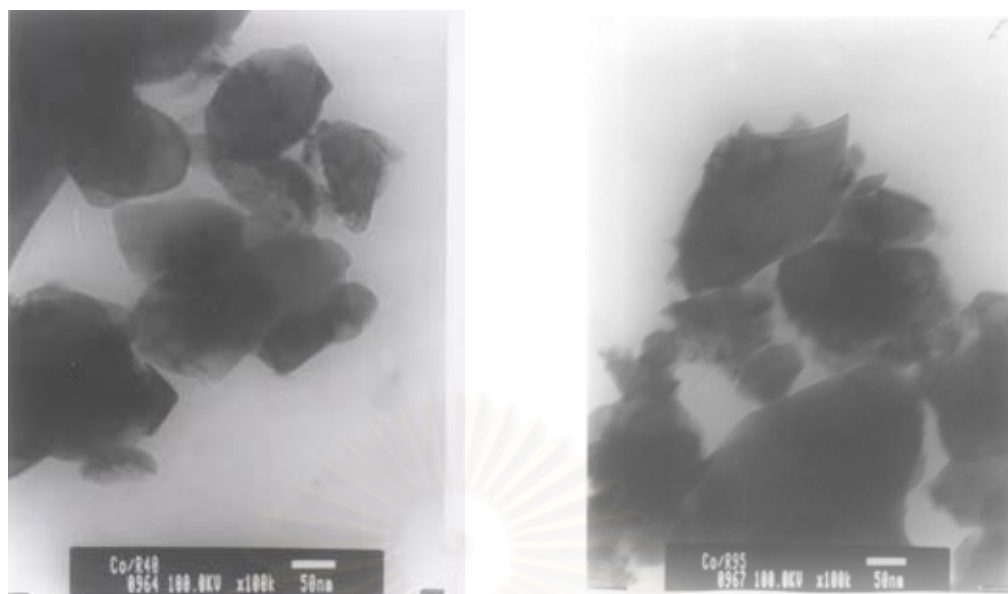


Figure 5.10 TEM micrographs of Co/R0, Co/R3 and Co/R19 catalysts.



Co/R40 (119 nm)

Co/R96 (144 nm)



Co/R99 (148 nm)

Figure 5.11 TEM micrographs of Co/R40, Co/R96 and Co/R99 catalysts.

5.1.1.9 Reaction study in CO hydrogenation

In order to measure the catalytic properties of the catalyst samples with various ratios of rutile to anatase in titania. Normally, after calcinations at 300°C for 10 h. Cobalt is in the form of cobalt oxide phase (Co_3O_4 or Co_2O_3). Cobalt oxide has to be reduced to cobalt metal (Co^0) prior to reaction since cobalt metal is known to be the most active phase for CO hydrogenation, not its oxide. Before reaction, the catalyst was reduced in-situ in H_2 flow 50 cc/min at 350°C for 3 h in order to obtain metallic phase cobalt.

CO hydrogenation was performed in a fixed-bed flow reactor and was carried out at 220°C, 1 atm, and H_2/CO ratio = 10 for all the catalyst samples. A relatively high H_2/CO ratio was used in order to minimize catalyst deactivation due to carbon deposition during reaction. The results are shown in Table 5.5. It indicated that the reaction rate ranged between 1.4 and 33.23 $\text{gCH}_2/\text{g}_{\text{cat}}\text{h}^{-1}$ (initial) and between 0.8 and 26.52 $\text{gCH}_2/\text{g}_{\text{cat}}\text{h}^{-1}$ (steady-state). The CO conversion ranged between 3.70 to 89.05% (initial) and 2.10 to 71.07% (steady state). This also showed that activities of the samples increased with the presence of rutile phase in titania up to a maximum at 19% of rutile phase (Co/R19) before decreasing when greater amounts of rutile phase were present. Considering selectivity to methane, it was found that the presence of rutile phase in titania resulted in an increased selectivity to methane.

Based on the reaction study, it can be concluded that the catalytic properties of Co/TiO_2 depend on the ratio of rutile/anatase. The results revealed that the presence of rutile phase of an optimum of the rutile phase (i.e., Co/R19) result in an increased catalytic activity during CO hydrogenation. It is proposed that the presence of rutile phase in titania can facilitate the reduction process of cobalt oxides species resulting in lower reduction temperatures. The presence of some rutile phase also resulted in an increased number of reduced cobalt metal surface atoms available for catalyzing the reaction. However, higher ratios (more than 19%) of rutile to anatase in titania decreased the catalyst activities. It should be mentioned that besides the ratios of rutile to anatase in titania, there are also other factors such as preparation methods, titania precursors, particle sizes, modes and types of reactions that would

affect the characteristics and catalytic properties of titania used both as a catalyst support or a catalyst itself.

Table 5.5 Reaction rate for CO hydrogenation on the various ratios of rutile to anatase phase of titania-supported Co catalysts.

Samples	CO conversion (%) ^a		Rate($\times 10^2$ gCH ₂ /g _{cat} h ⁻¹) ^b		CH ₄ selectivity (%)		C ₂ -C ₄ + selectivity (%)	
	Initial ^c	SS ^d	Initial	SS	Initial	SS	Initial	SS
	Co/R0	3.70	2.10	1.40	0.80	71	68	29
Co/R3	44.08	10.83	16.45	4.04	99	99	1	1
Co/R19	89.05	71.07	33.23	26.52	98	98	2	2
Co/R40	66.92	66.82	24.97	24.93	97	96	3	4
Co/R96	67.80	67.18	25.3	25.07	99	99	1	1
Co/R99	22.41	6.14	8.36	2.29	94	94	6	6

^a CO hydrogenation was carried out at 220°C, 1 atm, and H₂/CO/Ar = 20/2/8 cc/min.

^b Error $\pm 5\%$

^c After 5 min of reaction

^d After 5 h of reaction

สถาบันวิทยบริการ
จุฬาลงกรณ์มหาวิทยาลัย

5.1.2 Various percent loading of zirconia modified titania-supported Co catalysts

To increase catalyst activity, many promoters such as Ru (Iglesia *et.al.*, 1992 and Kogelbauer *et.al.*, 1996), Zr (Ali *et.al.*, 1995 and Rohr *et.al.*, 2000), Pt (Schanke *et.al.*, 1995) and etc. have been investigated for Co catalyst. It has been proposed that a variety of these promoters can increase the reducibility of Co, preserve the activity by preventing the formation of coke, exhibit cluster and ligand effects, act as a source of hydrogen spillover, and enhance the dispersion. A number of investigations have been focused on zirconium as a promoter for the supported cobalt catalyst such as silica (Ali *et.al.*, 1995 and Moradi *et.al.*, 2002) and alumina (Rohr *et.al.*, 2000, Jongsomjit *et.al.*, 2003 and Xiong *et.al.*, 2005). However, no studies have investigate the effect of zirconia modified titania support for Co FTS catalysts. The many percent of zirconia modified titania-supported Co catalysts were characterized by different method and their catalytic performances were tested in a fixed-bed flow reactor for CO hydrogenation reaction.

5.1.2.1 BET surface area

BET surface areas of various percent of zirconia modified titania unsupported and supported Co catalyst samples are shown in Table 5.6. The BET surface areas of the zirconia modified titania supports decreased from 70 m²/g for the R0 sample (pure anatase titania) to 47 m²/g for the R0Z5 sample (5% zirconia modified pure anatase titania support) and from 49 m²/g for the R19 sample (19% rutile in titania) to 33 m²/g for the R19Z5 sample (5% zirconia modified 19% rutile in titania support). Apparently, the zirconia modified titania-supported Co catalyst samples had BET surface areas lower than the support as reacted. The BET surface areas decrease with increasing the amounts of zirconia. The various percent loading of zirconia modified titania-supported Co catalysts ranged between 25-52 m²/g. The significant decrease in surface area of the original support material suggests that cobalt was deposited significantly in the pores of zirconia modified titania support.

Table 5.6 BET surface area measurement of various percent loading of zirconia modified titania unsupported and supported Co catalysts.

Supports	BET surface area (m ² /g) ^a	Catalyst samples	BET surface area (m ² /g) ^a
R0	70	Co/R0	52
R0Z0.5	55	Co/R0Z05	43
R0Z1	53	Co/R0Z1	42
R0Z5	47	Co/R0Z5	36
R19	49	Co/R19	34
R19Z0.5	38	Co/R19Z05	27
R19Z1	34	Co/R19Z1	25
R19Z5	33	Co/R19Z5	25

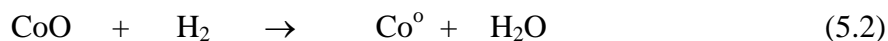
^a Measurement error is $\pm 2\%$.

5.1.2.2 Temperature programmed reduction (TPR)

The results of TPR at temperature 35-800°C of the various percent loading of zirconia modified titania-supported Co catalyst samples are shown in Table 5.7. The zirconia added in the anatase phase of titania (R0) support can result in a decrease in reducibility which also shown in Table 5.7. Whereas, the reducibilities of zirconia modified the rutile phase of titania (R19)-supported Co catalyst samples increased as seen for Co/R19Z0.5 and Co/R19Z1 samples (increase up to 7-10%) and decreased for Co/R19Z5 sample.

In addition, TPR was performed to obtain information on the reduction behaviors of the catalyst samples. Figure 5.12 was illustrated for TPR profiles of various percent loading of zirconia-modified titania-supported Co catalysts. And from these profiles the initial, final and maximum temperatures for each catalyst sample are given in Table 5.8. It can be perceived that bulk Co₃O₄ and all the samples after various pretreatment conditions indicated only one strong

reduction peak. This peak can be assigned to the overlap of two-step reduction of Co_3O_4 (Kraum and Baern, 1999; Voß *et al.*, 2003).



There was only one reduction peak located at ca. 370-695°C (max. at 550°C) for the Co/R0 sample. TPR profiles of all zirconia modified pure anatase in titania supported-Co catalysts were shifted about 15-30°C higher as shown in Figure 5.12. For the Co/R19 sample, TPR peak was located at ca. 320-735°C (max. at 530°C). There was a little shift occurred with the presence of zirconia in 19% of rutile in titania support.

This was suggested that the addition of zirconia on the pure anatase in titania not stabilized the titania support. It should be mentioned that Co-support compound formation (Co-SCF) in titania-supported cobalt catalyst still occurs during standard reduction resulting in a lower reducibility of catalyst (Jongsomjit *et al.*, 2004). Zhang *et al.* (1999) investigated the reducibilities of $\text{CoRu}/\gamma\text{-Al}_2\text{O}_3$ during standard reduction and TPR in the presence of added water vapor. They found that water has a significant effect on the reduction behavior of $\text{CoRu}/\gamma\text{-Al}_2\text{O}_3$. It was suggested that water vapor present during reduction leads to a decrease in the degree of reduction of the cobalt perhaps in two ways: (i) inhibition of the reduction of well-dispersed CoO interacting with the alumina support, possibly by increasing the cobalt-alumina interaction, and (ii) facilitation of the migration of cobalt ions into probable tetrahedral sites of $\gamma\text{-Al}_2\text{O}_3$ to form a non-reducible (at temperatures < 900°C) spinel. However, considering the Co-SCF in Co/TiO_2 , Jongsomjit *et al.* (2004) studied Co-support compound formation in titania-supported cobalt catalyst. They reported that the compound of cobalt and titania formed referred as “Co-titanate” was considered to be non-reducible at temperatures < 800°C and this “Co-titanate” formed resulted in a decrease in the reduction behaviors.

In the case of zirconia modified 19% of rutile in titania supported-Co catalysts (Co/R19Z0.5 and Co/R19Z1), the addition of zirconia resulted in an

increase in reducibility of the catalyst and reduction lower temperature. These results were consistent with Andreas *et al.* (1999). They reported that a weaker cobalt-zirconium interaction was observed and the addition of zirconium led to the increase of reducibility. Moradi *et al.* (2003) claimed that the interaction of cobalt-silica is replaced by the Co-Zr interaction which favors the reduction of the catalyst at lower temperature. Moreover, Jongsomjit *et al.* (2003) studied effect of zirconia-modified alumina on the properties of Co/ γ -Al₂O₃ catalysts. They suggested that the reducibility for TPR 30 to 800°C increased somewhat with Zr modification (ZrO₂ = 2-11 wt %) In addition, they found that there was no Ramon evidence for the formation of Co “aluminate” for the Zr-modified catalysts. They concluded that Zr modification decreased the impact of water vapor during reduction, possibly by partially blocking Co “aluminate” formation. This suggests that the increase in reducibility with Zr modification appeared to be caused by a decrease in the amount of Co-SCF in titania-supported cobalt catalyst.

Table 5.7 TPR and H₂ chemisorption results for the various percent loading of zirconia modified titania-supported Co catalysts.

Catalyst samples	Reducibility (%) during TPR at 35-800°C ^{a,b}	Total H ₂ chemisorption ($\mu\text{mol H}_2/\text{g}_{\text{cat}}$) ^c
Co/R0	92	0.93
Co/R0Z0.5	88	0
Co/R0Z1	59	0
Co/R0Z5	62	0.85
Co/R19	78	2.44
Co/R19Z0.5	86	9.05
Co/R19Z1	84	8.54
Co/R19Z5	60	2.37

^a The reduced samples were recalcined at the original calcination conditions prior to performing TPR.

^b Measurement error is $\pm 5\%$.

^c Error = $\pm 5\%$ of measurement of H₂ chemisorption.

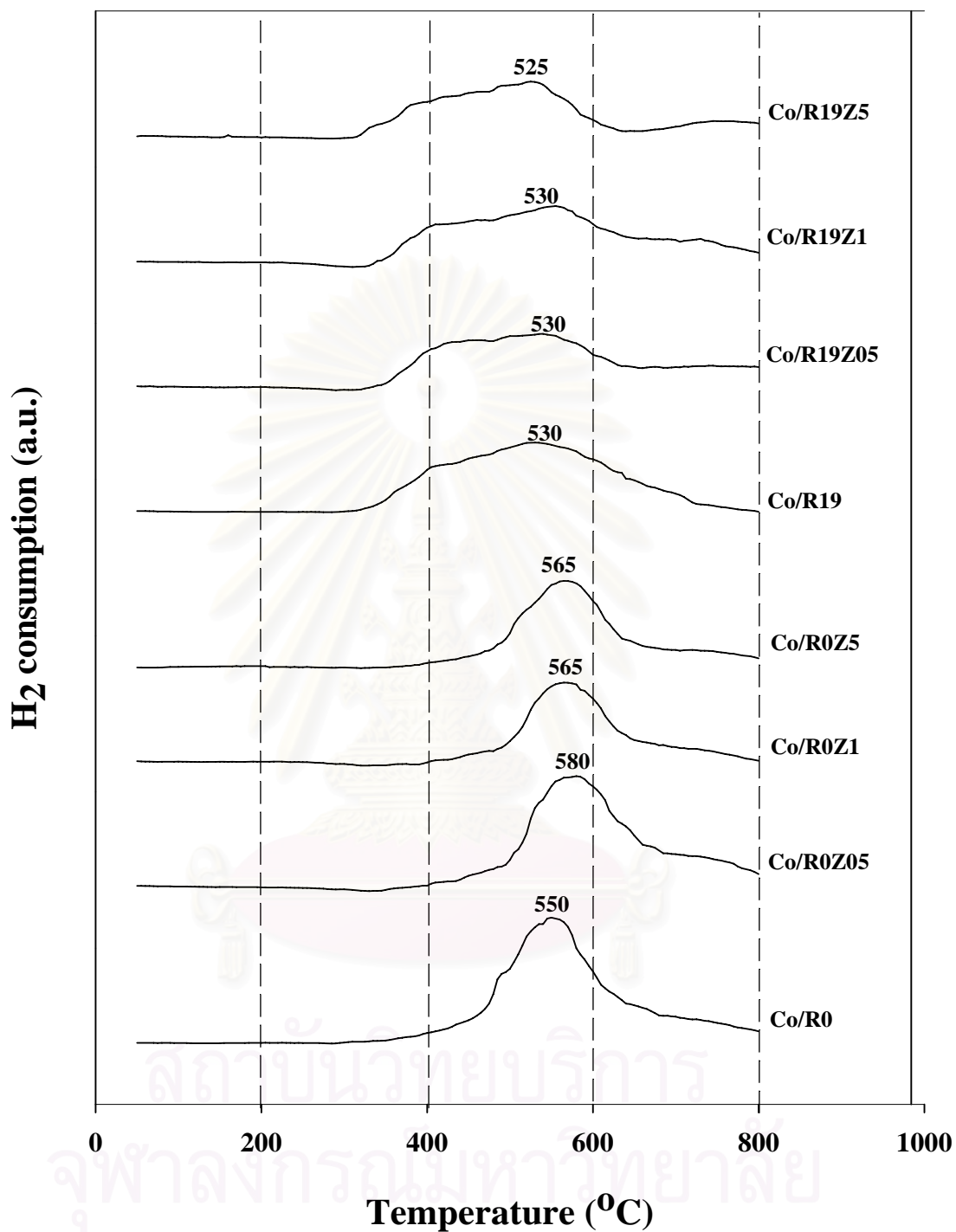


Figure 5.12 TPR profiles of various percent loading of zirconia modified titania-supported Co catalysts.

Table 5.8 Initial, final and maximum temperatures from TPR profiles of various percent loading of zirconia modified titania-supported Co catalysts.

Catalyst samples	Temperature (°C)		
	Initial	Final	Maximum
Co/R0	370	695	550
Co/R0Z0.5	400	735	580
Co/R0Z1	440	760	565
Co/R0Z5	440	780	565
Co/R19	320	735	530
Co/R19Z0.5	315	760	530
Co/R19Z1	315	750	530
Co/R19Z5	310	625	525

5.1.2.3 H₂ chemisorption

The results of H₂ chemisorption for various percent loading of zirconia modified titania-supported Co catalysts are given in Table 5.7. The amounts of H₂ adsorbed of the Co/R0Z0.5, Co/R0Z1 and Co/R0Z5 samples were lower than Co/R0 sample about 0.1-0.9 %. In the amount of H₂ adsorbed the zirconia modified 19% rutile in titania-supported Co catalysts increased with the presence of zirconia up to a maximum at 1% of zirconia (Co/R19Z1) before decreasing when greater amounts of the zirconia were present (Co/R19Z5). The total H₂ chemisorption was 9.05, 8.54 and 2.37 $\mu\text{mol H}_2/\text{g}_{\text{cat}}$ for Co/R19Z0.5, Co/R19Z1 and Co/R19Z5, respectively.

5.1.2.4 X-ray diffraction (XRD)

The XRD patterns for the calcined Co catalysts (with and without Zr modification) are shown in Figure 5.13. It was observed that they had identical XRD patterns. XRD patterns of the Co/R0, Co/R0Z0.5, Co/R0Z1 and Co/R0Z5 catalysts showed diffraction peaks at 25° (major), 37°, 48°, 55°, 56°, 62°, 71°, and 75° indicating the TiO₂ in the anatase form. XRD patterns of the Co/R19, Co/R19Z0.5, Co/R19Z1 and Co/R19Z5 catalysts showed diffraction peaks at 25° (major), 37°, 48°, 55°, 56°, 62°, 71°, and 75° indicating the TiO₂ in the anatase form and the diffraction peaks at 28° (major), 36°, 42° and 57° explaining the TiO₂ in the rutile form. No peaks of ZrO₂ or any other Zr compound, however, were detected. This indicates that Zr was present in a highly dispersed form (Ali *et al.*, 1995, Jongsomjit *et al.*, 2003)

After impregnation with the cobalt precursor and calcination, all catalyst samples were again identified using XRD. The XRD patterns of all calcined samples are shown in Figure 5.14. After calcination, all samples exhibited XRD peaks, which were identical with those for the corresponding zirconia modified titania supports used as seen in Figure 5.13. All calcined samples also exhibited weak XRD peaks at 31°, 36°, and 65°, which were assigned to the presence of Co₃O₄. Based on XRD results, it indicated that the presence of Co₃O₄ was apparently in the highly dispersed form.

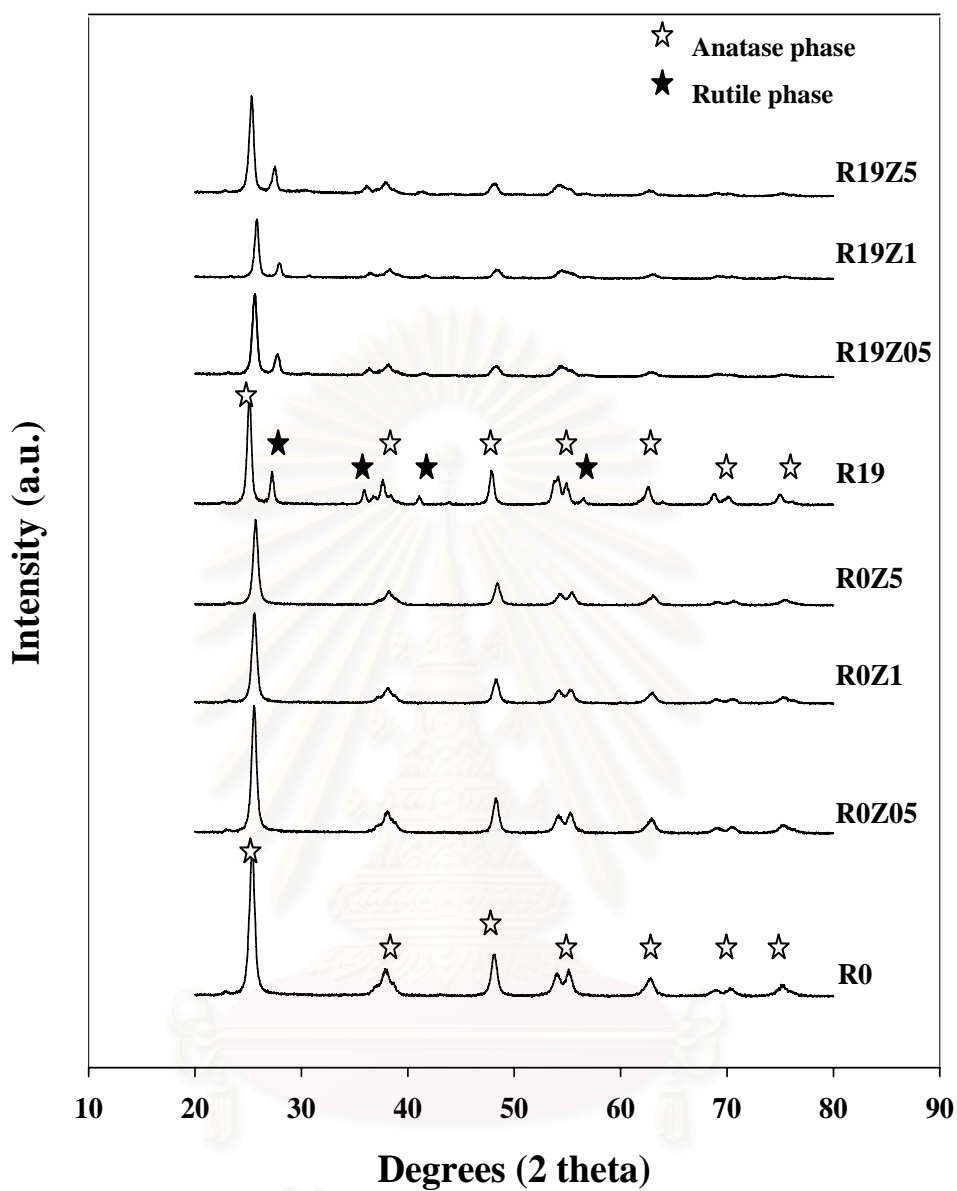


Figure 5.13 XRD patterns of various percent loading of zirconia modified titania support.

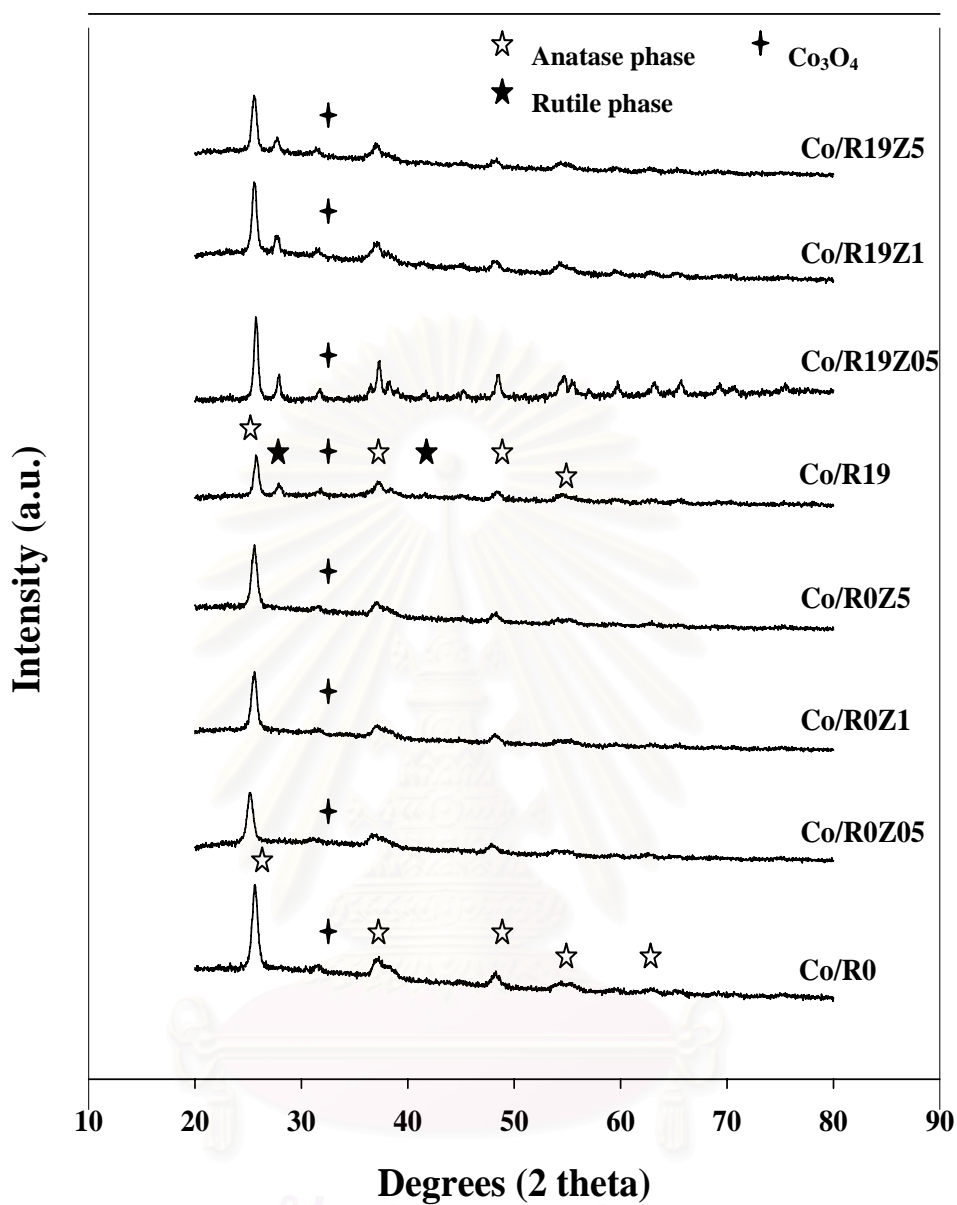


Figure 5.14 XRD patterns of various percent loading of zirconia modified titania-supported Co catalysts.

5.1.2.5 Electron microscopy

SEM and EDX were used to determine the catalyst granule morphology and elemental distribution of the catalyst particles, consecutively. The typical SEM micrographs along with the EDX mapping (for Co, Ti, and O) are illustrated in Figure 5.15-5.18 for the Co/R0Z1, Co/R0Z5, Co/R19Z1 and Co/R19Z5. It can be perceived that cobalt patches (white spots shown in all figures) were well distributed all over the external surface of catalyst granules. EDX gave the useful information about the elemental distribution on the catalyst granules, it can be seen that the cobalt oxide species were well dispersed and distributed (shown on mapping) all over the catalyst granule in all the modified titania supports.



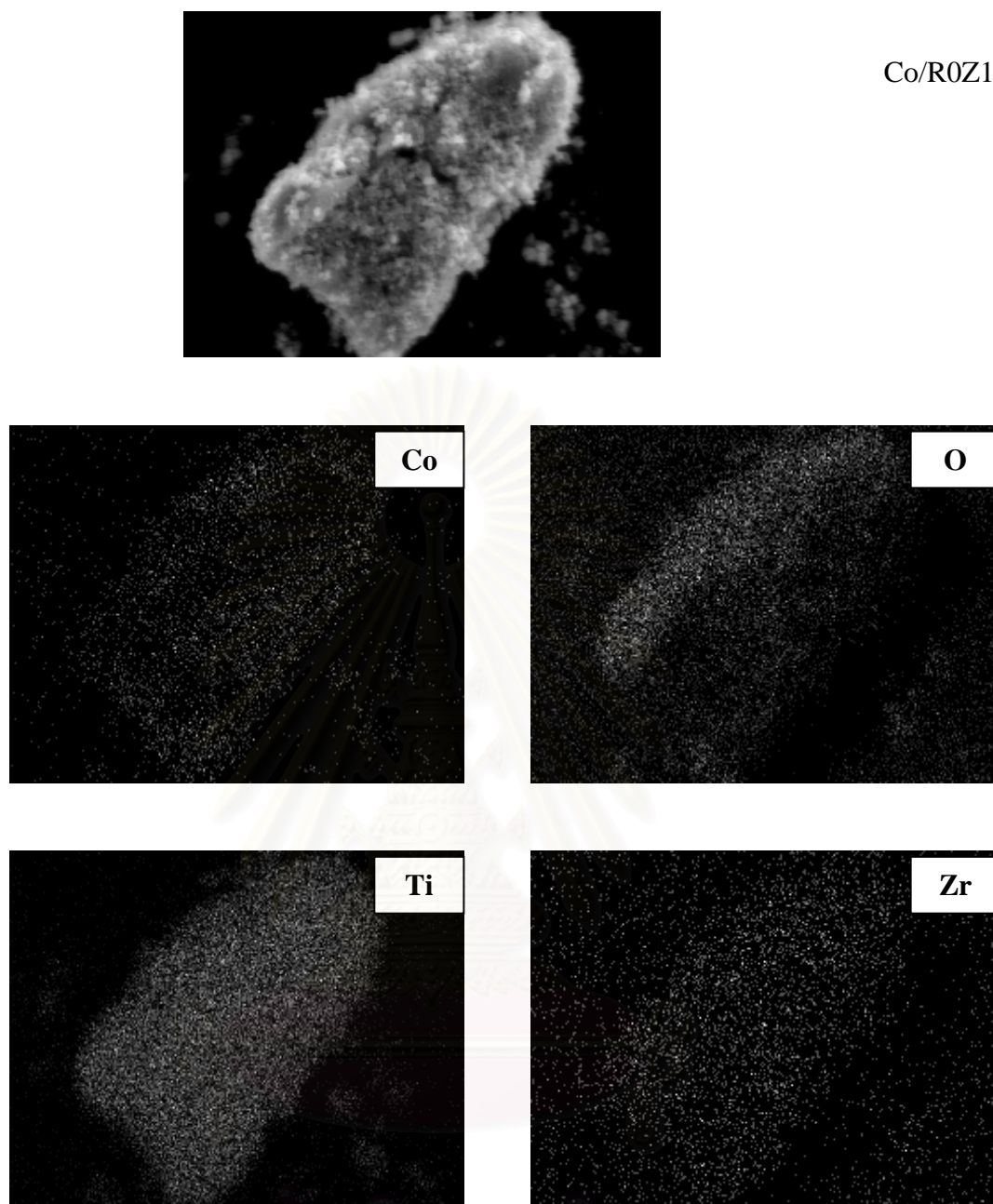


Figure 5.15 SEM micrograph and EDX mapping of Co/R0Z1 catalyst granule.

สถาบันวิทยบริการ
จุฬาลงกรณ์มหาวิทยาลัย

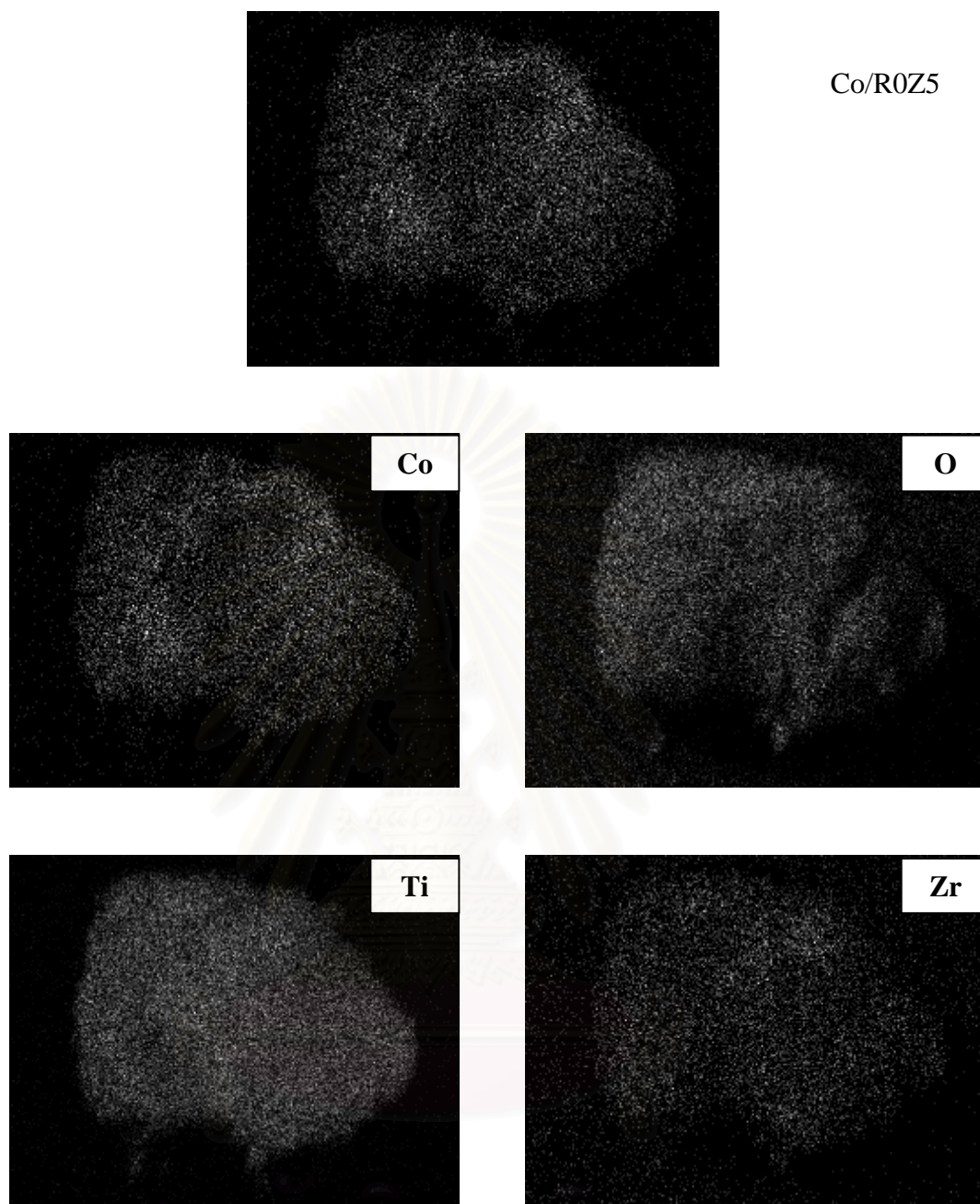


Figure 5.16 SEM micrograph and EDX mapping of Co/R0Z5 catalyst granule.

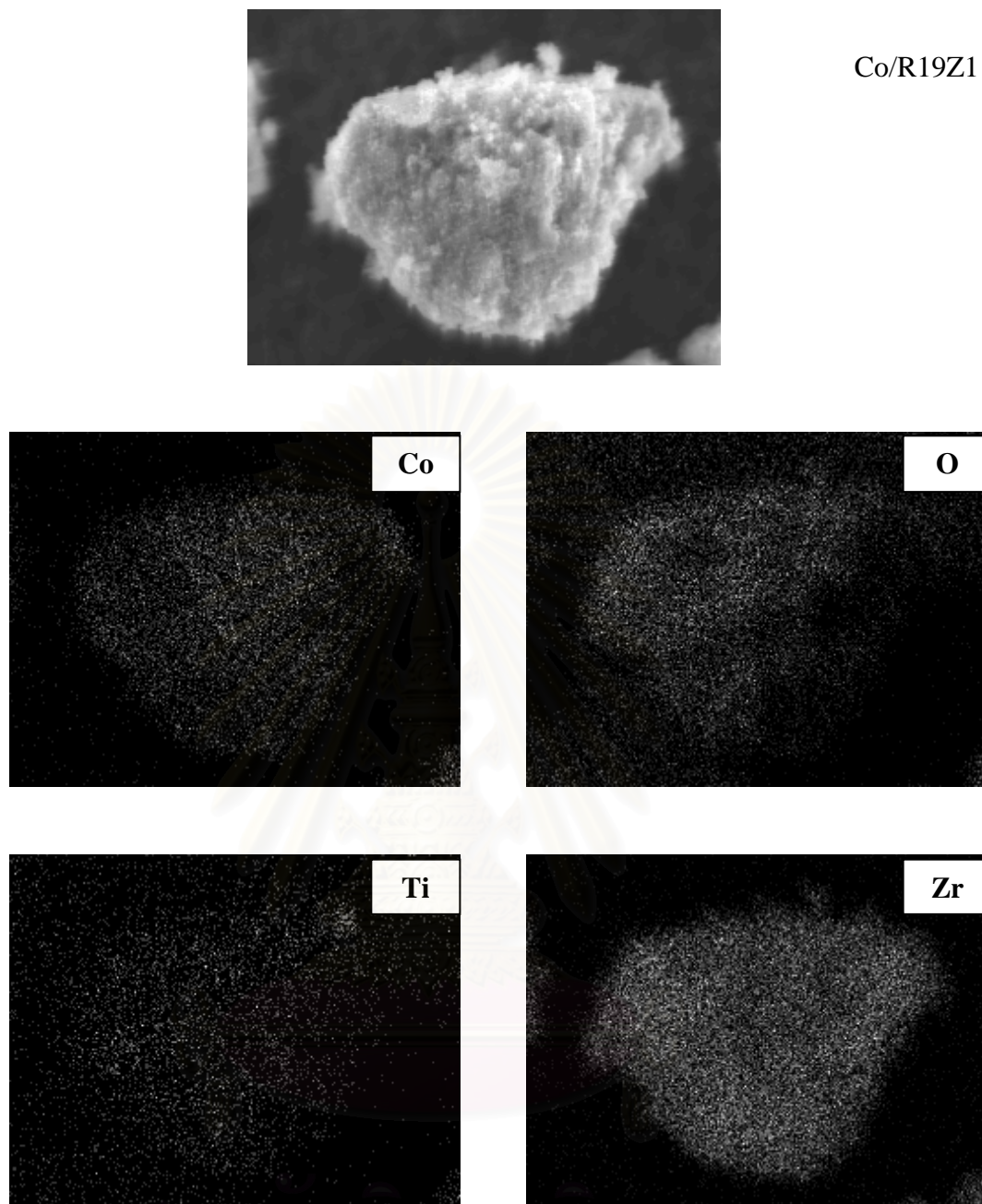


Figure 5.17 SEM micrograph and EDX mapping of Co/R19Z1 catalyst granule.

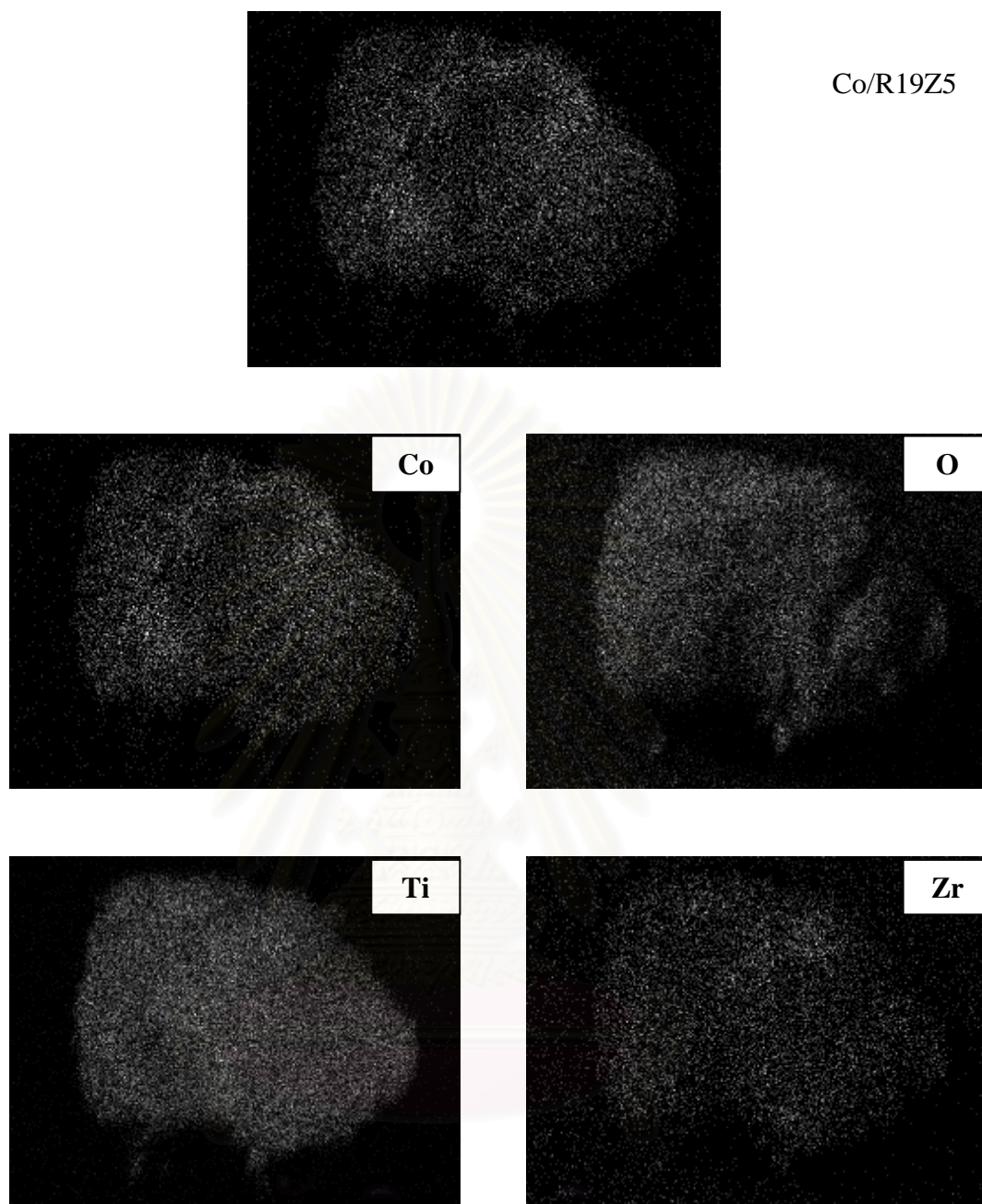


Figure 5.18 SEM micrograph and EDX mapping of Co/R19Z5 catalyst granule.

5.1.2.6 Transmission Electron Microscopy (TEM)

The TEM micrographs for all samples are shown in Figure 5.19. The dark spots represented cobalt oxide species present after calcination of samples dispersing on zirconia modified titania support. The average cobalt particle/cluster sizes from TEM are given in Table 5.9. It was found that the average cobalt particle/cluster diameters of cobalt oxide particles were 14.6, 16.2, 18.2 and 23.6 nm for Co/R0Z1, Co/R0Z5, Co/R19Z1 and Co/R19Z5, respectively. From these results, it was found that the diameter of cobalt oxide particles increased with increasing amount of zirconia.

Table 5.9 The average diameters of cobalt metals sizes from TEM for various percent loading of zirconia modified titania-supported Co catalysts.

Catalyst samples	The average diameters of cobalt metals sizes (nm)
Co/R0Z1	14.6
Co/R0Z5	16.3
Co/R19Z1	18.2
Co/R19Z5	23.6

สถาบันวิทยบริการ
จุฬาลงกรณ์มหาวิทยาลัย

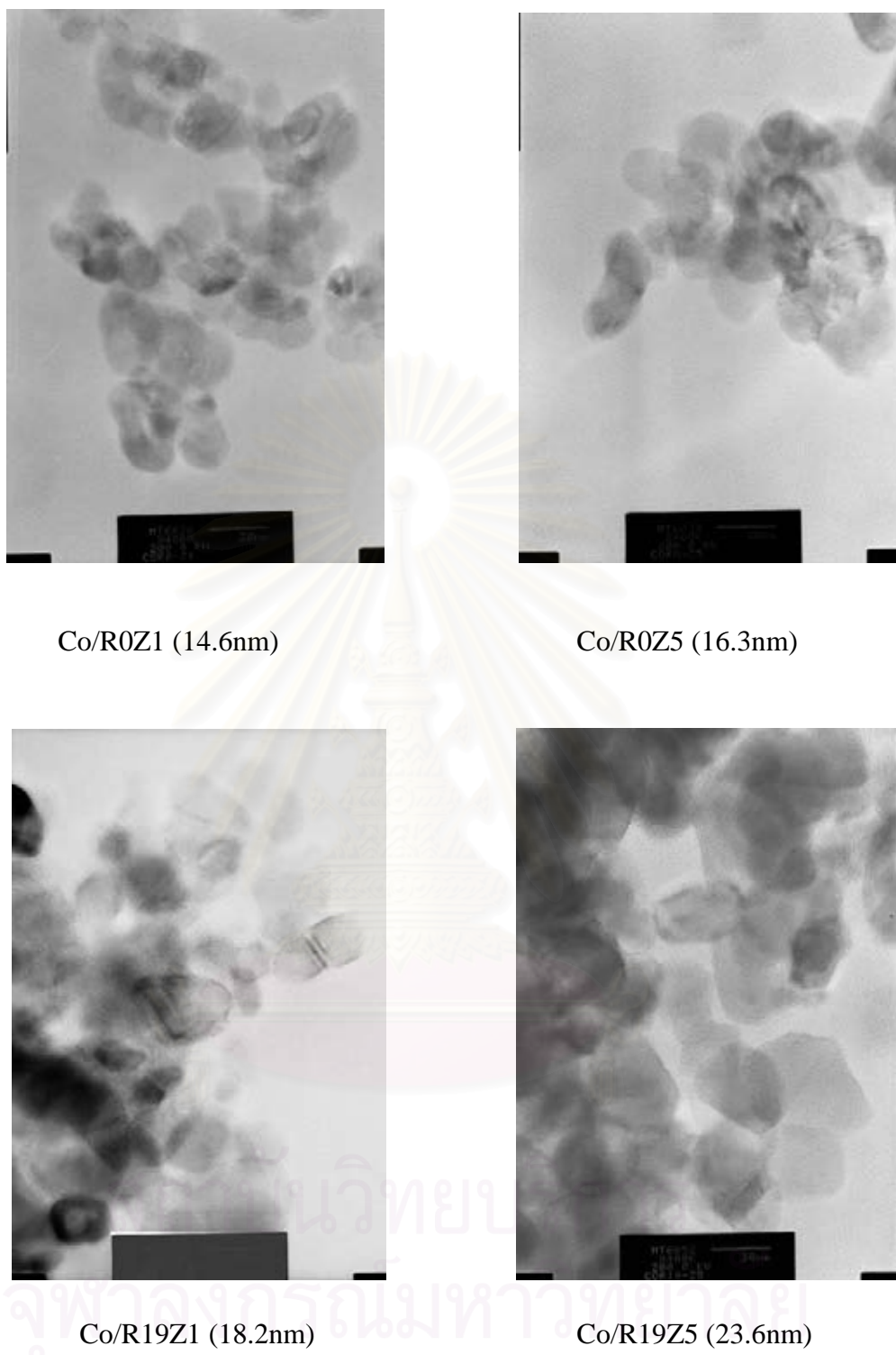


Figure 5.19 TEM micrographs of Co/R0Z1, Co/R0Z5, Co/R19Z1 and Co/R19Z5 catalysts.

5.1.2.7 Reaction study in CO hydrogenation

CO hydrogenation reaction was performed to determine the overall activity and product distribution of the Co catalysts with and without Zr modification. The results are shown in Table 5.10. It indicated that the reaction rate ranged between 0.009 and 1.4 $\text{gCH}_2/\text{g}_{\text{cat}}\text{h}^{-1}$ (initial) and between 0.009 and 0.8 $\text{gCH}_2/\text{g}_{\text{cat}}\text{h}^{-1}$ (steady-state) and CO conversion ranged between 0.025 to 3.7% (initial) and 0.023 to 2.1% (steady state) for pure anatase in titania-supported Co catalysts with and without Zr modification. It can be seen that reaction rate and CO conversion decreased with increasing the amount of zirconia. For 19% rutile in titania-supported Co catalysts with and without Zr modification, the reaction rate ranged between 28.8 and 37.44 $\text{gCH}_2/\text{g}_{\text{cat}}\text{h}^{-1}$ (initial) and between 26.52 and 37.44 $\text{gCH}_2/\text{g}_{\text{cat}}\text{h}^{-1}$ (steady-state) and CO conversion ranged between 76.92 to 100% (initial) and 71.07 to 100% (steady state). This also showed that the presence of zirconia (0.5-1%) as a support modifier increased significantly both the initial and the steady state. However, higher loading of zirconia (5%) tended to decrease the activity. Considering the product distribution, it can be observed that the addition of the Zr modifier resulted in no effect on selectivity of products, except in the case of Zr modified pure anatase in titania-supported Co catalysts.

It was found that the addition of zirconia on pure anatase in titania support did not enhance the activity for CO hydrogenation reaction. A low activity was due to the low reducibility during TPR at 35-800°C of cobalt species in the former catalysts, probably in the form of cobalt titanate as discussed before. For the Co/R19Z0.5 and Co/R19Z1, the increase in catalyst activity appears to be mainly due to the increase of cobalt active sites (from H_2 chemisorption) and reducibility. Nevertheless, there is no significant change in $\text{C}_2\text{-C}_4+$ selectivity of the hydrocarbon product. It should be mentioned there is no effect on selectivity with the increase of zirconia loading. Similar to what has been reported by Iglesia *et al.* (1992, 1997), the increase of the surface cobalt active site leads to the increase of the density of Co surface atoms on the support induced by addition of Zr, enhancing the activity for FTS reaction. Xiong *et al.* (2005) studied the catalytic performance of zirconium-modified $\text{Co}/\text{Al}_2\text{O}_3$ for Fischer-Tropsch synthesis. They reported that increasing zirconium loading effectively inhibited the formation of CoAl_2O_4 phase on the

catalysts. It gave rise to the increase of Co metal active sites and reducibility, leading to the increase of CO hydrogenation activity. In addition, Moradi *et al.* (2003) suggested that Co-silica interaction was replaced by a Co-zirconia interaction. It leads to a higher degree of reduction of cobalt and increase in the metallic atoms on the surface. However, higher loading of zirconia (Co/R19Z5) acted to partially block the cobalt metal sites (Ali 1995). For these results it appears that there was an optimum percent zirconia loading, beyond which some Co site blockage may have occurred.

Table 5.10 Reaction rate for CO hydrogenation on the various percent loading of zirconia modified titania-supported Co catalysts.

Samples	CO conversion (%) ^a		Rate (gCH ₂ /g _{cat} h ⁻¹) ^b		CH ₄ selectivity (%)		C ₂ -C ₄ + selectivity (%)	
	Initial ^c	SS ^d	Initial	SS	Initial	SS	Initial	SS
	Co/R0	3.70	2.10	1.40	0.80	71	68	29
Co/R0Z0.5	3.09	0.60	1.16	0.22	32	31	68	69
Co/R0Z1	0.054	0.042	0.020	0.016	97	96	3	4
Co/R0Z5	0.025	0.023	0.0093	0.0086	98	90	2	10
Co/R19	89.05	71.07	33.23	26.52	98	98	2	2
Co/R19Z0.5	100.00	100.00	37.33	37.33	98	98	2	2
Co/R19Z1	100.00	100.00	37.44	37.44	97	96	3	4
Co/R19Z5	76.92	72.10	28.80	27.00	97	97	3	3

^a CO hydrogenation was carried out at 220°C, 1 atm, and H₂/CO/Ar = 20/2/8 cc/min.

^b Error ±5%

^c After 5 min of reaction

^d After 5 h of reaction

5.1.3 Titania-Silica mixed oxide-supported Co catalysts

The TiO₂-SiO₂ mixed oxide has been considered to be very attractive as catalysts and supports, which have brought much attention in recent years. It was reported that TiO₂-SiO₂ mixed materials have been used as catalysts and supports for various reactions (Gao *et al.*, 1999). However, the use of this mixed oxide support here with the cobalt catalyst has not been reported yet. This TiO₂-SiO₂ mixed oxide would lead to robust catalytic supports of cobalt catalyst for carbon monoxide (CO) hydrogenation reaction. The ratios of TiO₂/SiO₂ used were varied. The mixed oxide supports and catalyst precursors were prepared, characterized and tested for CO hydrogenation.

5.1.3.1 BET surface area

BET surface areas of Titania-Silica mixed oxide unsupported and supported Co catalysts are also shown in Table 5.11. BET surface areas of Titania-Silica mixed oxide support increased from 70 m²/g for the Ti/Si = 1/0 sample (pure titania) to 300 m²/g for the Ti/Si = 0/1 sample (pure silica). It found that the BET surface area increased with increasing amount of silica. After loading 20 %wt Co, BET surface areas decreased. The loss of surface area due to adding cobalt on mixed oxide support. The BET surface area of Titania-Silica mixed oxide-supported Co catalysts were ranged between 52 to 262 m²/g for the Co_1/0 to Co_0/1 sample. The significant decrease in surface area of the original mixed oxide support material suggests that cobalt was deposited significantly in the pores of support.

Table 5.11 BET surface area measurement of Titania-Silica mixed oxide unsupported and supported Co catalysts.

Supports	BET surface area (m ² /g) ^a	Catalyst samples	BET surface area (m ² /g) ^a
Ti/Si = 1/0	70	Co_1/0	52
Ti/Si = 8/2	138	Co_8/2	83
Ti/Si = 6/4	196	Co_6/4	145
Ti/Si = 4/6	239	Co_4/6	166
Ti/Si = 2/8	257	Co_2/8	230
Ti/Si = 0/1	300	Co_0/1	262

^a Measurement error is $\pm 2\%$.

5.1.3.2 Temperature programmed reduction (TPR)

Temperature-programmed reduction (TPR) on the calcined samples needs to be performed in order to give a better understanding according to such a reduction behavior. The TPR profiles for all samples are shown in Figure 5.20. From these profiles the initial, final and maximum temperatures for each catalyst sample are given in Table 5.12. It was found that there was only one reduction peak, however, at different reduction temperatures for all calcined samples. This peak can be assigned to the overlap of two-step reduction of Co₃O₄ (Kraum and Baern, 1999; Voß *et al.*, 2003). These peaks have been related to the following reduction steps: Co₃O₄ → CoO and CoO → Co⁰ (Co metal). However, prolonged calcination or reduction and recalcination results in complete decomposition of any cobalt nitrates present (Kogelbauer *et al.*, 1996).

The lowest reduction temperatures located at ca. 280– 600°C (max. at 450°C) was observed on the Co/SiO₂ sample (Co_0/1) as shown in Table 5.12. However, the reduction temperatures were found to dramatically shift to lower temperatures with increasing the amounts of silica present in the mixed oxide

supports. Thus, the highest reduction temperatures located at ca. 370-695°C (max. at 550°C) can be observed for the Co/TiO₂ sample (Co_1/0). The presence of titania can be attributed to the strong support interaction between the cobalt oxides and titania (Riva *et al.*, 2000). This was suggested that with the presence of silica it was easier for the cobalt oxide species to be reduced at the specified condition than those in titania itself. However, since the catalyst samples were reduced at different temperatures, it may not be useful to compare the reducibility of samples at this condition.

Table 5.12 Initial, final and maximum temperatures from TPR profiles and H₂ chemisorption results for Titania-Silica mixed oxide-supported Co catalysts.

Catalyst samples	Temperature (°C)			Total H ₂ chemisorption ($\mu\text{mol H}_2/\text{g}_{\text{cat}}$) ^a
	Initial	Final	Maximum	
Co_1/0	370	695	550	0.42
Co_8/2	365	720	565	0
Co_6/4	340	685	535	0.22
Co_4/6	340	680	510	1.85
Co_2/8	335	675	475	10.70
Co_0/1	280	600	450	11.11

^a Error = \pm 5% of measurement of H₂ chemisorption.

5.1.3.3 H₂ chemisorption

Besides, the number of reduced Co metal surface atoms can be calculated directly from the H₂ chemisorption results, which is more acceptable since all catalysts samples are reduced at the standard reduction condition. It is known that the active form of supported cobalt FTS catalysts is cobalt metal (Co⁰). Thus, reduction of cobalt oxide species is essentially performed in order to transform cobalt oxide species obtained after calcination process into the active cobalt metal atoms for catalyzing the reaction. Therefore, the static H₂ chemisorption on the reduced cobalt samples was used to determine the number of reduced cobalt metal surface atoms. This is usually related to the overall activity of the catalyst during carbon monoxide (CO) hydrogenation. The resulted H₂ chemisorption for all samples are shown in Table 5.12. It revealed that the number of reduced cobalt metal surface atoms increased with the amounts of silica present in the mixed oxide supports and no number of reduced cobalt metal surface atoms occurred in the Co_{8/2} catalyst (total H₂ chemisorption equal zero). These results were corresponding with those from the TPR as mentioned before.

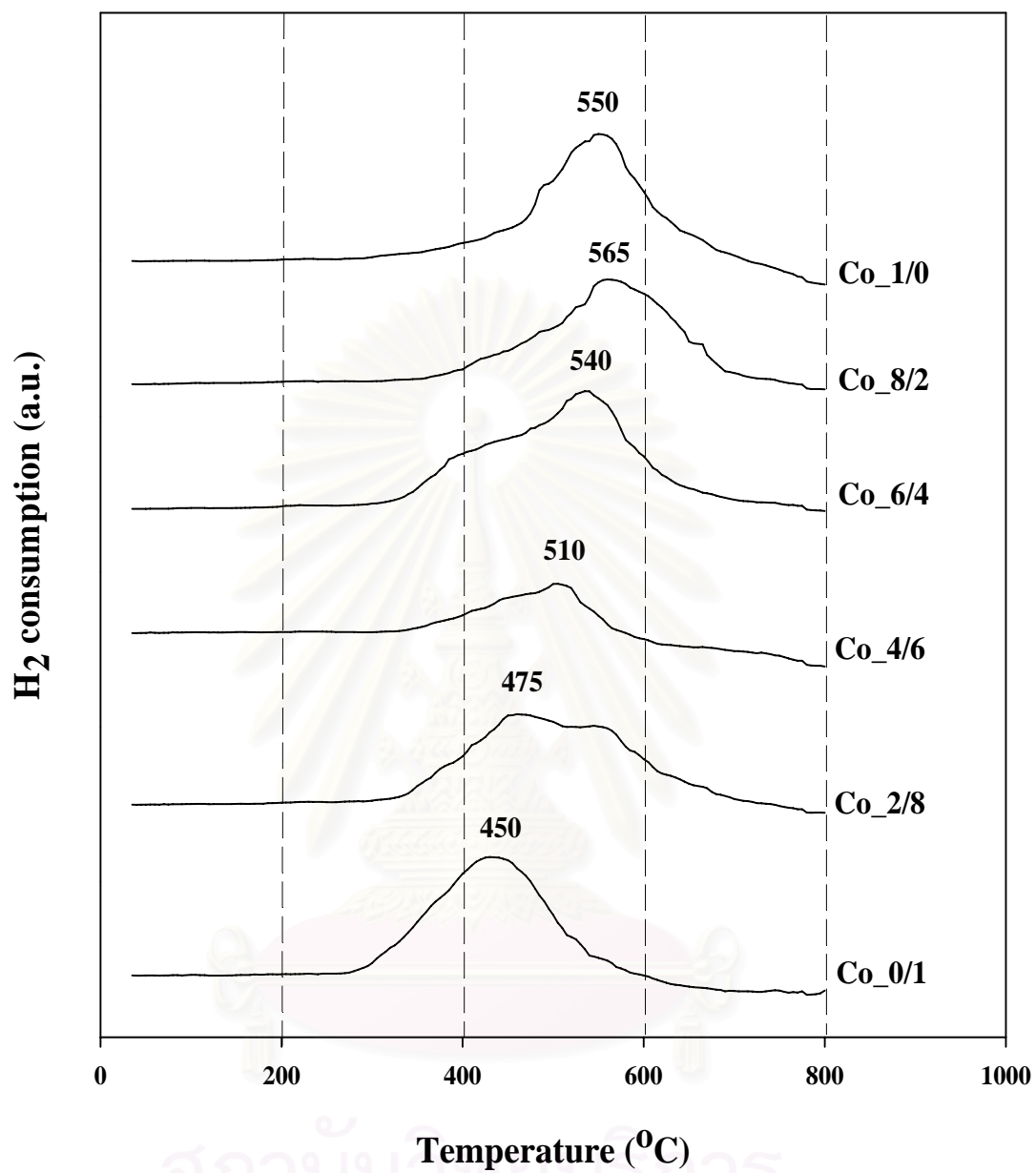


Figure 5.20 TPR profiles of Titania-Silica mixed oxide-supported Co catalysts.

5.1.3.4 X-ray diffraction (XRD)

The XRD patterns of mixed $\text{TiO}_2\text{-SiO}_2$ supports before impregnation with the cobalt precursor are shown in Figure 5.21. It was observed that the pure silica exhibited a broad XRD peak assigning to the conventional amorphous silica. Similar to the pure silica, the XRD patterns of pure titania indicated only the characteristic peaks of anatase titania at 25° (major), 37° , 48° , 55° , 56° , 62° , 71° , and 75° . XRD patterns of the mixed oxide supports containing various ratios of titania and silica revealed the combination of titania and silica supports based on their contents. It can be seen that the intensity of XRD characteristic peaks for both supports was changed based on the ratios of titania and silica.

After impregnation with the cobalt precursor and calcination, all samples of $\text{Co/TiO}_2\text{-SiO}_2$ catalyst were again identified using XRD. The XRD patterns of all calcined samples are shown in Figure 5.22. After calcination, all samples exhibited XRD peaks, which were identical with those for the corresponding mixed oxide supports used as seen in Figure 5.21. This indicated that there was no further phase transformation from anatase to rutile occurred after calcination (at temperature ca. 500°C for 4 h). The amorphous silica also exhibited good stability upon the same calcination process. Besides the corresponding mixed oxide supports detected, all calcined samples also exhibited weak XRD peaks at 31° , 36° , and 65° , which were assigned to the presence of Co_3O_4 . Based on XRD results, it indicated that the presence of Co_3O_4 was apparently in the highly dispersed form.

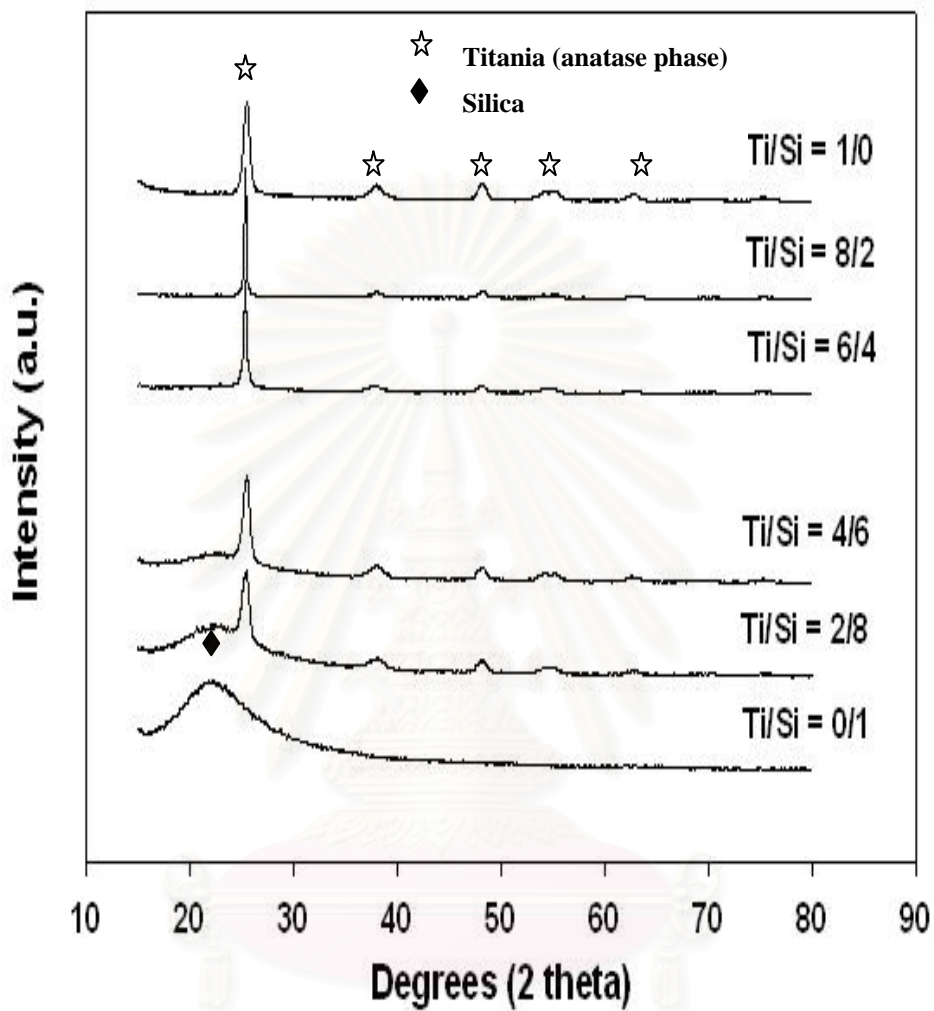


Figure 5.21 XRD patterns of Titania-Silica mixed oxide support samples.

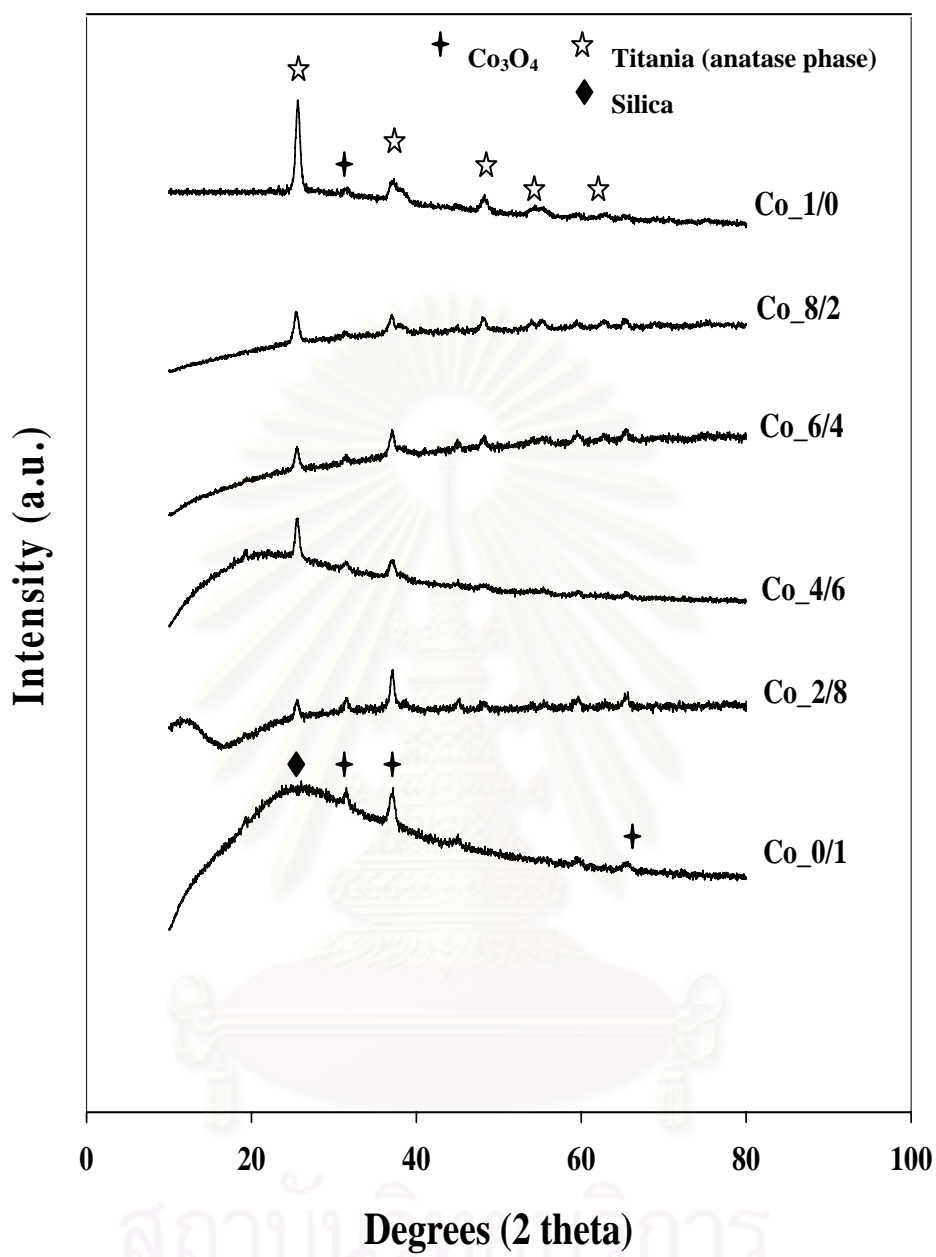


Figure 5.22 XRD patterns of Titania-Silica mixed oxide-supported Co catalyst samples.

5.1.3.5 Raman spectroscopy

Raman spectroscopy is one of the most powerful techniques used to identify the metal oxide species present. It was found that the titania support exhibited the Raman bands at 640, 514 and 397 cm^{-1} for TiO_2 in its anatase form (Jongsomjit *et al.*, 2005) whereas silica was the Raman insensitive upon the scanning range applied. The Raman spectra for all calcined samples as shown in Figure 5.23 exhibited the Raman bands of the titania support as mentioned above with two shoulders at 690 and 480 cm^{-1} , assigned to Co_3O_4 (Jongsomjit *et al.*, 2001; 2003; 2005) with corresponding to those with XRD.



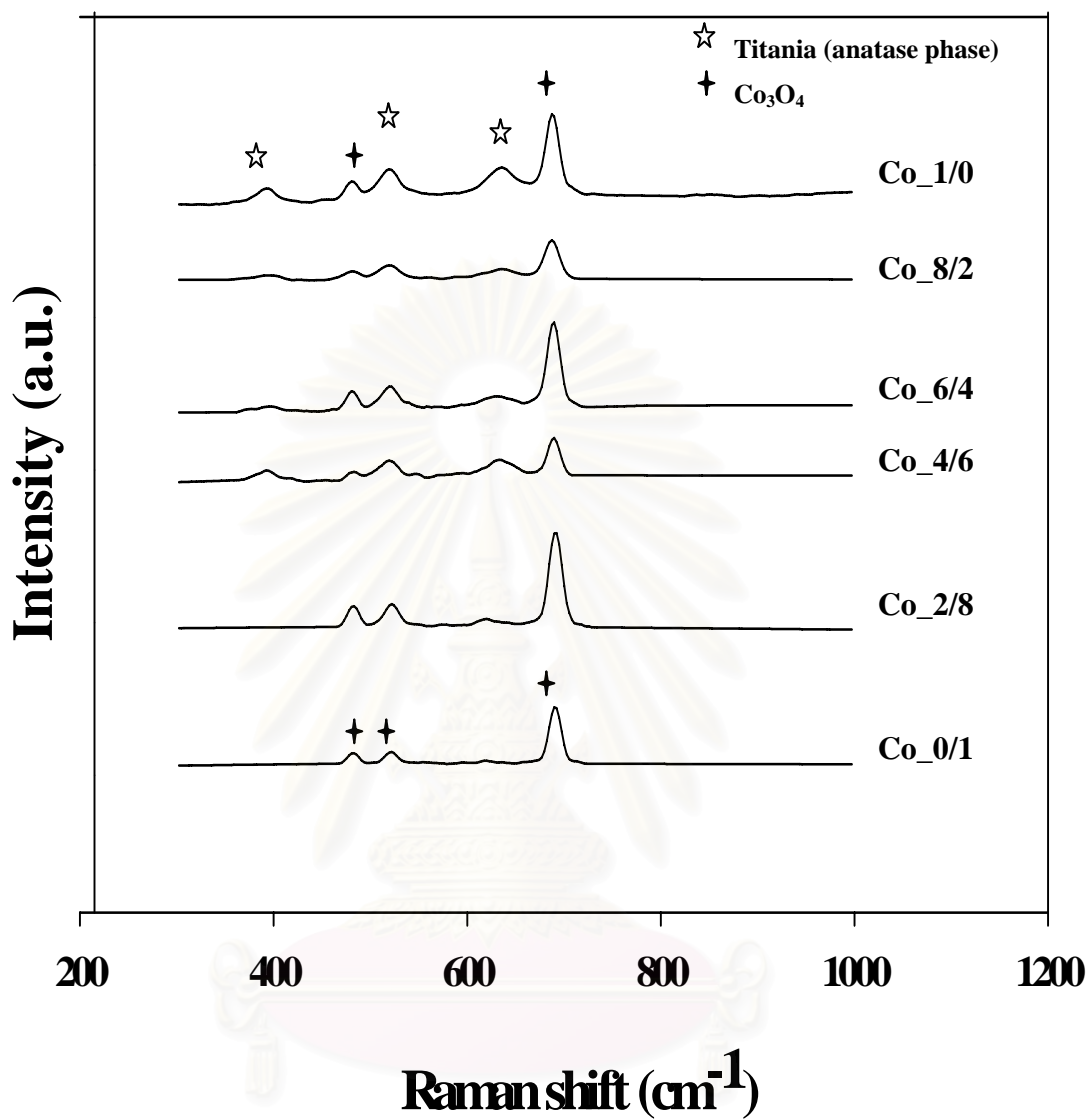


Figure 5.23 Raman spectra of Titania-Silica mixed oxide-supported Co catalysts.

5.1.3.6 Electron microscopy

The morphologies of the catalyst samples and elemental distributions of the catalyst samples were determined using SEM and EDX, respectively. Apparently, SEM micrographs and EDX mapping exhibited similar trends of morphologies and elemental (Co, Si, Ti, and O) distributions. The typical SEM micrographs along with the EDX mapping (for Co, Si, and O) of Co₀/1 sample (Co/SiO₂) are illustrated in Figure 5.24 indicating the external surface of the sample granule. It can be seen that the cobalt oxide species were well distributed (shown on EDX mapping) all over the sample granule.

In order to determine the morphologies and elemental distributions of cobalt oxides on the mixed TiO₂-SiO₂ supports, the typical SEM micrographs along with the EDX mapping (for Co, Si, Ti, and O) are shown in Figure 5.25-5.28 for Co₂/8, Co₄/6, Co₆/4 and Co₈/2 samples, respectively, which is similar with those as seen in Co₀/1 sample. And the typical SEM micrograph along with the EDX mapping (for Co, Ti, and O) for Co₁/0 sample (Co/TiO₂) is illustrated in Figure 5.29. However, as obvious charged surface under SEM electron bombarding is visible in Co₀/1 sample. Besides the observation of well distribution for cobalt oxide species, it indicated that titania was apparently located on the outer surface of silica. The connectivity of Si-O-Ti can be confirmed by the IR spectroscopy indicating the IR bands at ca. 980 and 1100 cm⁻¹ (Dutoit *et al.*, 1995; Jongsaomjit *et al.*, 2005).

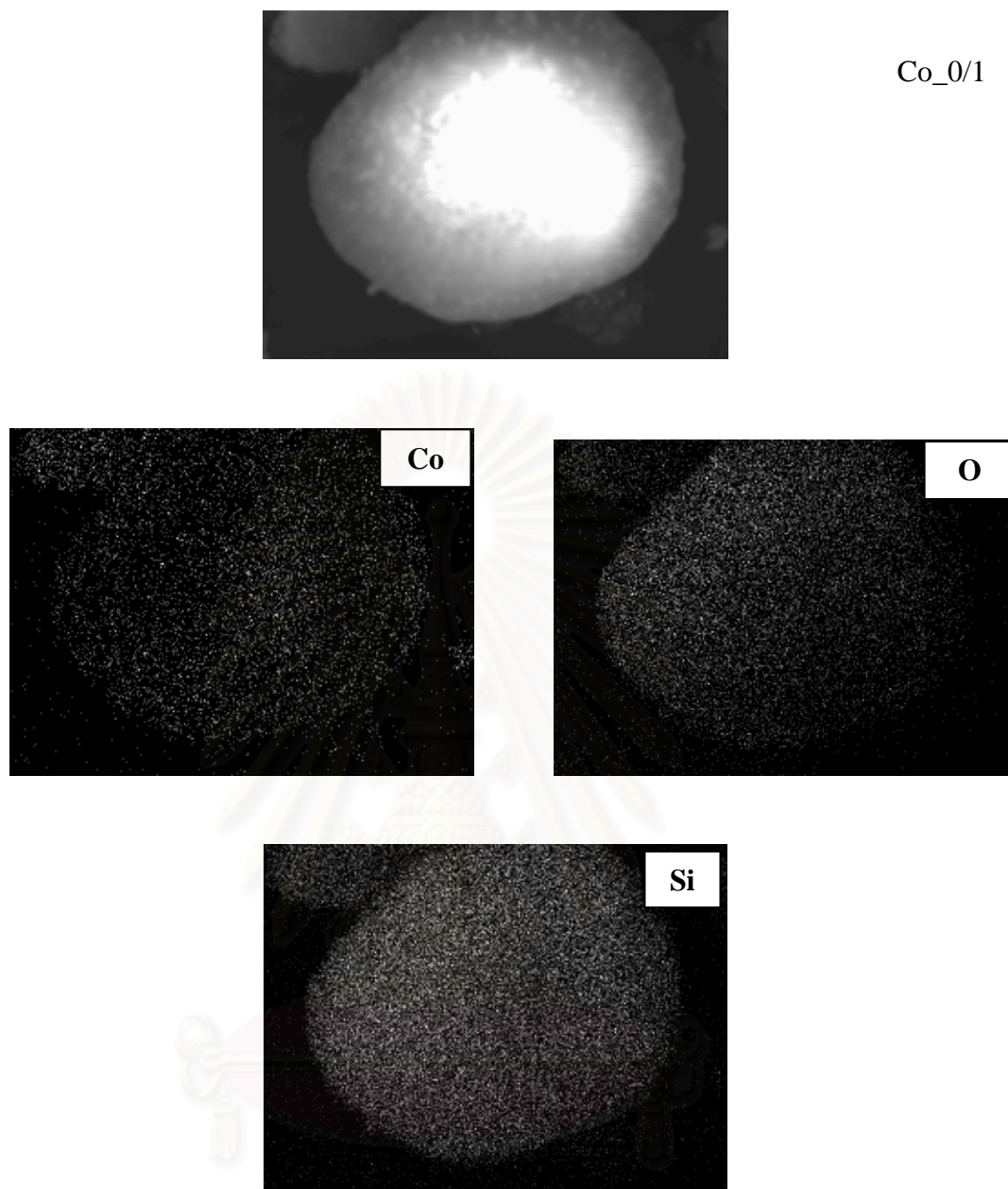


Figure 5.24 SEM micrographs and EDX mapping of Co₀/1 catalyst granule.

สภามหาวิทยาลัย
จุฬาลงกรณ์มหาวิทยาลัย

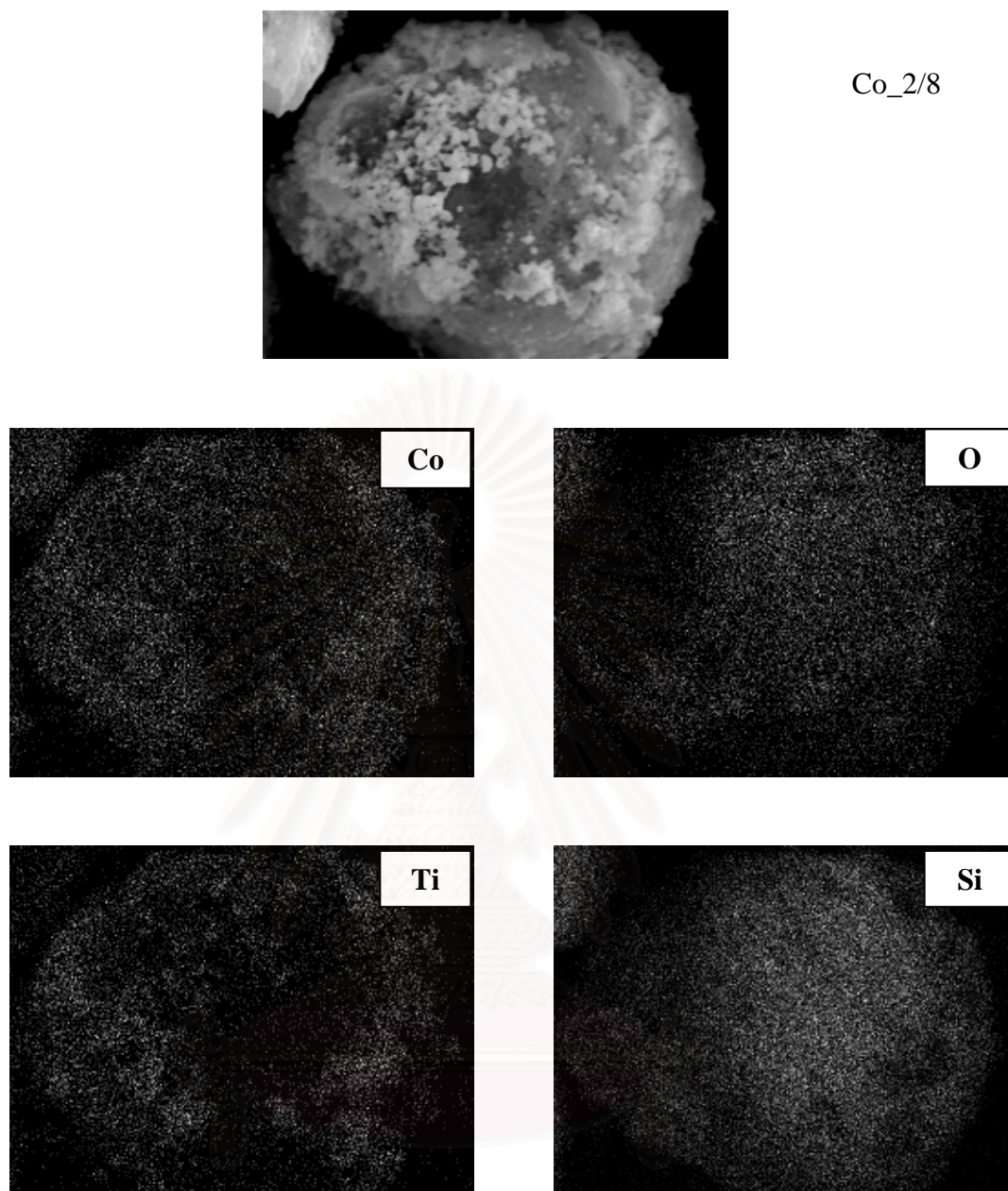


Figure 5.25 SEM micrographs and EDX mapping of Co₂/8 catalyst granule.

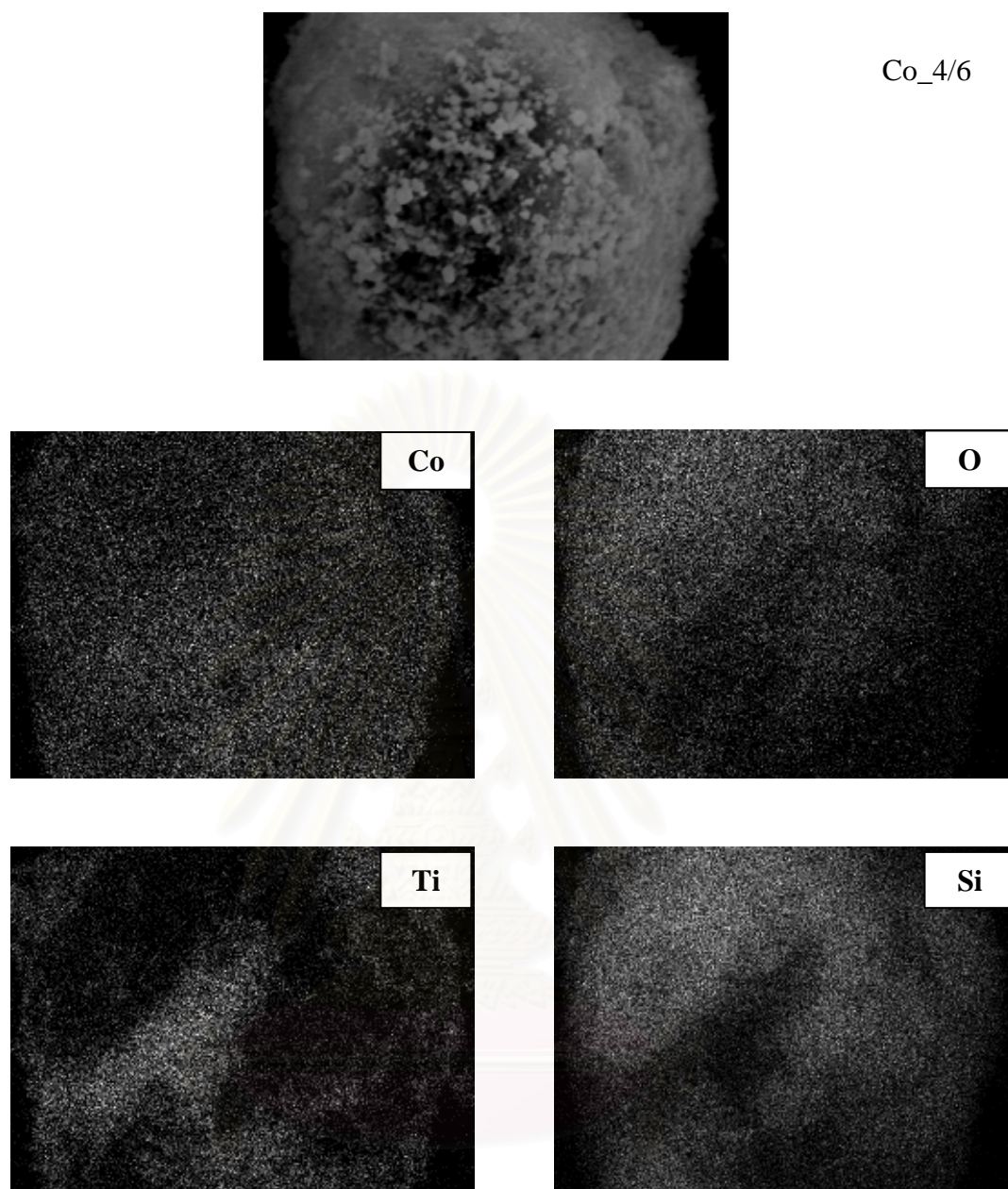


Figure 5.26 SEM micrograph and EDX mapping of Co_{4/6} catalyst granule.

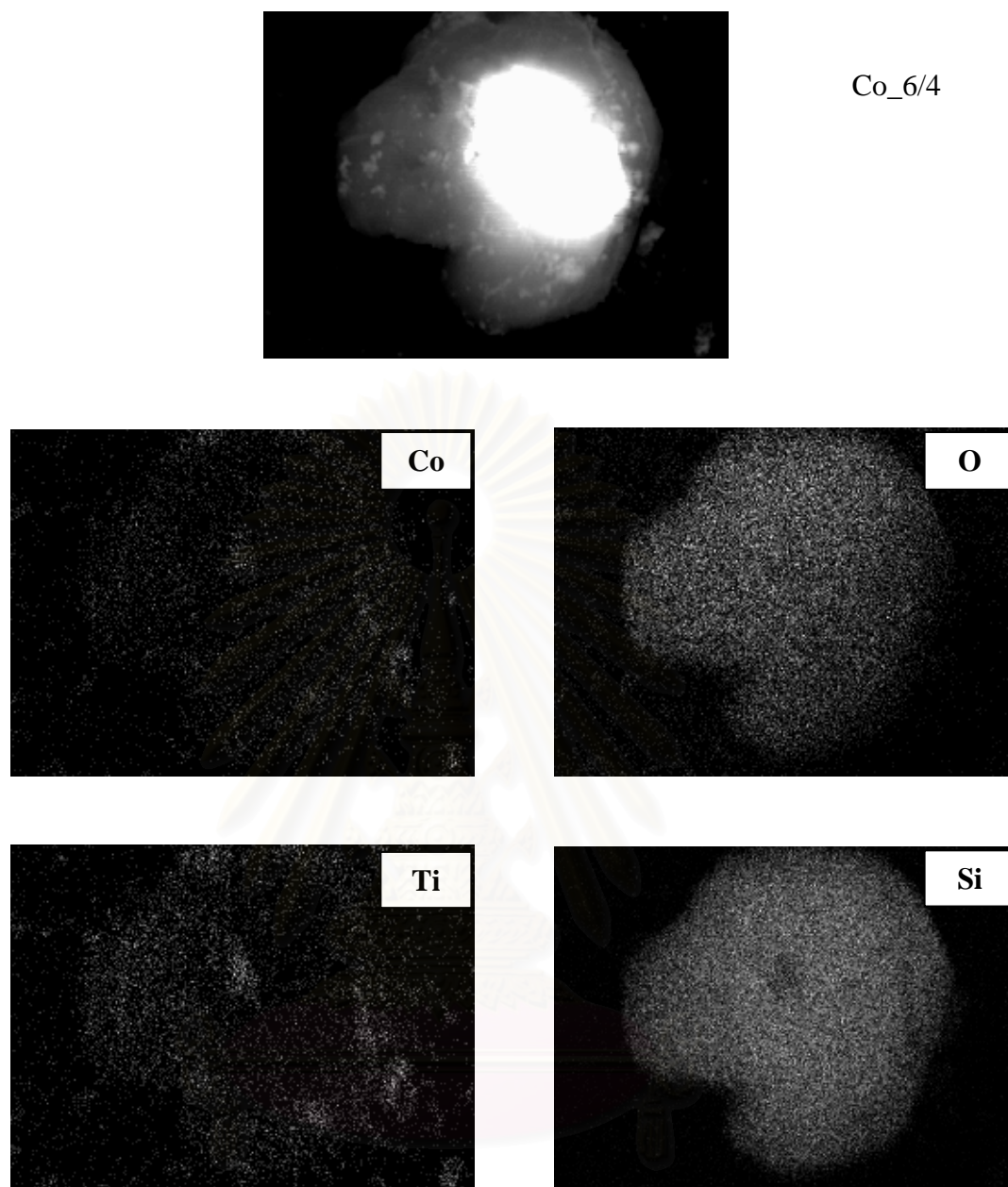


Figure 5.27 SEM micrograph and EDX mapping of Co_{6/4} catalyst granule.

สงวนลิขสิทธิ์
จุฬาลงกรณ์มหาวิทยาลัย

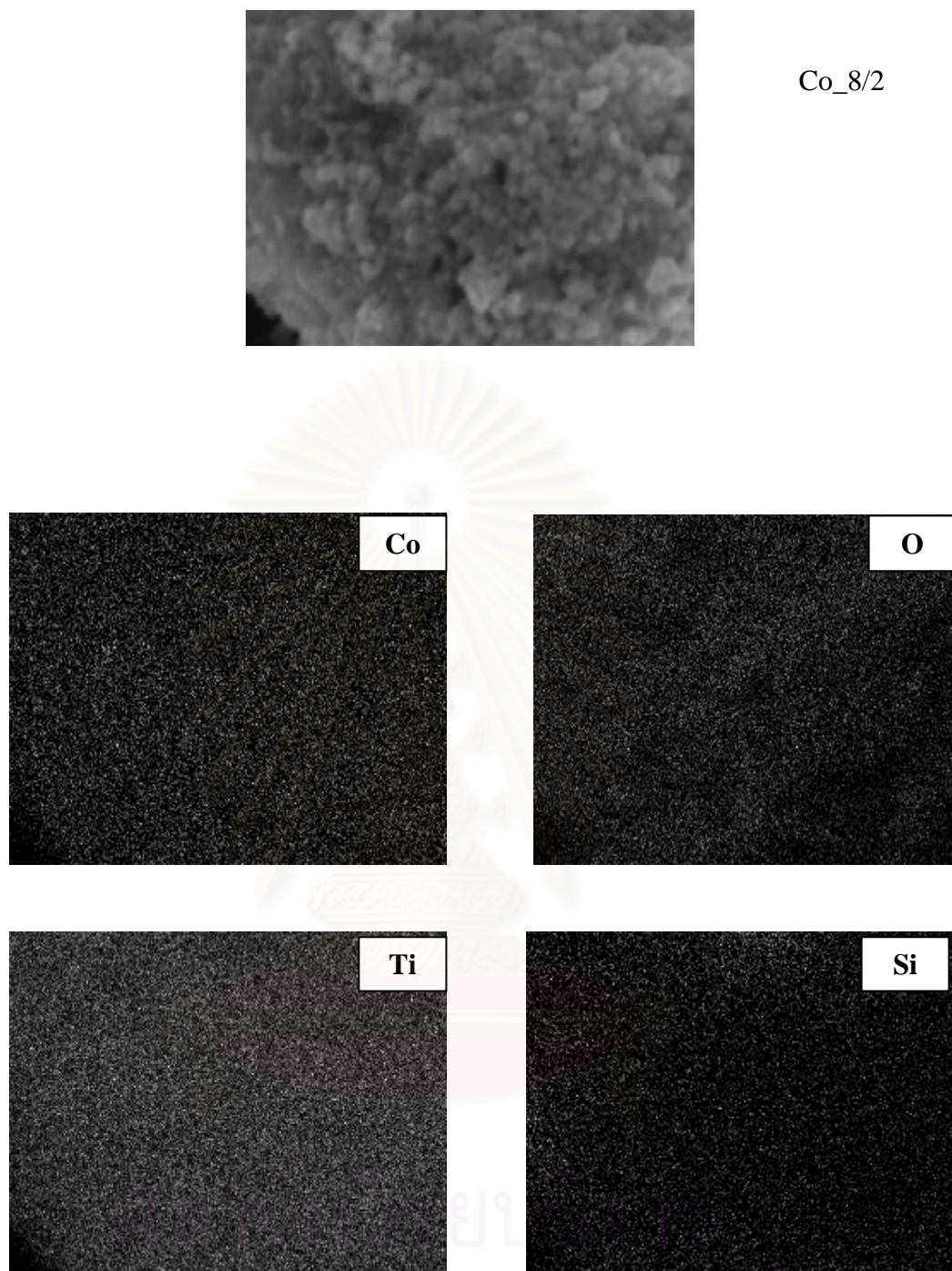


Figure 5.28 SEM micrograph and EDX mapping of Co_{8/2} catalyst granule.

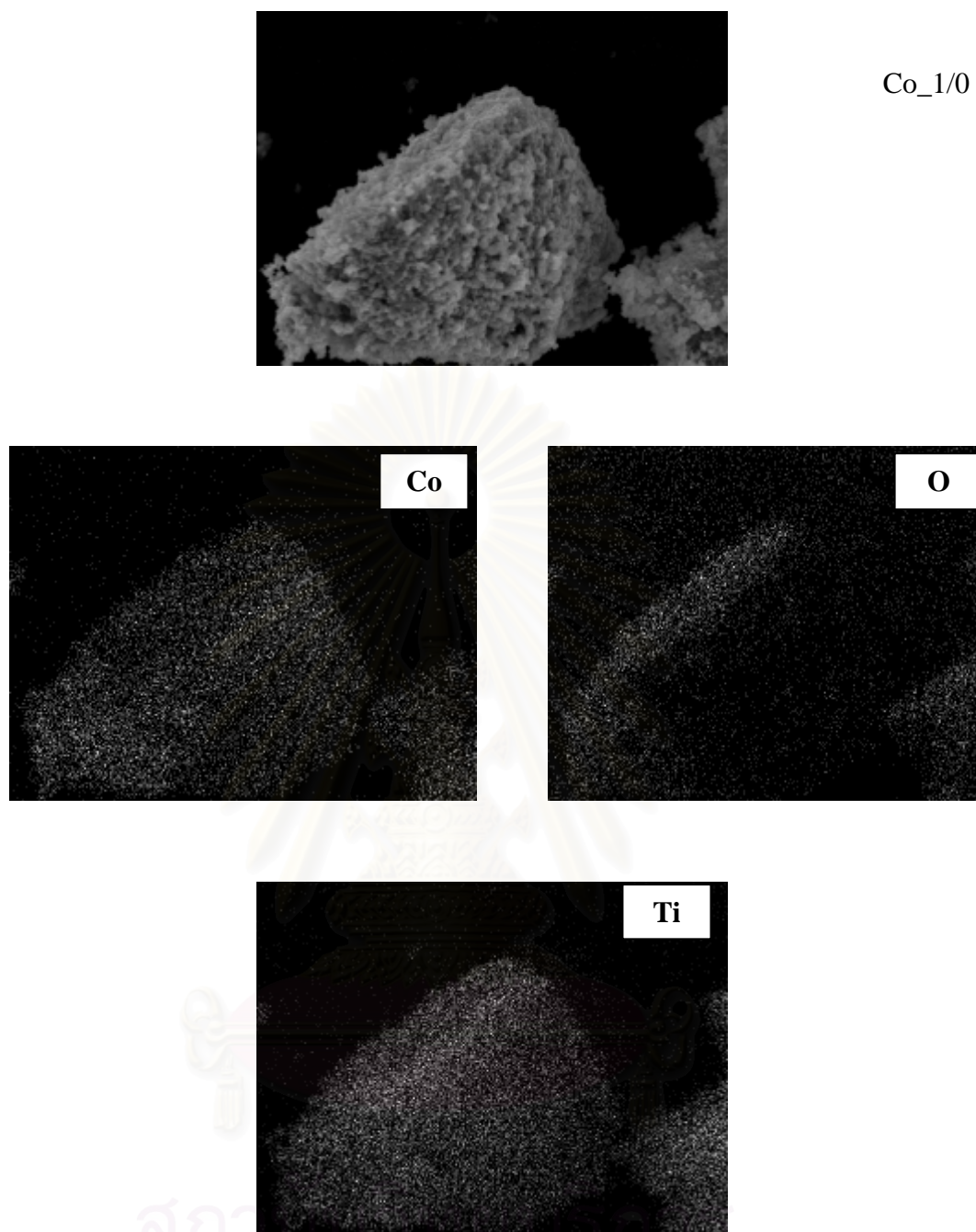


Figure 5.29 SEM micrograph and EDX mapping of Co₁/0 catalyst granule.

5.1.3.7 Transmission Electron Microscopy (TEM)

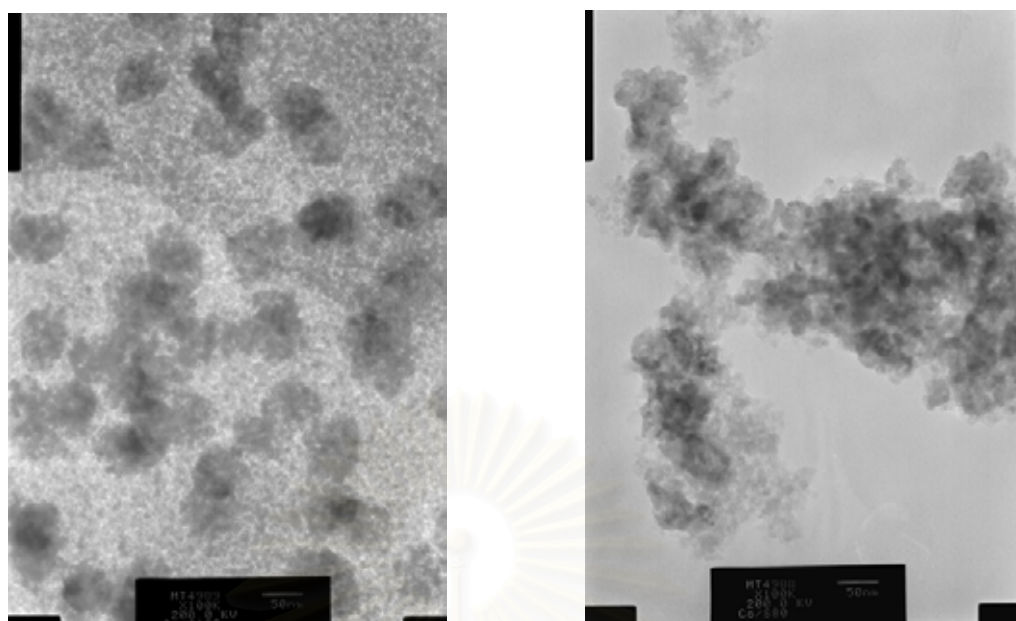
In order to determine the dispersion of cobalt oxide species on the various mixed oxide supports, a more powerful technique such as TEM was applied to all samples. The TEM micrographs for all samples are shown in Figure 5.30 and 5.31, respectively. The dark spots represented cobalt oxide species or patches dispersing on the various mixed $\text{TiO}_2\text{-SiO}_2$ supports. The average cobalt particle/cluster sizes from TEM are given in Table 5.13. It was found that the average cobalt particle/cluster diameters of cobalt oxide particles were ranged between 10.5 to 15.2 nm and increased with increasing amount of silica.

It can be observed that a highly dispersed form of cobalt oxide species trended to be achieved with the presence of titania in the mixed oxide supports resulting in an appearance of smaller cobalt oxide patches. When combined the Raman spectroscopic results with those from TEM, it is likely that larger shoulders at 690 and 480 cm^{-1} would result in more dispersion of Co. It should be mentioned that although the more highly dispersed cobalt oxide patches with the presence of titania their distributions seen by TEM were not as good as those seen in the pure silica support. On the other hand, the cobalt oxide patches present on the pure silica support exhibited better distribution, however, with lower degree of dispersion than any other samples. This can be attributed to higher surface areas of the silica support itself. It should be mentioned that high surface area of support could result in better distribution of Co, but somehow does not guarantee good dispersion (small Co patches). Besides, the highly dispersed form of cobalt oxide species could not guarantee the large number of reduced cobalt metal surface atoms. In addition, the highly dispersed form of cobalt oxide species, the interaction of those with the specified supports has to be essentially considered.

Table 5.13 The average diameters of cobalt metals sizes from TEM for various ratios of rutile to anatase phase of titania-supported Co catalysts.

Catalyst samples	The average diameters of cobalt metals sizes (nm)
Co_1/0	10.5
Co_8/2	10.7
Co_6/4	11.9
Co_4/6	12.5
Co_2/8	14.4
Co_0/1	15.2

สถาบันวิทยบริการ
จุฬาลงกรณ์มหาวิทยาลัย



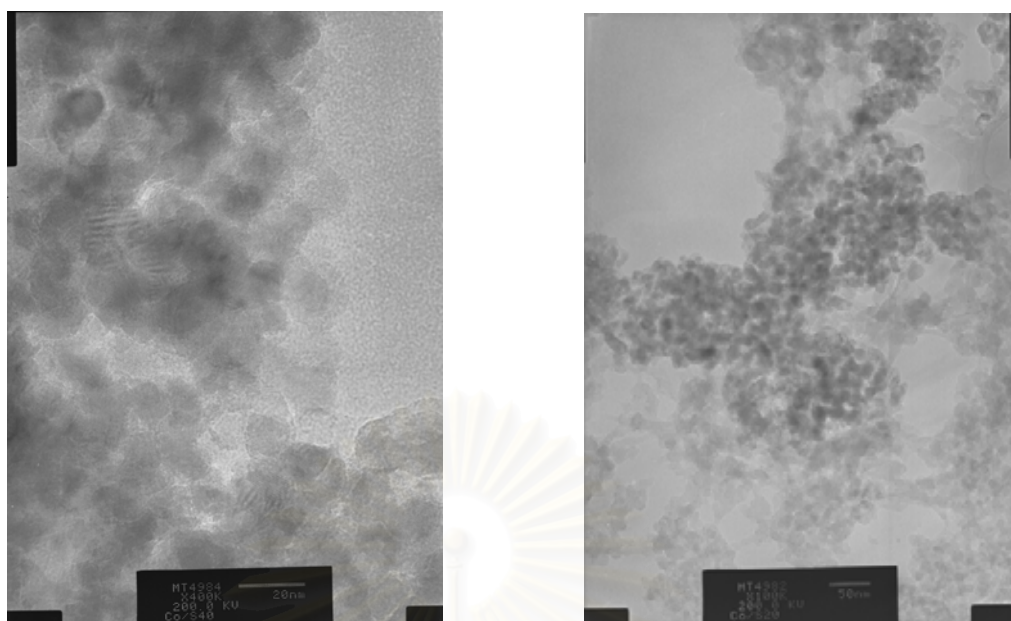
Co_0/1 (15.2 nm)

Co_2/8 (14.4 nm)



Co_4/6 (12.5 nm)

Figure 5.30 TEM micrographs of Co_0/1, Co_2/8 and Co_4/6 catalysts.

Co_{6/4} (11.9 nm)Co_{8/2} (10.7 nm)Co_{1/0} (10.5 nm)**Figure 5.31** TEM micrographs of Co_{6/4}, Co_{8/2} and Co_{1/0} catalysts.

5.1.3.8 Reaction study in CO hydrogenation

The resulted reaction study is also shown in Table 5.14. As expected, based on the H₂ chemisorption results, the overall activities for both initial and steady-state rates dramatically increased with the amounts of silica present on the mixed oxide supports. This was basically due to the large number of reduced cobalt metal surface atoms with the presence of silica as seen by the H₂ chemisorption results along with higher surface area of silica as mentioned earlier. However, with some consideration on the product selectivity obtained, an interesting discovery can be observed.

Considering the selectivity of product, it showed that the selectivity to methane essentially increased with the amounts of silica in the supports. On the other hand, more amounts of longer chain hydrocarbons (C₂-C₅) can be obtained with the presence of titania in the mixed supports. It is known that CO hydrogenation is a kind of polymerization reactions where insertion of the -CH₂- (methylene group) occurs through the active center. Thus, the product distribution strongly depends on the nature of active centers, rate of propagation, and rate of termination. Obviously, the termination of chain growth occurs and is recognized as the chain growth probability. Based on product selectivity found here, it can be concluded that the presence of titania in the mixed supports apparently inhibited the chain growth probability resulting in the observation of longer chain hydrocarbons even at the specified methanation condition. In order to study this effect in more details, the reaction intermediates at specified conditions must be further investigated with more powerful techniques such as the steady-state isotropic transient kinetic analysis (SSITKA) which has been successfully done by Goodwin and coworkers (Ali *et al.*, 1995, Vada *et al.*, 1995, Ali *et al.*, 1998, Panpranot *et al.*, 2002; Jongsomjit *et al.*, 2003).

Table 5.14 Reaction rate for CO hydrogenation on the Titania-Silica mixed oxide-supported Co catalysts.

Samples	CO conversion (%) ^a		Rate (gCH ₂ /g _{cat} h ⁻¹) ^b		CH ₄ selectivity (%)		C ₂ -C ₄ + selectivity (%)	
	Initial ^c	SS ^d	Initial	SS	Initial	SS	Initial	SS
	Co_1/0	3.7	2.1	1.4	0.8	71	68	29
Co_8/2	0	0	0	0	0	0	0	0
Co_6/4	7.2	1.8	2.7	0.7	82	74	18	26
Co_4/6	38.1	26.7	14.2	10.0	87	87	13	13
Co_2/8	86.4	81.5	32.2	30.4	95	95	5	5
Co_0/1	96.3	92.0	38.9	34.3	99	99	1	1

^a CO hydrogenation was carried out at 220°C, 1 atm, and H₂/CO/Ar = 20/2/8 cc/min.

^b Error ±5%

^c After 5 min of reaction

^d After 5 h of reaction

สถาบันวิทยบริการ
จุฬาลงกรณ์มหาวิทยาลัย

CHAPTER VI

CONCLUSIONS AND RECOMMENDATION

This chapter is focused upon the conclusions of the experimental details of the characteristics and catalytic properties of Co/TiO₂ for various rutile:anatase ratios, effect of zirconia-modified titania consisting of different phases on catalytic properties of Co/TiO₂ catalysts and catalytic behaviors of mixed TiO₂-SiO₂-supported cobalt Fischer-Tropsch catalysts which was described in section 6.1. In addition, Recommendations for further study are given in section 6.2.

6.1 Conclusions

6.1.1 Various ratios of rutile to anatase phase of titania-supported Co catalysts

A dependence of the characteristics and catalytic properties during CO hydrogenation on the ratio of rutile/anatase in titania revealed that the presence of 19% rutile phase in titania for Co/TiO₂ (Co/R19) exhibited the highest activity during CO hydrogenation. It appeared that the increase in activity was due to two reasons; i) the presence of rutile phase in titania can facilitate the reduction process of cobalt oxide species into reduced cobalt metal, and ii) the presence of some rutile phase resulted in a larger number of reduced cobalt metal surface atoms, which is related to the activity during CO hydrogenation. However, if the ratio of rutile to anatase was over 19%, the activity dramatically decreased. No further phase transformation of the supports occurred during calcination of the catalyst samples and reaction.

6.1.2 Various percent loading of zirconia modified titania-supported Co catalysts

Zr modification of the titania support had a significant impact on the properties of Co/TiO₂ catalysts. For the pure anatase in titania support, the overall catalytic activity during CO hydrogenation decreased upon Zr modification. Lower activities were due to low reducibilities (TPR at 35-800°C of cobalt species) perhaps

resulting from the Co-support compound formation (Co-SCF) in titania-supported cobalt catalyst or “Co-titanate”. In contrast, the activity increased with Zr modification for the 19% rutile in titania support. Most of this increase appeared due to an increase in reducibility during standard reduction. Zr modification may result in a stabilization of the titania support by blocking “Co-titanate” formation by minimizing the impact of water vapor on the formation of compound. Considering the product distribution, it was illustrated that the addition of zirconia tended to have no effect on selectivity of products during CO hydrogenation.

6.1.3 Titania-Silica mixed oxide-supported Co catalysts

The impact of various mixed TiO_2 - SiO_2 -supported cobalt catalysts on their catalytic behaviors was discussed. It was found that both initial and steady-state rates during CO hydrogenation dramatically decreased with the amounts of titania present in the mixed supports. The decreased activities had to be attributed to the less number of reduced cobalt metal surface atoms for catalyzing the reaction. At the specified conditions, the selectivity of the longer chain hydrocarbons (C_2 - C_5) was more pronounced with the presence of titania in the mixed supports. It can be concluded that the presence of titania apparently inhibited the chain growth probability during CO hydrogenation.

6.2 Recommendations

1. Effect of titania supports mixed with other inorganic oxides should be further investigated in order to determine which the best support for cobalt catalysts.
2. Effect of titania supports contained other promoters or modifiers should be further investigated in order to determine which the best support for cobalt catalysts.
3. The reaction study under commercial Fischer-Tropsch synthesis conditions using Co/TiO_2 catalysts is also recommended.

REFERENCES

- Ali, S., Chen, B., and Goodwin, Jr., J.G. Zr promotion of Co/SiO₂ for Fisher-Tropsch Synthesis. J. Catal. 157 (1995): 35-41.
- Brik, Y., Kacimi, M., Ziyad, M., and Bozon-Verduraz, F. Titania-supported cobalt and cobalt-phosphorus catalysts: Characterization and performances in ethane oxidative dehydrogenation. J. Catal. 202 (2001): 118-128.
- Choi, J.G. Reduction of supported cobalt catalysts by hydrogen. Catal Lett. 35 (1995): 291-296.
- Coville, N.J., and Li, J. Effect of boron source on the catalyst reducibility and Fisher-Tropsch synthesis activity of o/TiO₂ catalysts. Catal. Today. 71 (2002): 403-410.
- Dalai, A.K., Das, T.K., Chaudhari, K.V., Jacobs, G., and Davis, B.H. Fischer-Tropsch synthesis: Water effects on Co supported on narrow and wide-pore silica. Appl. Catal. A: General. 289 (2005): 135-142
- Duvenhage, D.J., and Coville, N.J. Fe:Co/TiO₂ bimellic catalysts for the Fischer-Tropsch reaction Part 2. The effect of calcination and reduction temperature. Appl. Catal. A 233(2002): 63-75.
- Farrauto, R.J. and Bartholomew, C.H. Fundamentals of industrial catalytic processes. 1 st ed. London: Chapman & Hall, 1997.
- Feller, A., Claeys, M., and Steen, EV. Cobalt cluster effects in zirconium promoted Co/SiO₂ Fischer-Tropsch Catalysts. J. Catal. 185 (1995): 20-130.
- Fujishima, A., Hashimoto, K., and Watanabe, T., TiO₂ photocatalysis: fundamental and applications. 1 st ed. Tokyo:BKC, 1999.
- Gao, X., and Wachs, I.E. Titania-silica as catalysts: molecular structural characteristics and physico-chemical properties. Catal. Today. 51 (1999): 233-254.
- George, A.O. and Arpad, M. Hydrocarbon chemistry. New York:John Wiley & Sons, Inc.,1995.
- Hu, S., Willey, R.J., and Notari, B. An investigation on the catalytic properties of titania-silica materials. J. Catal. 220 (2003): 240-248.
- Iglesis, E., Soled, S.L., Fiato, R.A., and Via, G.H. Dispersion, Support and bimetallic effects in Fischer-Tropsch synthesis on cobalt catalysts. Natural Gas Conversion II. 81 (1994):433-442.
- Jacob, K., William, J.A., Jr., Ernest, G. Inorganic chemistry. Boston: D.C. Heath and

- company, 1960.
- Jacobs, G., Das, T.K., Zhang, Y., Li, J., Racoillet, G., and Davis, B.H. Fischer-Tropsch synthesis: support, loading, and promoter effects on the reducibility of cobalt catalysts. Appl. Catal. A 233 (2002): 263-281.
- John, J.M. Chemical processing handbook. New York: Marcel Dekker, Inc., 1993.
- Jongsomjit, B., and Goodwin, J.G., Jr. Co-support compound formation in Co/Al₂O₃ catalysts: effect of reduction gas containing CO. Catal. Today 77 (2002): 191-204.
- Jongsomjit, B., Panpranot, J., and Goodwin, J.G., Jr. Co-support compound formation in alumina-supported cobalt catalysts. J. Catal. 204 (2001): 98-109.
- Jongsomjit, B., Panpranot, J., and Goodwin, J.G., Jr. Effect of zirconia-modified alumina on the properties of Co/g-Al₂O₃ catalysts. J. Catal. 215 (2003): 66-77.
- Jongsomjit, B., Sakdamnusun, C., and Praserthdam, P. Dependence of crystalline phases in titania on catalytic properties during CO hydrogenation of Co/TiO₂ catalysts. Mat. Chem. and Phys. 89 (2005): 395-401.
- Jongsomjit, B., Sakdamnusun, C., Goodwin, J.G., Jr., and Praserthdam, P. Co-support compound formation in titania-supported cobalt catalyst. Catal. Lett. 94 (2004): 209-215.
- Jung, K.Y., and Park, S.B. Anatase-phase titania: preparation by embedding silica and photocatalytic activity for the decomposition of trichloroethylene. J. of Photochem. and Photobio. A: Chemistry. 127 (1999): 177-122.
- Kogelbauer, A., Weber, J.C., and Goodwin, J.G., Jr. The formation of cobalt silicates on Co/SiO₂ under hydrothermal conditions. Catal Lett. 34 (1995): 259-267.
- Kraum, M., and Baerns, M. Fischer-Tropsch synthesis: the influence of various cobalt compounds applied in the preparation of supported cobalt catalysts on their performance. Appl. Catal. A 186 (2002): 189-200.
- Li, J., and Coville, N.J. Effect of boron on the sulfur poisoning of Co/TiO₂ Fischer-Tropsch catalysts. Appl. Catal. A 208 (2002): 177-184.
- Li, J., and Coville, N.J. Effect of boron source on the catalyst reducibility and Fischer-Tropsch synthesis activity of Co/TiO₂ catalysts. Catal. Today 71 (2002): 403-410.
- Li, J., and Coville, N.J. The effect of boron on the catalyst reducibility and activity of Co/TiO₂ Fischer-Tropsch catalysts. Appl. Catal. A 181(1999): 201-208.
- Li, J., Jacobs, G., Zhang, Y., Das, T., and Davis, B.H. Fisher-Tropsch synthesis: effect of small amounts of boron, ruthenium and rhenium on Co/TiO₂ catalysts.

- Appl. Catal. A: General. 223 (2002): 195-203.
- Li, J., Jacobs, G., Zhang, Y., Das, T., and Davis, B.H. Fisher-Tropsch synthesis: effect of water on the catalytic properties of a ruthenium promoted Co/TiO₂ catalysts. Appl. Catal. A: General. 233 (2002): 255-262.
- Li, J.L., Xu, L.G., Keogh, R., and Davis, B. Fischer-Tropsch synthesis. Effect of CO pretreatment on a ruthenium promoted Co/TiO₂. Catal Lett. 70 (2000): 127-130.
- Madikizela, N.N., and Coville, N.J. A study of Co/Zn/TiO₂ catalysts in the Fischer-Tropsch reaction. J. Mol. Catal. A 181 (2002): 129-136.
- Mohamed, M.M., Salama, T.M., and Yamaguchi, T. Synthesis, characterization and catalytic properties of titania-silica catalysts Colloids and Surfaces A: Physicochemical and Engineering Aspects. 207 (2002): 25-32.
- Moradi, G.R., Basir, M.M., Taeb, A., and Kiennemann, A. Promotion of Co/SiO₂ Fischer-Tropsch catalysts with zirconium. Catal. Comm. 4 (2003): 27-32.
- Nagaoka, K., Takanabe, K., and Aika, K. Influence of the reduction temperature on catalytic activity of Co/TiO₂ (anatase-type) for high pressure dry reforming of methane. Appl. Catal. A. 255 (2003): 13-21.
- Nagaoka, K., Takanabe, K., and Aika, K. Modification of Co/TiO₂ for dry reforming of methane at 2 MPa by Pt, Ru or Ni. Appl. Catal. A: General. 268 (2004): 151-158.
- Nobuntu, N., Madikizela, M., and Coville, N.J. Surface and reactor study of the effect of zinc on titania-supported Fischer-Tropsch cobalt catalysts. Appl. Catal. A: General 272 (2004): 339-346.
- Othmer, K. Encyclopedia of chemical technology. Vol. 6. 4 th ed. New York: A Wiley-Interscience Publication, John Wiley&Son, 1991.
- Panpranot, J., Goodwin, J.G., Jr., and Sayari, A. CO hydrogenation on Ru-promoted Co/MCM-41 catalysts. J. Catal. 211 (2002): 530-539.
- Pradyot Patnaik, Ph.D. Handbook of inorganic chemicals. New York: McGraw-Hill, 2002.
- Price, J.G., Glasser, D., Hildebrandt, D., and Coville, N.J. Fischer-Tropsch synthesis: DRIFTS and SIMS surface investigation of Co and Co/Ru on titania supports. Natural Gas Conversion IV. 107 (1997): 243-248.
- Rana, M.S., Maity, S.K., Ancheyta, J., Murali Dhar, G., and Prasada Raob, T.S.R. TiO₂-SiO₂ supported hydrotreating catalysts: physico-chemical characterization and activities. Appl. Catal. A: General. 253 (2003): 165-176.

- Reuel, R.C., and Bartholomew, C.H. The stoichiometries of H₂ and CO adsorption on cobalt: effects of support and preparation. J. Catal. 85 (1984): 63-77.
- Riva, R., Miessner, H., and Piero, G.D. Metal-support interaction in Co/SiO₂ and Co/TiO₂. Appl. Catal. A 196 (2000): 111-123.
- Rohr, F., Lindvåga, O.A., Holmen, A., and Blekkan, E.A. Fischer–Tropsch synthesis over cobalt catalysts supported on zirconia-modified alumina. Catal. Today. 58 (2000): 247-254.
- Schanke, D., Hilmen, A.M., Bergene, E., Kinnari, K., Rytter, E., Adnanes, E., and Holmen, A. Study of the deactivation mechanism of Al₂O₃-supported cobalt Fischer-Tropsch catalysts. Catal Lett. 34 (1995): 269-284.
- Shinoda, M., Zhang, Y., Yoneyama, Y., Hasegawa, K., and Tsubaki, N. New bimodal pore catalysts for Fischer–Tropsch synthesis. Fuel Processing Tech. 86 (2004): 73-85.
- Storsæter, S., Borg, Ø., Blekkan, E.A., and Holmen, A. Study of the effect of water on Fischer–Tropsch synthesis over supported cobalt catalysts. J. Catal. 231 (2005): 405-419.
- Sun, S., Fujimoto, K., Yoneyama, Y., and Tsubaki, N. Fisher-Tropsch synthesis using Co/SiO₂ catalysts prepared from mixed precursors and addition effect of noble metals. Fuel 81 (2002): 1583-1591.
- Theinkaew, S., Synthesis of large-surface area silica modified titanium (IV) oxide ultrafine particles, Master's thesis, Faculty of Engineering, Chulalongkorn University, (2002).
- Tsubaki, N., Sun, S., and Fujimoto, K. Different function of the noble metals added to cobalt catalysts for Fischer-Tropsch synthesis. J. Catal. 199 (2001): 236-246.
- Vob, M., Borgmann, D., and Wedler, G. Characterization of alumina, silica, and titania supported cobalt catalysts. J. Catal. 212 (2002): 10-21.
- West, A. R.; Solid State Chemistry and its Application. Brisbane: John Wiley&Sons, 1997.
- Xiong, H., Zhang, Y., Liew, K., and Li, J. Catalytic performance of zirconium-modified Co/Al₂O₃ for Fischer–Tropsch synthesis. J. of Molecular Catal. A: Chemical 231 (2005): 145-151.
- Young, R.S. COBALT: Its Chemistry, Metallurgy, and Uses. New York: Reinhold Publishing Corporation, 1960.
- Zennaro, R., Tagliabue, M., and Bartholomew, C.H. Kinetics of Fischer-Tropsch synthesis on titania-supported cobalt. Catal. Today 58 (2000): 309-319.

Zhang, Y., Shinoda, M., and Tsubaki, N. Development of bimodal cobalt catalysts for Fischer–Tropsch synthesis. *Catal. Today*. 93-95 (2004): 55-63.

Zhang, Y., Wei, D., Hammache, S., and Goodwin, J.G., Jr. Effect of water vapor on the reduction of Ru-promoted Co/Al₂O₃. *J. Catal.* 188 (1999): 281-290.



สถาบันวิทยบริการ
จุฬาลงกรณ์มหาวิทยาลัย



APPENDICES

สถาบันวิทยบริการ
จุฬาลงกรณ์มหาวิทยาลัย

APPENDIX A

CALCULATION FOR CATALYST PREPARATION

Preparation of Zr-modified TiO₂ support and 20%Co/TiO₂ catalysts by the incipient wetness impregnation method are shown as follows:

- Reagent:
- Zirconia (IV) propoxide (C₁₂H₂₈O₄Zr) 70 wt.% solution in 1-propanol
Molecular weight = 327.57
 - Cobalt (II) nitrate hexahydrate (Co(NO₃)₂ · 6H₂O)
Molecular weight = 290.93
 - Support: - Titania [TiO₂]

Calculation for the preparation of Zr-modified TiO₂ support

For 0.5 % Zr-modified TiO₂ support

Based on 100 g of titania used, the composition of the support will be as follows:

$$\text{Titania} = 99.5 \text{ g}$$

$$\text{Zirconia} = 0.5 \text{ g}$$

For 5 g of titania

$$\text{Zirconia required} = 5 \times (0.5/99.5) = 0.025 \text{ g}$$

Zirconia 0.025 g was prepared from C₁₂H₂₈O₄Zr and molecular weight of Zr is 91.224.

$$\begin{aligned} \text{C}_{12}\text{H}_{28}\text{O}_4\text{Zr required} &= \frac{\text{MW of C}_{12}\text{H}_{28}\text{O}_4\text{Zr} \times \text{Zirconia required}}{\text{MW of Zr}} \\ &= (327.57/91.224) \times 0.025 = 0.09 \text{ g} \end{aligned}$$

C₁₂H₂₈O₄Zr 0.09 g was prepared from C₁₂H₂₈O₄Zr 70 wt.% solution in 1-propanol

$$\begin{aligned} \text{C}_{12}\text{H}_{28}\text{O}_4\text{Zr 70 wt.\% solution in 1-propanol required} \\ &= \frac{\text{percent of solution} \times \text{C}_{12}\text{H}_{28}\text{O}_4\text{Zr required}}{\text{percent of C}_{12}\text{H}_{28}\text{O}_4\text{Zr in solution}} \\ &= (100/70) \times 0.09 = 0.13 \text{ g} \end{aligned}$$

Loading the amount of zirconia from calculation on titania by incipient wetness impregnation method.

Calculation for the preparation of cobalt loading catalyst (20%Co/TiO₂)

Based on 100 g of catalyst used, the composition of the catalyst will be as follows:

$$\begin{aligned} \text{Cobalt} &= 20 \text{ g} \\ \text{Titania} &= 100-20 = 80 \text{ g} \end{aligned}$$

For 5 g of titania

$$\text{Cobalt required} = 5 \times (20/80) = 1.25 \text{ g}$$

Cobalt 1.25 g was prepared from $\text{Co}(\text{NO}_3)_2 \cdot 6\text{H}_2\text{O}$ and molecular weight of Co is 58.93

$$\begin{aligned} \text{Co}(\text{NO}_3)_2 \cdot 6\text{H}_2\text{O} \text{ required} &= \frac{\text{MW of Co}(\text{NO}_3)_2 \cdot 6\text{H}_2\text{O} \times \text{cobalt required}}{\text{MW of Co}} \\ &= (290.93/58.93) \times 1.25 = 6.17 \text{ g} \end{aligned}$$

Since the pore volume of the titania support is 0.8 ml/g and 1 ml/g for JRC-TIO1, JRC-TIO4, respectively. Thus, the total volume of impregnation solution which must be used is 4 ml for JRC-TIO1 and 5 ml for JRC-TIO4 by the requirement of incipient wetness impregnation method, the de-ionized water is added until equal pore volume for dissolve Cobalt (II) nitrate hexahydrate.

สถาบันวิทยบริการ
จุฬาลงกรณ์มหาวิทยาลัย

APPENDIX B

CALCULATION OF BET SURFACE AREA BY THE SINGLE POINT METHOD

From Brunauer-Emmett-Teller (BET) equation:

$$\frac{X}{V(1-X)} = \frac{1}{V_m C} + \frac{(C-1)X}{V_m C} \quad (\text{B.1})$$

Where: X = relative partial pressure of N_2 , P/P_0

P_0 = saturated vapor pressure of N_2 (or adsorbed gas) at the experimental temperature

P = equilibrium vapor pressure of N_2

V = volume of gas adsorbed at a pressure P ; ml at the NTP/ g of sample

V_m = volume of gas adsorbed at monolayer, ml. at the NTP / g of sample

C = constant

Assume $C \rightarrow \infty$, then

$$\frac{X}{V(1-X)} = \frac{X}{V_m} \quad (\text{B.2})$$

$$V_m = V (1-P/P_0)$$

From the gas law,

$$\frac{P_b V}{273} = \frac{P_t V}{T} \quad (\text{B.3})$$

Where: V = constant volume

P_b = pressure at 0°C

P_t = pressure at $t^\circ\text{C}$

$T = 273.15 + t$, K

$$P_t = 1 \text{ atm} \quad \text{and thus,} \quad P_b = (273.15 / T)$$

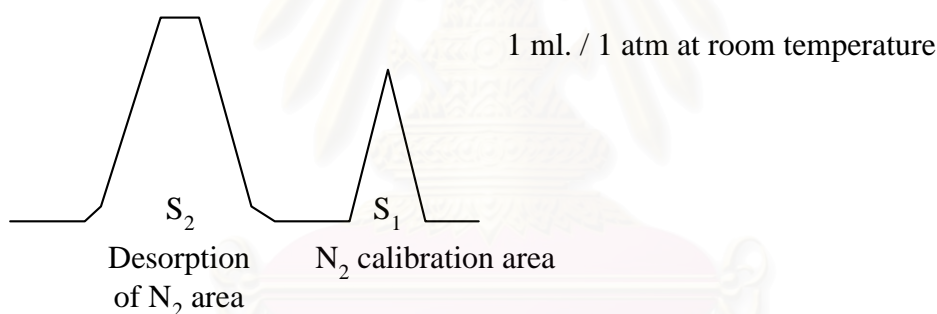
Partial pressure of Nitrogen:

$$\begin{aligned} P &= \frac{[\text{Flow of (He+N}_2\text{)} - \text{Flow of He}]}{\text{Flow of (He+N}_2\text{)}} & \text{(B.4)} \\ &= 0.3 \text{ atm} \end{aligned}$$

N₂ saturated vapor pressure, P_o = 1.1 atm

$$p = P / P_o = P / 1.1 = 0.3/1.1 = 0.2727$$

How to measure V



$$V = \frac{S_2}{S_1} \times \frac{1}{W} \times \frac{273.15}{T} \text{ ml. / g of catalyst} \quad \text{(B.5)}$$

Where, S₁ = Nitrogen 1 ml/1 atm of room temperature area

S₂ = Desorption of nitrogen area

W = Weight of the sample (g)

T = Room temperature (K)

Therefore,

$$\begin{aligned} V_m &= \frac{S_2}{S_1} \times \frac{1}{W} \times \frac{273.15}{T} \times (1-p) \\ V_m &= \frac{S_2}{S_1} \times \frac{1}{W} \times \frac{273.15}{T} \times 0.7273 & \text{(B.6)} \end{aligned}$$

Surface area of catalyst:

$$S = \frac{N\sigma V_m}{M}$$

Where, N = Avogadro number = 6.02×10^{23}

σ = area occupied by one molecule of adsorbed nitrogen = 16.2×10^{-20}

M = volume of one mole nitrogen = $22410 \text{ cm}^3/\text{mol}$

Then,

$$S = 4.352 V_m$$

$$S = \frac{S_2}{S_1} \times \frac{1}{W} \times \frac{273.15}{T} \times 0.7273 \times 4.352$$

$$S = \frac{S_2}{S_1} \times \frac{1}{W} \times \frac{273.15}{T} \times 3.1582 \quad (\text{B.7})$$

สถาบันวิทยบริการ
จุฬาลงกรณ์มหาวิทยาลัย

APPENDIX C

CALCULATION FOR REDUCIBILITY

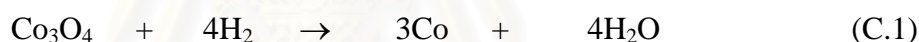
For supported cobalt catalyst, it can be assumed that the major species of calcined Co catalysts is Co_3O_4 . H_2 consumption of Co_3O_4 is calculated as follows:

$$\begin{aligned} \text{Molecular weight of Co} &= 58.93 \\ \text{Molecular weight of } \text{Co}_3\text{O}_4 &= 240.79 \end{aligned}$$

Calculation of the calibration of H_2 consumption using cobalt oxide (Co_3O_4)

$$\begin{aligned} \text{Let the weight of } \text{Co}_3\text{O}_4 \text{ used} &= 0.01 \text{ g} \\ &= 4.153 \times 10^{-5} \text{ mole} \end{aligned}$$

From equation of Co_3O_4 reduction;



$$\begin{aligned} \text{H}_2 &= 4 \text{ Co}_3\text{O}_4 \\ &= 4 \times 4.153 \times 10^{-5} = 1.661 \times 10^{-4} \text{ mole} \end{aligned}$$

$$\text{Integral area of } \text{Co}_3\text{O}_4 \text{ after reduction} = 396572.5 \text{ unit}$$

Thus, the amount of H_2 that can be consumed at 100 % reducibility is 1.661×10^{-4} mole which related to the integral area of Co_3O_4 after reduction 396572.5 unit.

Calculation of reducibility of supported cobalt catalyst

$$\begin{aligned} \text{Integral area of the calcined catalyst} &= X \text{ unit} \\ \text{The amount of } \text{H}_2 \text{ consumption} &= [1.661 \times 10^{-4} \times (X) / 396572.5] \text{ mole} \\ \text{Let the weight of calcined catalyst used} &= W \text{ g} \\ \text{Concentration of Co (by AAS)} &= Y \text{ \% wt} \\ \text{Mole of Co} &= [(W \times Y) / 58.93] \text{ mole} \\ \text{Mole of } \text{Co}_3\text{O}_4 &= [(W \times Y) / 3 \times 58.93] \text{ mole} \end{aligned}$$

$$\begin{aligned} \text{Mole of H}_2 \text{ can be consumed} &= [(W \times Y) \times 4/3 \times 58.93] \text{ mole} \\ \text{Reducibility (\% of supported Co catalyst)} &= \frac{[1.661 \times 10^{-4} \times (X) / 396572.5] \times 100}{[(W \times Y) \times 4/3 \times 58.93]} \end{aligned}$$



สถาบันวิทยบริการ
จุฬาลงกรณ์มหาวิทยาลัย

APPENDIX D

CALCULATION FOR TOTAL H₂ CHEMISORPTION AND DISPERSION

Calculation of the total H₂ chemisorption and metal dispersion of the catalyst, a stoichiometry of H/Co = 1, measured by H₂ chemisorption is as follows:

Let the weight of catalyst used	=	W	g
Integral area of H ₂ peak after adsorption	=	A	unit
Integral area of 45 μl of standard H ₂ peak	=	B	unit
Amounts of H ₂ adsorbed on catalyst	=	B-A	unit
Concentration of Co (by AAS)	=	C	% wt
Volume of H ₂ adsorbed on catalyst	=	45×[(B-A)/B]	μl
Volume of 1 mole of H ₂ at 100°C	=	28.038	μl
Mole of H ₂ adsorbed on catalyst	=	[(B-A)/B]×[45/28.038]	μmole
Total hydrogen chemisorption	=	[(B-A)/B]×[45/28.038]×[1/W]	μmole /g of catalyst
	=	N	μmole /g of catalyst
Molecular weight of cobalt	=	58.93	
Metal dispersion (%)	=	$\frac{2 \times H_{2 \text{ tot}} / \text{g of catalyst} \times 100}{\text{No } \mu\text{mole Co}_{\text{tot}} / \text{g of catalyst}}$	
	=	$\frac{2 \times N \times 100}{\text{No } \mu\text{mole Co}_{\text{tot}}}$	
	=	$\frac{2 \times N \times 58.93 \times 100}{C \times 10^6}$	
	=	$\frac{1.179 \times N}{C}$	

APPENDIX E

CALIBRATION CURVES

This appendix showed the calibration curves for calculation of composition of reactant and products in CO hydrogenation reaction. The reactant is CO and the main product is methane. The other products are linear hydrocarbons of heavier molecular weight that are C₂-C₄ such as ethane, ethylene, propane, propylene and butane.

The thermal conductivity detector, gas chromatography Shimadzu model 8A was used to analyze the concentration of CO by using Molecular sieve 5A column. The chromatograms of catalyst sample are shown in Figure E.1.

The VZ10 column are used with a gas chromatography equipped with a flame ionization detector, Shimadzu modal 14B, to analyze the concentration of products including of methane, ethane, ethylene, propane, propylene and butane. The chromatograms of catalyst sample are shown in Figure E.2. Conditions uses in both GC are illustrated in Table E.1.

Mole of reagent in y-axis and area reported by gas chromatography in x-axis are exhibited in the curves. The calibration curves of CO, methane, ethane, ethylene, propane, propylene and butane are illustrated in the following figures.

สถาบันวิทยบริการ
จุฬาลงกรณ์มหาวิทยาลัย

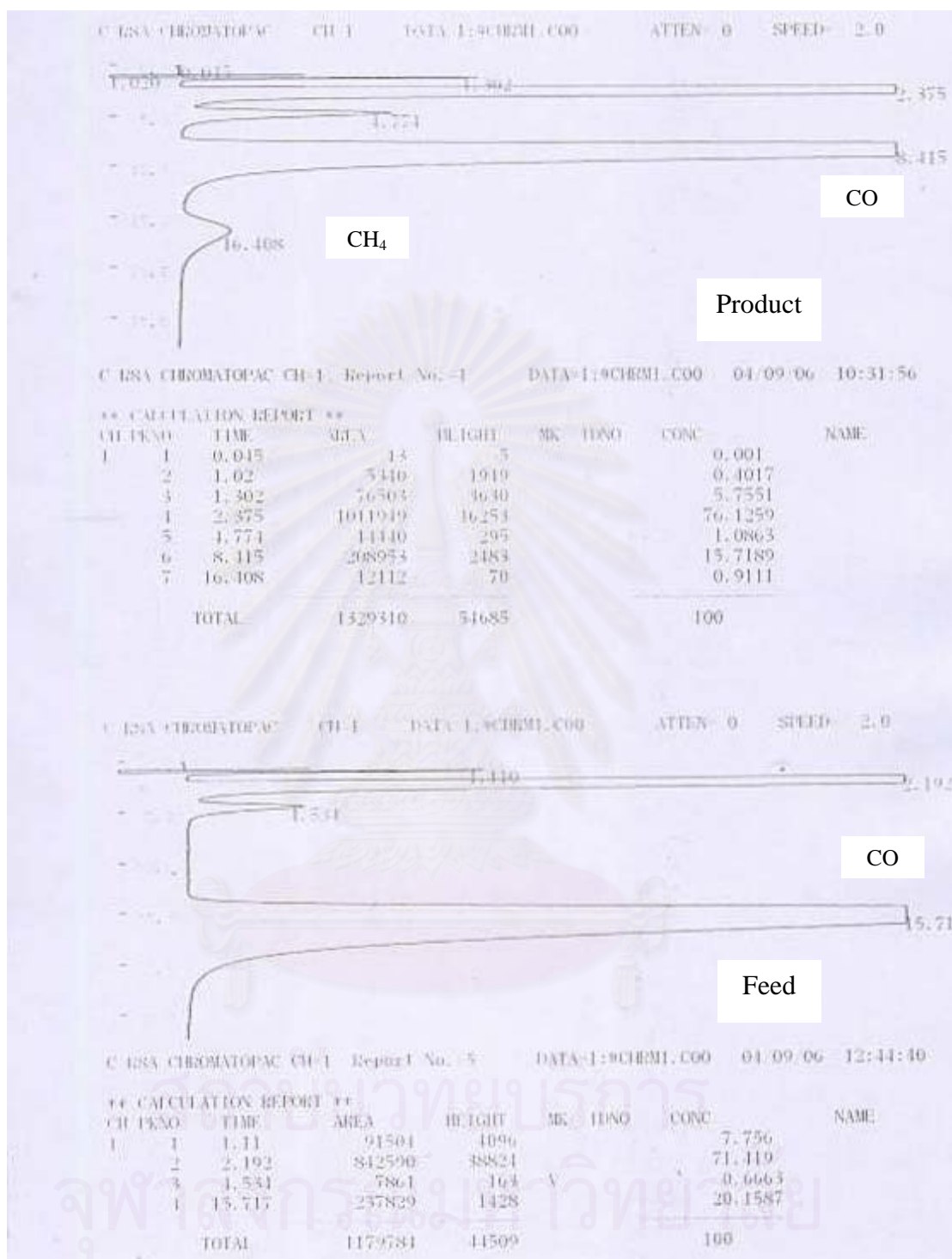


Figure E.1 The chromatograms of catalyst sample from thermal conductivity detector, gas chromatography Shimadzu model 8A (Molecular sieve 5A column).

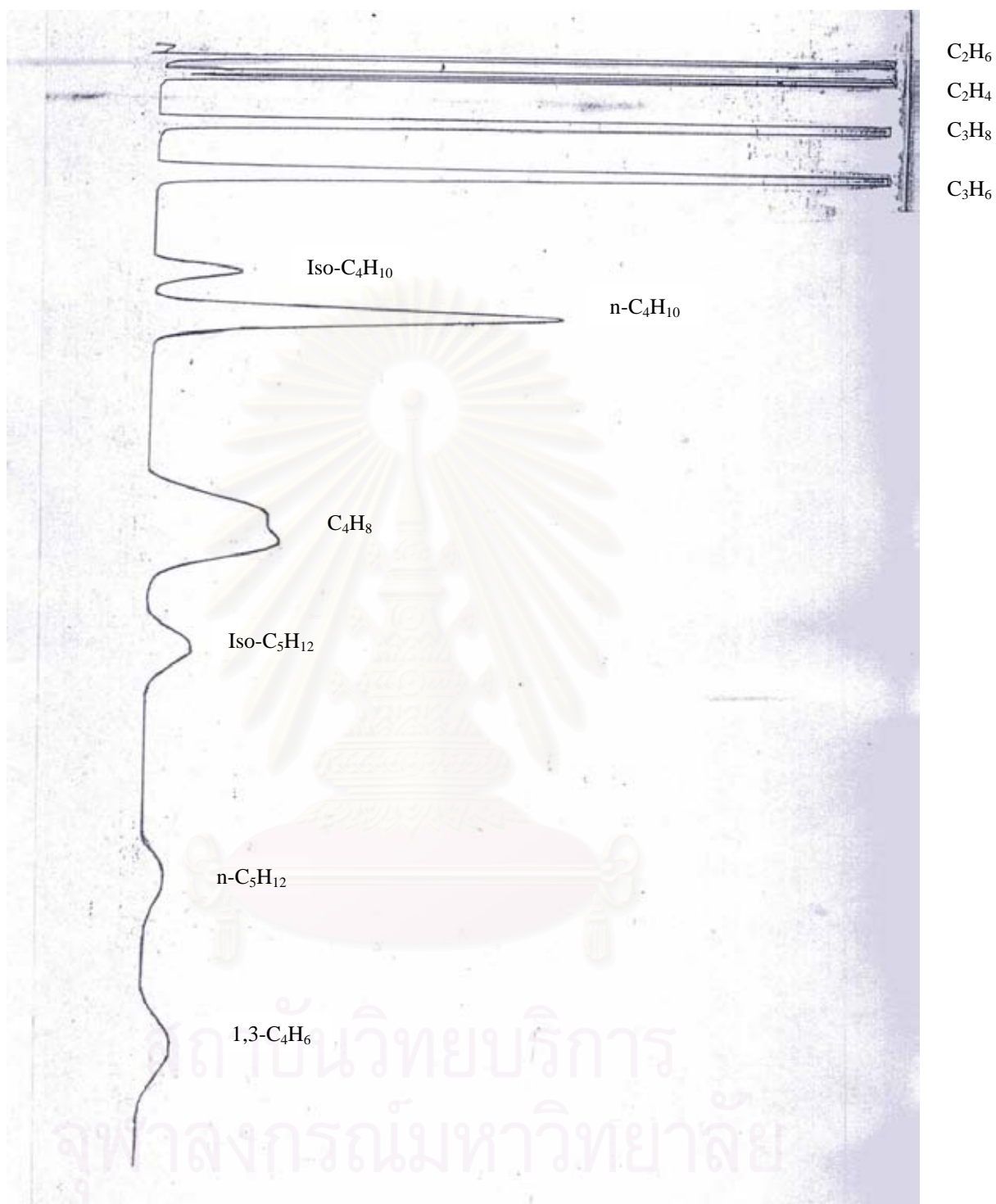


Figure E.2 The chromatograms of catalyst sample from flame ionization detector, gas chromatography Shimadzu modal 14B (VZ10 column).

Table E.1 Conditions use in Shimadzu modal GC-8A and GC-14B.

Parameters	Condition	
	Shimadzu GC-8A	Shimadzu GC-14B
Width	5	5
Slope	50	50
Drift	0	0
Min. area	10	10
T.DBL	0	0
Stop time	50	60
Atten	0	0
Speed	2	2
Method	41	41
Format	1	1
SPL.WT	100	100
IS.WT	1	1

สถาบันวิทยบริการ
จุฬาลงกรณ์มหาวิทยาลัย

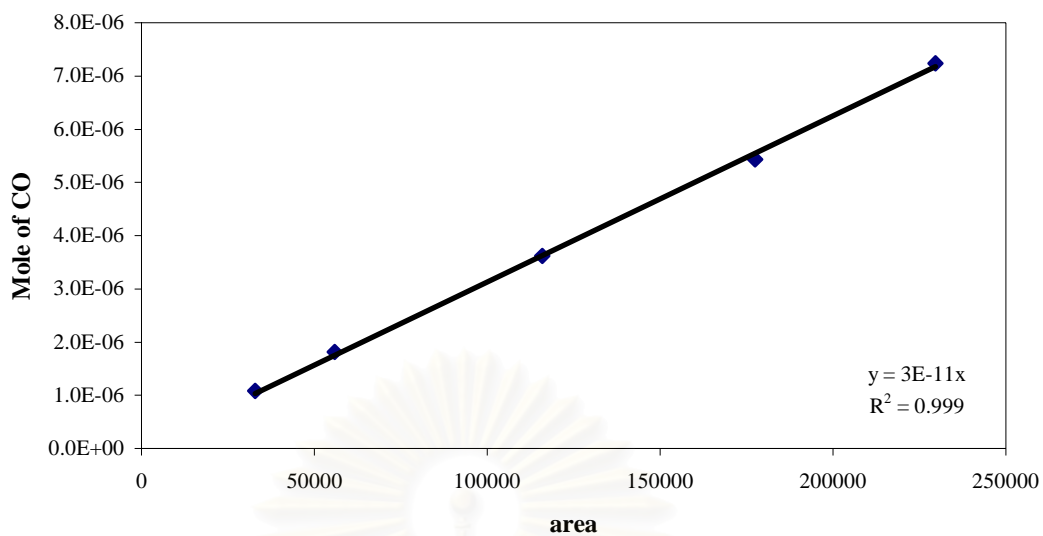


Figure E.3 The calibration curve of CO.

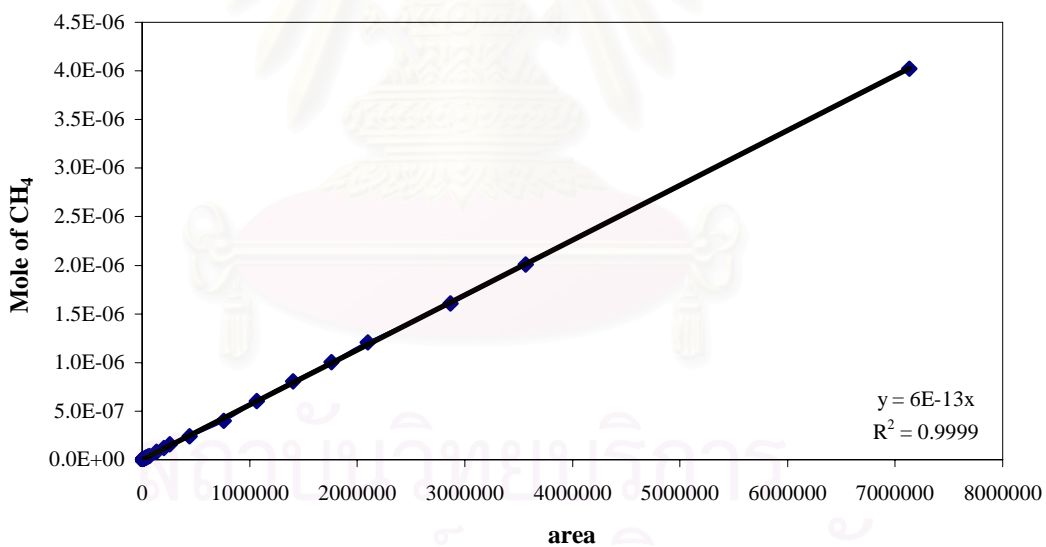


Figure E.4 The calibration curve of methane.

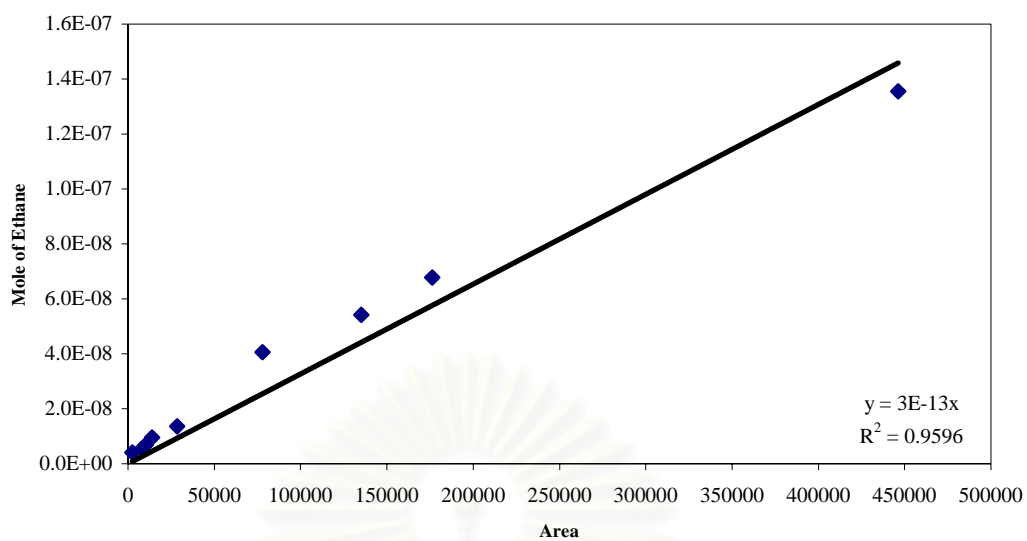


Figure E.5 The calibration curve of ethane.

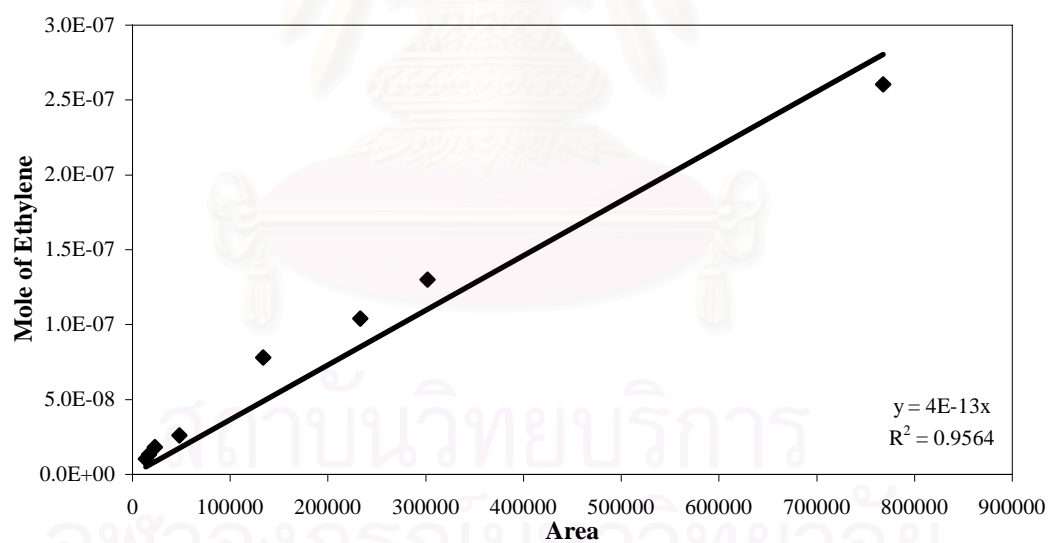


Figure E.6 The calibration curve of ethylene.

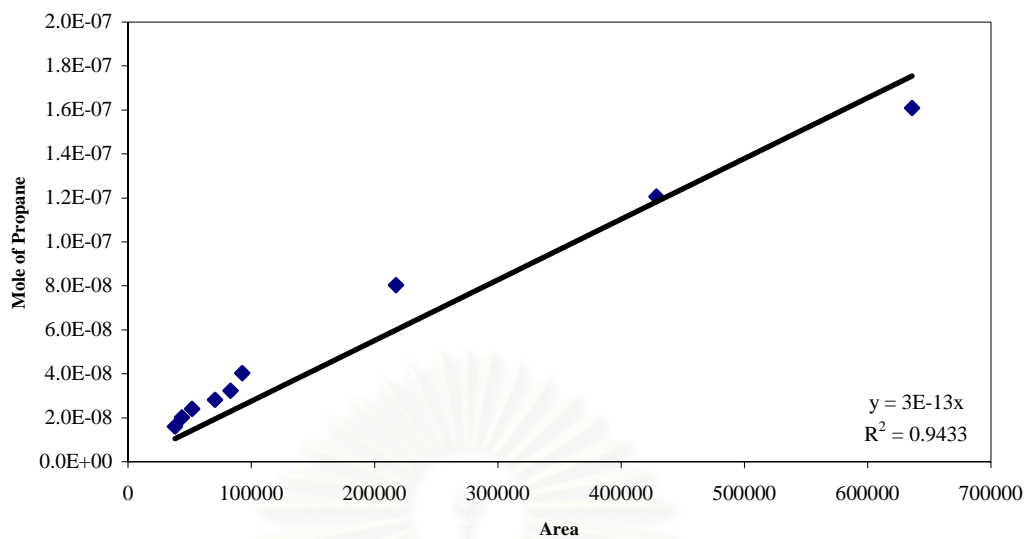


Figure E.7 The calibration curve of propane.

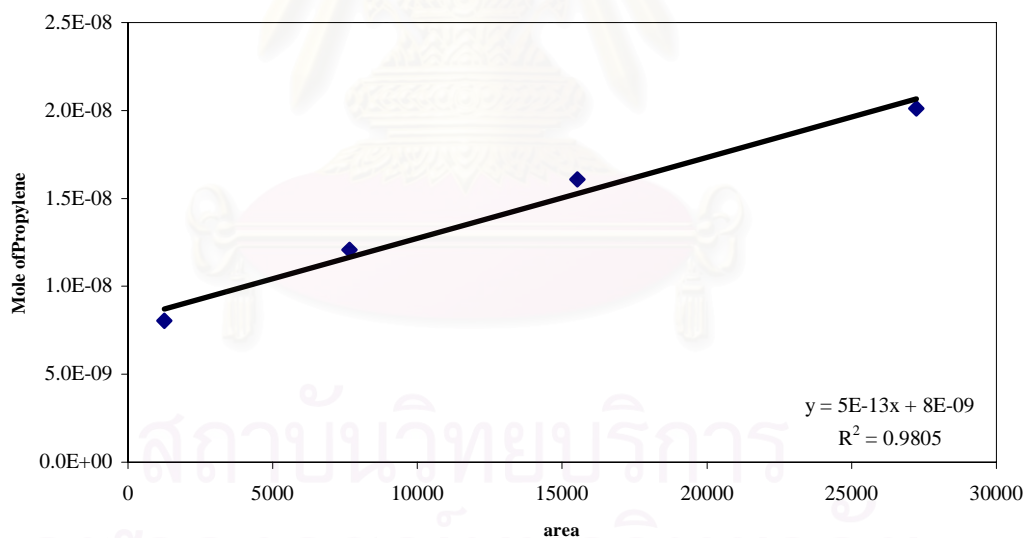


Figure E.8 The Calibration curve of propylene.

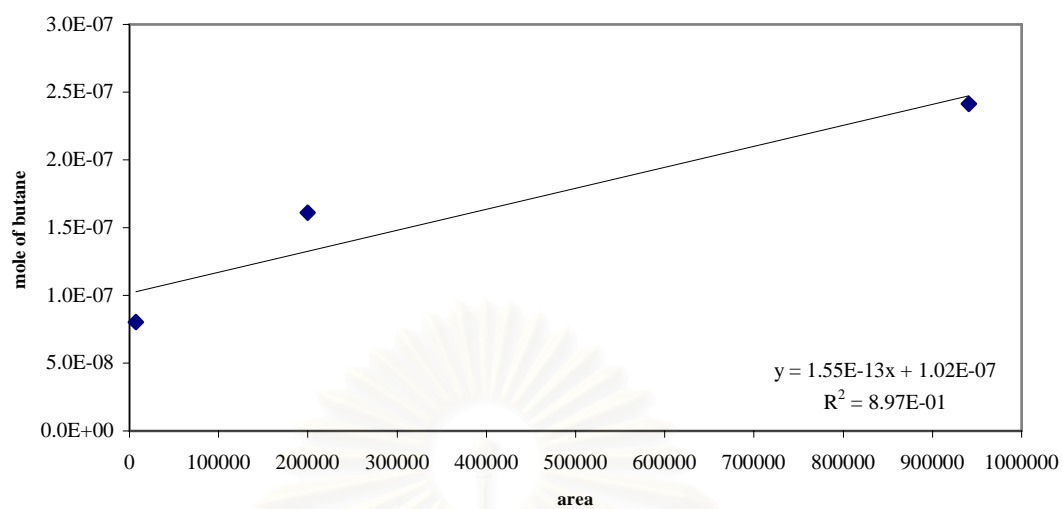


Figure E.9 The calibration curve of butane

สถาบันวิทยบริการ
จุฬาลงกรณ์มหาวิทยาลัย

APPENDIX F

CALCULATION OF CO CONVERSION, REACTION RATE AND SELECTIVITY

The catalyst performance for the CO hydrogenation was evaluated in terms of activity for CO conversion reaction rate and selectivity.

Activity of the catalyst performed in term of carbon monoxide conversion and reaction rate. Carbon monoxide conversion is defined as moles of CO converted with respect to CO in feed:

$$\text{CO conversion (\%)} = \frac{100 \times [\text{mole of CO in feed} - \text{mole of CO in product}]}{\text{mole of CO in feed}} \quad (\text{i})$$

where mole of CO can be measured employing the calibration curve of CO in Figure E.1, Appendix E., i.e.,

$$\text{mole of CO} = (\text{area of CO peak from integrator plot on GC-8A}) \times 3 \times 10^{-11} \quad (\text{ii})$$

Reaction rate was calculated from CO conversion that is as follows:

Let the weight of catalyst used	=	W	g
Flow rate of CO	=	2	cc/min
Reaction time	=	60	min
Weight of CH ₂	=	14	g
Volume of 1 mole of gas at 1 atm	=	22400	cc
Reaction rate (g CH ₂ /g of catalyst/h)	=	$\frac{[\% \text{ conversion of CO}/100] \times 60 \times 14 \times 2}{W \times 22400} \quad (\text{iii})$	

Selectivity of product is defined as mole of product (B) formed with respect to mole of CO converted:

$$\text{Selectivity of B (\%)} = 100 \times [\text{mole of B formed}/\text{mole of total products}] \quad (\text{iv})$$

Where B is product, mole of B can be measured employing the calibration curve of products such as methane, ethane, ethylene, propane, propylene and butane in Figure E.4-E.9, Appendix E.,i.e.,

$$\text{mole of CH}_4 = (\text{area of CH}_4 \text{ peak from integrator plot on GC-14B}) \times 6 \times 10^{-13} \quad (\text{ii})$$



สถาบันวิทยบริการ
จุฬาลงกรณ์มหาวิทยาลัย

APPENDIX G**LIST OF PUBLICATIONS**

1. Bunjerd Jongsomjit, Tipnapa Wongsalee and Piyasan Prasertthdam, “Study of cobalt dispersion on titania consisting various rutile:anatase”, *Materials Chemistry and Physics*, 92 (2005): 572-577.
2. Bunjerd Jongsomjit, Tipnapa Wongsalee and Piyasan Prasertthdam, “Characteristics and catalytic properties of Co/TiO₂ for various rutile:anatase ratios”, *Catalysis Communications*, (in press).
3. Bunjerd Jongsomjit, Tipnapa Wongsalee and Piyasan Prasertthdam, “Catalytic Behaviors of Mixed TiO₂-SiO₂-Supported Cobalt Fischer-Tropsch Catalysts for Carbon Monoxide Hydrogenation”, *Materials Chemistry and Physics*, (in press).



สถาบันวิทยบริการ
จุฬาลงกรณ์มหาวิทยาลัย



Study of cobalt dispersion on titania consisting various rutile: anatase ratios

Bunjerd Jongsomjit*, Tipnapa Wongsalee, Piyasan Praserttham

*Center of Excellence on Catalysis and Catalytic Reaction Engineering, Department of Chemical Engineering,
Faculty of Engineering, Chulalongkorn University, Bangkok 10330, Thailand*

Received 29 October 2004; received in revised form 25 January 2005; accepted 16 February 2005

Abstract

The number of reduced cobalt metal surface atoms in Co/TiO₂ was found to increase with the presence of rutile phase. It was suggested that the increased number of reduced cobalt metal surface atoms be attributed to highly dispersed cobalt oxide species as seen by the transmission electron microscopy (TEM) technique. Besides the dispersion of cobalt oxide species, it should be noted that the presence of rutile phase in titania could facilitate the reduction of highly dispersed cobalt oxides species into the reduced cobalt metal surface atoms. It was concluded that both highly dispersed cobalt oxide species and the presence of rutile phase could result in the large number of reduced cobalt metal surface atoms.

© 2005 Elsevier B.V. All rights reserved.

Keywords: Titania; Cobalt; Catalyst; TEM; Chemisorption

1. Introduction

Inorganic materials such as silica (SiO₂), alumina (Al₂O₃), and titania (TiO₂) are commonly used as a carrier or support for catalytic materials due to their high surface areas, high thermal stability and high mechanical resistance. Thus, an active catalytic phase such as metal or metal oxide species can be highly dispersed on the high surface area supports. It is noted that high dispersion of the active catalytic phase may lead to great accessibility to utilize the active sites for surface reaction. Supported cobalt (Co) catalysts are preferred for Fischer–Tropsch synthesis (FTS) based on natural gas [1] due to their high activities for FTS, high selectivity for long chain hydrocarbons and low activities for the competitive water–gas shift (WGS) reaction [2,3]. Many inorganic supports such as silica [4–8], alumina [9–14], titania [15–17] and zeolites [18] have been extensively studied for supported Co catalysts for years. It is known that in general, the catalytic properties depend on reaction conditions, catalyst composition, type of inorganic support and the degree of metal dispersion as well.

It is reported that during the past decades, titania-supported Co catalysts have been investigated widely by many authors, especially for the application of FTS in a continuously stirred tank reactor (CSTR) [15–17]. However, it should be noted that titania itself has different crystalline phases such as anatase, brookite and rutile phase. Thus, the differences in compositions of crystalline phases could result in changes on physical and chemical properties of titania, then consequently for the dispersion of cobalt. In order to give a better understanding of those, the focus of this present study was to investigate the cobalt dispersion on titania consisting various ratios of rutile:anatase. The Co/TiO₂ was prepared and then characterized using different characterization techniques.

2. Experimental

2.1. Material preparation

2.1.1. Preparation of titania support consisting various rutile:anatase ratios

The various ratios of rutile:anatase in titania support were obtained by calcination of pure anatase titania (obtained from

* Corresponding author. Tel.: +66 2 2186869; fax: +66 2 2186766.
E-mail address: bunjerd.j@chula.ac.th (B. Jongsomjit).

Ishihara Sangyo, Japan) in air at temperatures between 800 and 1000 °C for 4 h. The high space velocity of air flow (16,000 h⁻¹) insured the gradual phase transformation to avoid rapid sintering of samples. The ratios of rutile:anatase were determined by XRD according to the method described by Jung et al. [19] as follows:

$$\% \text{Rutile} = \frac{1}{\left[\left(\frac{A}{R}\right) 0.884 + 1\right]} \times 100$$

where, A and R are the peak area for major anatase ($2\theta = 25^\circ$) and rutile phase ($2\theta = 28^\circ$), respectively.

2.1.2. Preparation of Co/TiO₂ samples

A 20 wt.% of Co/TiO₂ was prepared by the incipient wetness impregnation. A designed amount of cobalt nitrate [Co(NO₃)₃·6H₂O] was dissolved in deionized water and then impregnated onto TiO₂ containing various ratios of rutile:anatase obtained from Section 2.1.1. The sample was dried at 110 °C for 12 h and calcined in air at 500 °C for 4 h.

2.2. Nomenclature

The nomenclature used for Co/TiO₂ samples in this study is following:

- Rn: titania support consisting *n*% of rutile phase (R);
- Co/Rn: titania support containing *n*% of rutile phase (R)-supported cobalt.

2.3. Characterization

2.3.1. BET surface area

BET surface area of the samples with various rutile:anatase ratios of titania was performed to determine if the total surface area changes. It was determined using N₂ adsorption at 77 K in a Micromeritics ASAP 2010.

2.3.2. X-ray diffraction

XRD was performed to determine the bulk crystalline phases of samples. It was conducted using a SIEMENS D-5000 X-ray diffractometer with Cu Kα ($\lambda = 1.54439 \text{ \AA}$). The spectra were scanned at a rate of 2.4° min⁻¹ in the range $2\theta = 20\text{--}80^\circ$.

2.3.3. Scanning electron microscopy and energy dispersive X-ray spectroscopy

SEM and EDX were used to determine the sample morphologies and elemental distribution throughout the sample granules, respectively. The SEM of JEOL model JSM-5800LV was applied. EDX was performed using Link Isis series 300 program.

2.3.4. Hydrogen chemisorption

Static H₂ chemisorption at 100 °C on the reduced samples was used to determine the number of reduced surface cobalt

metal atoms. This is related to the overall activity of the samples during CO hydrogenation. Gas volumetric chemisorption at 100 °C was performed using the method described by Reuel and Bartholomew [20]. The experiment was performed in a Micromeritics ASAP 2010 using ASAP 2010C V3.00 software.

2.3.5. Transmission electron microscopy (TEM)

The dispersion of cobalt oxide species on the titania supports were determined using a JEOL-TEM 200CX transmission electron spectroscopy operated at 100 kV with 100k magnification.

3. Results and discussion

The present study focused on investigation of cobalt dispersion on titania consisting various ratios of rutile:anatase. After calcination of the pure anatase titania under calcination temperatures ranged between 800 and 1000 °C for 4 h, the phase transformation from anatase to rutile phase in titania technically occurred. The amounts of rutile phase formed during calcination depend on temperatures used. The high space velocity of the air flow at 16,000 h⁻¹ was applied during the calcination process in order to minimize the rapid sintering due to the phase transformation of titania. It was found that after calcination of the pure anatase sample, the amounts of rutile phase obtained ranged between 3 and 99%. The titania supports containing rutile phase of ca. 0, 3, 19, 40, 96, and 99% were named as R0, R3, R19, R40, R96, and R99, respectively. The surface areas of titania containing various rutile:anatase ratios essentially decreased from 70 m² g⁻¹ for the R0 sample (pure anatase titania) to 49 m² g⁻¹ for the R99 sample (99% rutile titania). XRD patterns of titania samples calcined at various temperatures between 800 and 1000 °C are shown in Fig. 1. For the pure anatase titania (R0), XRD peaks of the anatase phase of titania at 25° (major), 37°, 48°, 55°, 56°, 62°, 71°, and 75° were evident.

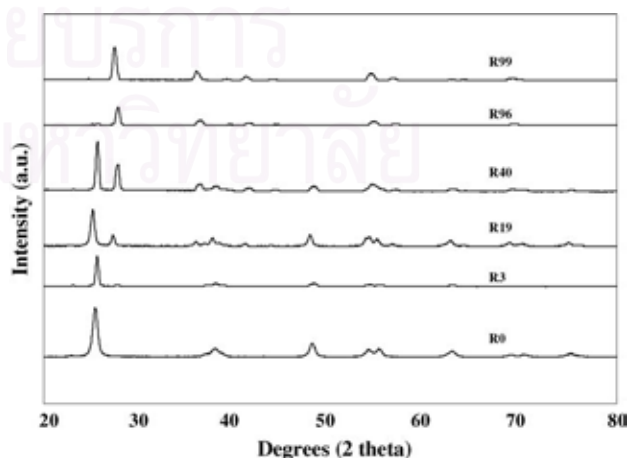


Fig. 1. XRD patterns of titania consisting various ratios of rutile:anatase phase.

After calcination of pure anatase titania sample, it was observed that besides the XRD peaks of pure anatase titania as shown above XRD peaks at 28° (major), 36° , 42° , and 57° were gradually seen. These peaks were assigned to the rutile phase essentially formed after calcination of the pure anatase titania. Apparently, the major peak at 28° of rutile phase gradually increased with increasing the calcination temperatures indicating higher content of rutile phase in titania was obtained. It was shown that the transformation from anatase to rutile phase (R99) was almost complete at temperature of ca. 1000°C resulting in the disappearance of XRD peaks for the anatase phase of titania. After various titania supports were obtained, the preparation of Co/TiO_2 via various rutile:anatase ratios of titania was consequently conducted in order to investigate the effect of various ratios of rutile:anatase in titania supports on characteristics, especially the cobalt dispersion of Co/TiO_2 .

A 20 wt.% of cobalt supported on titania consisting of various ratios of rutile:anatase phase was prepared by the conventional incipient wetness impregnation method. The XRD patterns for all calcined samples (Co/TiO_2) are shown in Fig. 2. After calcination, all calcined samples exhibited XRD peaks, which were identical with those for the corresponding titania supports. This indicated that there was no further phase transformation from anatase to rutile occurred after calcination (at temperature ca. 500°C for 4 h) of the samples. Besides the XRD peaks of the corresponding titania supports detected, all calcined samples also exhibited weak XRD peaks at 31° , 36° , and 65° , which were assigned to the presence of Co_3O_4 . However, at high content of rutile phase, the XRD peaks of Co_3O_4 were gradually diminished due to the hindrance of strong intensity of XRD peaks for the rutile phase of titania.

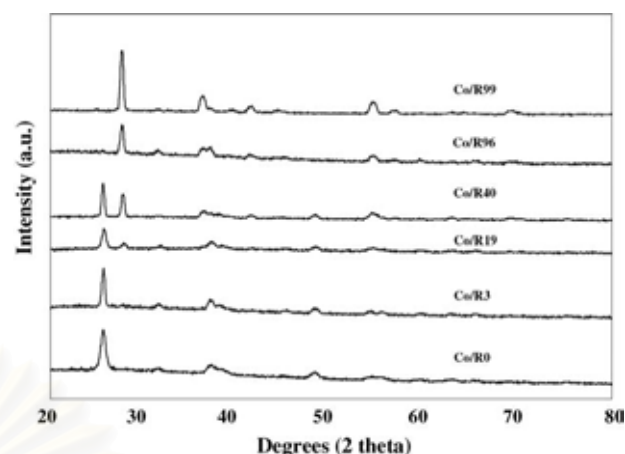


Fig. 2. XRD patterns of calcined Co/TiO_2 with various ratios of rutile:anatase phase.

Based on the XRD results, it was clear that Co_3O_4 species was definitely present in a highly dispersed form.

SEM and EDX were also conducted in order to study the morphologies and elemental distribution of the samples, respectively. Apparently, SEM micrographs and EDX mapping for all samples exhibited similar trends of morphologies and elemental (Co, Ti, and O) distributions. The typical SEM micrographs along with the EDX mapping (for Co, Ti, and O) for $\text{Co}/\text{R19}$ sample are illustrated in Fig. 3 indicating the external surface of the sample granule. It can be seen that the cobalt oxide species were well dispersed and distributed (shown on EDX mapping) all over the sample granule. Thus, SEM and EDX can not differentiate morphologies and elemental distributions of Co/TiO_2 consisting of various

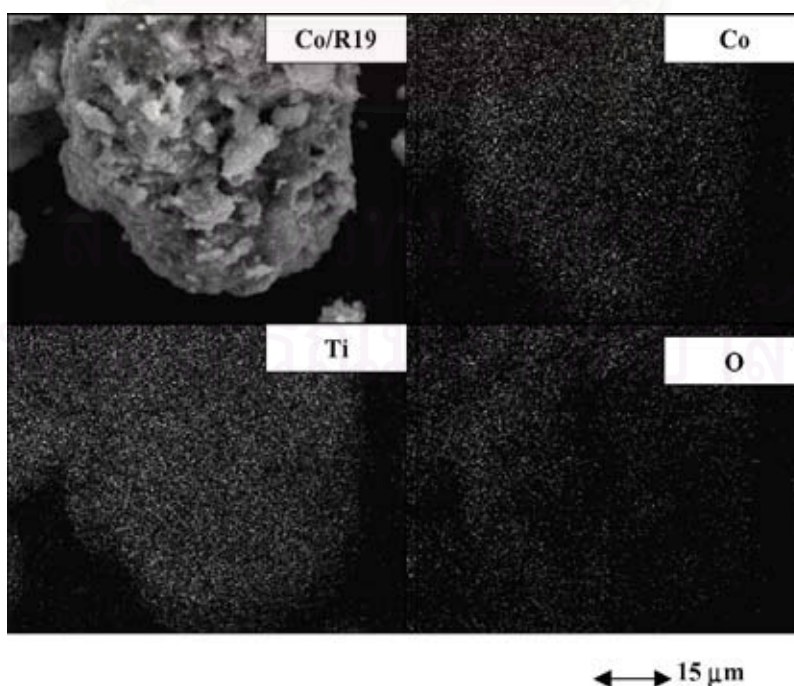


Fig. 3. SEM micrograph and EDX mapping of $\text{Co}/\text{R19}$ sample.

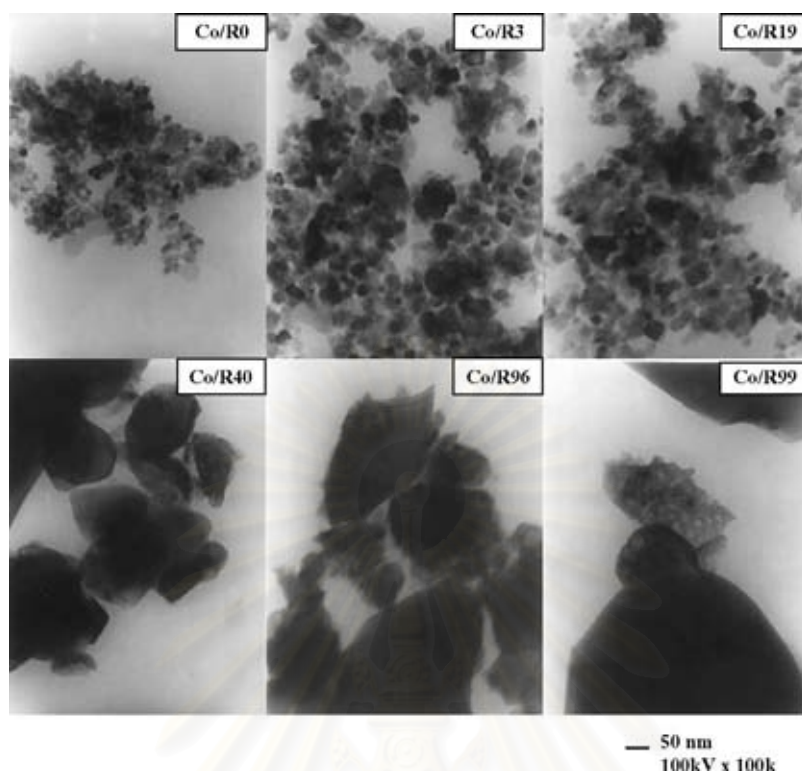


Fig. 4. TEM micrographs of Co/TiO₂ with various ratios of rutile:anatase phase.

ratios of rutile:anatase. In order to determine the dispersion of cobalt oxide species on titania, a more powerful technique such as TEM was applied to all samples. The TEM micrographs for all samples are shown in Fig. 4. The dark spots represented cobalt oxide species present after calcination of samples dispersing on titania consisting of various ratios of rutile:anatase. It can be observed that cobalt oxide species were highly dispersed on the titania supports for Co/R0, Co/R3, and Co/R19 samples resulting in an appearance of smaller cobalt oxide patches present. However, the degree of dispersion for cobalt oxide species essentially decreased with increasing the rutile phase in titania from 40 to 99% as seen for Co/R40, Co/R96, and Co/R99 samples resulting in the observation of larger cobalt oxide patches. It is suggested that the presence of the rutile phase in titania from 0 (pure anatase phase) to 19% exhibited the highly dispersed forms of cobalt oxide species for the calcined samples.

It is known that the active form of supported cobalt FTS catalysts is cobalt metal (Co⁰). Thus, reduction of cobalt oxide species is essentially performed in order to transform cobalt oxide species obtained after calcination process into the active cobalt metal atoms for catalyzing the reaction. Therefore, the static H₂ chemisorption on the reduced cobalt samples was used to determine the number of reduced Co metal surface atoms. This is usually related to the overall activity of the catalyst during carbon monoxide (CO) hydrogenation. The resulted H₂ chemisorption for all samples is shown in Fig. 5. It was found that the number of the reduced cobalt metal surface atoms increased with the presence of ru-

tile phase in titania up to a maximum at 19% of rutile phase (Co/R19) before decreasing with the greater amounts of rutile phase. Considering the number of cobalt metal atoms for Co/R0 (pure anatase titania), the number was apparently low even though highly dispersed cobalt oxides species. This was suggested that highly dispersed forms of cobalt oxide species be not only the factor that insures larger number of reduced cobalt metal surface atoms in Co/TiO₂. On the other hand, it can be observed that the number of reduced cobalt metal surface atoms for Co/R40 and Co/R96 (with the low degree of dispersion of cobalt oxide species as seen by TEM) was

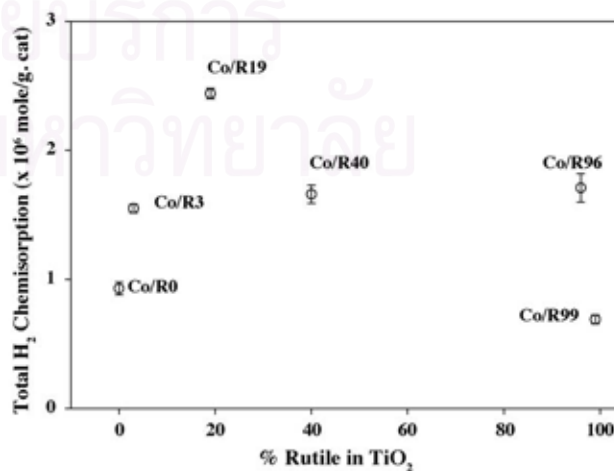


Fig. 5. A plot of the total H₂ chemisorption vs. % rutile in titania.

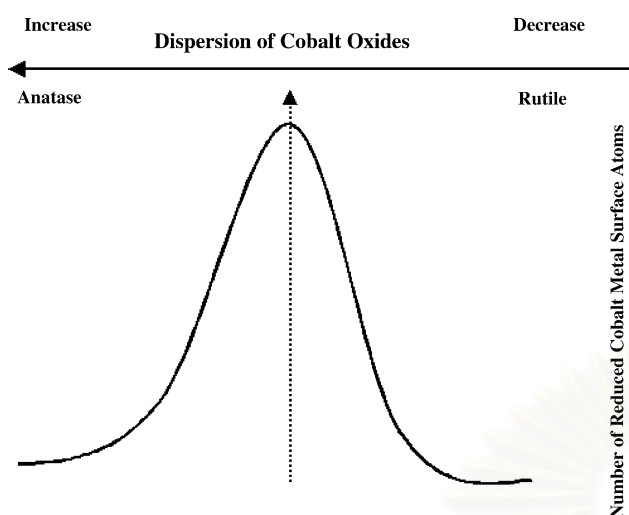


Fig. 6. A conceptual model on dependence of dispersion along with rutile phase on the number of reduced cobalt metal surface atoms for Co/TiO₂.

larger than that for Co/R0. This was due to the presence of rutile phase in Co/R40 and Co/R96. It should be mentioned that the largest number of reduced cobalt metal surface atoms for the Co/R19 sample was attributed to both highly dispersed cobalt oxide species and the presence of rutile phase in titania. In order to provide a better understanding for effects of both dispersion of cobalt oxide species and the presence of rutile phase in titania on the number of reduced cobalt metal surface atoms, a conceptual model of those is illustrated in Fig. 6. Thus, a large number of reduced cobalt metal surface atoms in Co/TiO₂ can be obtained with an optimum amount of rutile phase along with highly dispersed cobalt oxide species prior to reduction. It was suggested that the presence of rutile phase in titania can facilitate the reduction of cobalt oxide species as shown in Fig. 7. It was observed that the presence of rutile phase resulted in lowering the reduction temperature. However, the large amounts of rutile phase can result in a small number of reduced cobalt metal surface atoms. This is due to the low degree of dispersion for cobalt oxide species

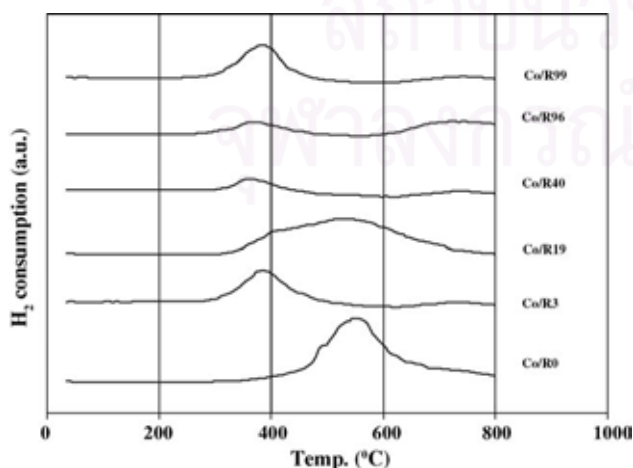


Fig. 7. TPR behaviors of Co/TiO₂ with various ratios of rutile:anatase phase.

with large amounts of rutile phase present. It should be also noted that part of the reason for the lower dispersion of Co is the lower BET surface area, especially for the rutile rich titania.

4. Conclusions

The present study showed dependence of both highly dispersed cobalt oxide species and the presence of rutile phase in titania on the number of reduced cobalt metal atoms in Co/TiO₂. It was found that the presence of rutile phase with optimum amounts in titania up to 19% resulted in highly dispersed cobalt oxide species as seen by TEM. Although with highly dispersed cobalt oxide species, Co/R0 (pure anatase titania) gave the low number of reduced cobalt metal surface atoms. On the other hand, Co/R40 and Co/R96 with a low degree of cobalt oxide dispersion apparently gave the higher number (compared to Co/R0) of reduced cobalt metal surface atoms. Thus, both highly dispersed cobalt oxide species along with the presence of rutile phase in titania could play an important role on the number of reduced cobalt metal surface atoms for Co/TiO₂.

Acknowledgements

We gratefully acknowledge the financial support by the National Research Council of Thailand (NRCT), the Thailand Research Fund (TRF) and Thailand–Japan Technology Transfer Project (TJTTP-JBIC). We would like to thank Prof. James G. Goodwin Jr. at Clemson University for initiating this kind of project.

References

- [1] H.P. Wither Jr., K.F. Eliezer, J.W. Mechell, *Ind. Eng. Chem. Res.* 29 (1990) 1807.
- [2] E. Iglesia, *Appl. Catal. A* 161 (1997) 59.
- [3] R.C. Brady, R.J. Pettie, *J. Am. Chem. Soc.* 103 (1981) 1287.
- [4] A. Martinez, C. Lopez, F. Marquez, I. Duaz, *J. Catal.* 220 (2003) 486.
- [5] J. Panpranot, J.G. Goodwin Jr., A. Sayari, *Catal. Today* 77 (2002) 269.
- [6] J. Panpranot, J.G. Goodwin Jr., A. Sayari, *J. Catal.* 211 (2002) 530.
- [7] S.L. Sun, I. Isubaki, K. Fujimoto, *Appl. Catal. A* 202 (2000) 121.
- [8] S. Ali, B. Chen, J.G. Goodwin Jr., *J. Catal.* 157 (1995) 35.
- [9] B. Jongsomjit, J. Panpranot, J.G. Goodwin Jr., *J. Catal.* 215 (2003) 66.
- [10] T. Das, G. Jacobs, P.M. Patterson, W.A. Conner, J.L. Li, B.H. Davis, *Fuel* 82 (2003) 805.
- [11] G. Jacobs, P.M. Patterson, Y.Q. Zhang, T. Das, J.L. Li, B.H. Davis, *Appl. Catal. A* 233 (2002) 215.
- [12] M. Rothaemel, K.F. Hanssen, E.A. Blekkan, D. Schanke, A. Holmen, *Catal. Today* 38 (1997) 79.
- [13] V. Ragaini, R. Carli, C.L. Bianchi, D. Lorenzetti, G. Vergani, *Appl. Catal. A* 139 (1996) 17.

- [14] V. Ragaini, R. Carli, C.L. Bianchi, D. Lorenzetti, G. Predieri, P. Moggi, *Appl. Catal. A* 139 (1996) 31.
- [15] J.L. Li, G. Jacobs, T. Das, B.H. Davis, *Appl. Catal. A* 233 (2002) 255.
- [16] G. Jacobs, T. Das, Y.Q. Zhang, J.L. Li, G. Racoillet, B.H. Davis, *Appl. Catal. A* 233 (2002) 263.
- [17] J.L. Li, L.G. Xu, R. Keogh, B.H. Davis, *Catal. Lett.* 70 (2000) 127.
- [18] X.H. Li, K. Asami, M.F. Luo, K. Michiki, N. Tsubaki, K. Fujimoto, *Catal. Today* 84 (2003) 59.
- [19] K.Y. Jung, S.B. Park, *J. Photochem. Photobio. A: Chem.* 127 (1999) 117.
- [20] R.C. Reuel, C.H. Bartholomew, *J. Catal.* 85 (1984) 63.



สถาบันวิทยบริการ
จุฬาลงกรณ์มหาวิทยาลัย

Available online at www.sciencedirect.com

SCIENCE @ DIRECT®

Catalysis Communications 6 (2005) 705–710

CATALYSIS
COMMUNICATIONSwww.elsevier.com/locate/catcom

Characteristics and catalytic properties of Co/TiO₂ for various rutile:anatase ratios

Bunjerd Jongsomjit *, Tipnapa Wongsalee, Piyasan Prasertthdam

Center of Excellence on Catalysis and Catalytic Reaction Engineering, Department of Chemical Engineering, Faculty of Engineering, Chulalongkorn University, Bangkok 10330, Thailand

Received 21 March 2005; received in revised form 5 July 2005; accepted 5 July 2005

Abstract

This present study revealed a dependence of rutile:anatase ratios in titania on the characteristics and catalytic properties of Co/TiO₂ catalysts during CO hydrogenation. In this study, Co/TiO₂ catalysts were prepared using various titania supports consisting of various rutile:anatase ratios of titania. In order to identify the characteristics, all catalyst materials were characterized using XRD, SEM/EDX, TPR, and hydrogen chemisorption. CO hydrogenation (H₂/CO = 10/1) was also performed to determine the overall activity and selectivity. It was found that both activity and selectivity were altered by changing the rutile:anatase ratios in the titania support.

© 2005 Elsevier B.V. All rights reserved.

Keywords: Cobalt catalyst; Titania; Chemisorption; CO; hydrogenation; Titania phase

1. Introduction

It has been known that supported cobalt (Co) catalysts are used for carbon monoxide (CO) hydrogenation because of their high activities based on natural gas [1], high selectivity to linear long chain hydrocarbons and also low activities for the competitive water–gas shift (WGS) reaction [2,3]. Many inorganic supports such as SiO₂ [4–8], Al₂O₃ [9–14], TiO₂ [15–17] and zeolites [18] have been extensively studied for supported Co catalysts for years. It is known that in general, the catalytic properties depend on reaction conditions, catalyst compositions, metal dispersion, and types of inorganic supports used. Thus, changes in the catalyst composition and/or even though the compositions of supports

used may lead to significant enhanced catalytic properties as well.

During the past decades, titania-supported Co catalysts have been widely investigated by many authors, especially for the application of FT synthesis in a continuously stirred tank reactor (CSTR) [15–17]. However, it should be noted that titania itself has different crystalline phases such as anatase, brookite and rutile phase. Differences in crystalline phases may result in changes in physical and chemical properties of titania. Thus, different crystalline phase compositions of titania could play an important role on the catalytic performance of titania-supported Co catalysts during CO hydrogenation as well.

Therefore, the main objective of this present research was to investigate influences of various rutile:anatase ratios in titania support on the characteristics and catalytic properties during CO hydrogenation of Co/TiO₂ catalysts. In the present study, the Co/TiO₂ catalysts were prepared using various titania supports containing different ratios of rutile:anatase phase. The catalysts

* Corresponding author. Tel.: +662 218 6869; fax: +662 218 6766/6877.

E-mail address: bunjerd.j@chula.ac.th (B. Jongsomjit).

were characterized using various characterization techniques and tested in order to evaluate the catalytic properties during CO hydrogenation.

2. Experimental

2.1. Material preparation

2.1.1. Preparation of titania support

The various ratios of rutile:anatase in titania support were obtained by calcination of pure anatase titania (obtained from Ishihara Sangyo, Japan) in air at temperatures between 800 and 1000 °C for 4 h. The high space velocity of air flow (16,000 h⁻¹) insured the gradual phase transformation to avoid rapid sintering of samples. The ratios of rutile:anatase were determined by XRD according to the method described by Jung and Park [19] as follows:

$$\% \text{ Rutile} = \frac{1}{[(A/R)0.884 + 1]} \times 100,$$

where *A* and *R* are the peak area for major anatase ($2\theta = 25^\circ$) and rutile phase ($2\theta = 28^\circ$), respectively.

2.1.2. Preparation of catalyst samples

A 20 wt% of Co/TiO₂ was prepared by the incipient wetness impregnation. A designed amount of cobalt nitrate [Co(NO₃)₃·6H₂O] was dissolved in deionized water and then impregnated onto TiO₂ containing various ratios of rutile:anatase obtained from Section 2.1.1. The catalyst precursor was dried at 110 °C for 12 h and calcined in air at 500 °C for 4 h.

2.2. Catalyst nomenclature

The nomenclature used for the catalyst samples in this study is following:

- *Rn*: titania support containing *n*% of rutile phase (R).
- *Co/Rn*: titania support containing *n*% of rutile phase (R)-supported cobalt.

2.3. Catalyst characterization

2.3.1. BET surface area

BET surface area of the samples with various rutile:anatase ratios of TiO₂ was performed to determine if the total surface area changes. It was determined using N₂ adsorption at 77 K in a Micromeritics ASAP 2010.

2.3.2. X-ray diffraction

XRD was performed to determine the bulk crystalline phases of catalyst. It was conducted using a SIEMENS D-5000 X-ray diffractometer with Cu *K*α ($\lambda = 1.54439$

Å). The spectra were scanned at a rate of 2.4 deg/min in the range $2\theta = 20\text{--}80^\circ$.

2.3.3. Scanning electron microscopy and energy dispersive X-ray spectroscopy

SEM and EDX were used to determine the catalyst morphologies and elemental distribution throughout the catalyst granules, respectively. SEM was carried out using a JEOL model JSM-5800LV. EDX was performed using Link Isis series 300 program.

2.3.4. Hydrogen chemisorption

Static H₂ chemisorption at 100 °C on the reduced cobalt catalysts was used to determine the number of reduced surface cobalt metal atoms. Prior to H₂ chemisorption, the catalyst sample was reduced in H₂ at 350 °C for 10 h. The resulting H₂ chemisorption is related to the overall activity of the catalysts during CO hydrogenation. Gas volumetric chemisorption at 100 °C was performed using the method described by Reuel and Bartholomew [20]. The experiment was performed in a Micromeritics ASAP 2010 using ASAP 2010C V3.00 software.

2.3.5. Temperature-programmed reduction

TPR was used to determine the reduction behaviors and reducibilities of the samples. It was carried out using 50 mg of a sample and a temperature ramp from 35 to 800 °C at 5 °C/min. The carrier gas was 5% H₂ in Ar. A cold trap was placed before the detector to remove water produced during the reaction. A thermal conductivity detector (TCD) was used to determine the amount of H₂ consumed during TPR. The H₂ consumption was calibrated using TPR of Ag₂O at the same conditions. The calculation of reducibilities was as described elsewhere [9,21–24].

2.4. Reaction

CO hydrogenation (H₂/CO = 10/1) was performed to determine the overall activity of the catalyst samples. Hydrogenation of CO was carried out at 220 °C and 1 atm. A flow rate of H₂/CO/He = 20/2/8 cm³/min in a fixed-bed flow reactor under differential conditions was used. A relatively high H₂/CO ratio was used to minimize deactivation due to carbon deposition during reaction. Typically, 20 mg of a catalyst sample was reduced in situ in flowing H₂ (30 cm³/min) at 350 °C for 10 h prior to the reaction. Reactor effluent samples were taken at 1 h intervals and analyzed by GC. In all cases, steady state was reached within 5 h.

3. Results and discussion

The present study showed the dependence of rutile:anatase ratios in titania on the catalytic properties during

CO hydrogenation of Co/TiO₂ catalysts. As mentioned, in general titania used contains mainly two phases; anatase and rutile phases. Phase transformation of titania depends on the preparation of titania such as sol–gel or solvothermal methods and also calcination temperatures. However, it was proposed that the different phase compositions in titania could play an important role on the catalytic properties during CO hydrogenation of Co/TiO₂ catalysts. Results and discussion are divided into two parts as follows.

3.1. Crystalline phases of titania

After calcination of the pure anatase titania under calcination temperatures ranging between 800 and 1000 °C for 4 h, the phase transformation from anatase to rutile phase should technically occur. The amounts of rutile phase formed during calcination depended on the temperature used. The high space velocity of the air flow at 16,000 h⁻¹ was applied during the calcination process in order to minimize the rapid sintering due to the phase transformation of titania. It was found that after calcination of the pure anatase sample, the amounts of rutile phase obtained ranged between 3% and 99%. The titania supports containing rutile phase of ca. 0%, 3%, 19%, 40%, 96%, and 99% were named as R0, R3, R19, R40, R96, and R99, respectively. The surface areas of titania containing various rutile:anatase ratios essentially decreased from 70 m²/g for the R0 sample (pure anatase titania) to 49 m²/g for the R99 sample (99% rutile titania). XRD patterns of titania samples calcined at various temperatures between 800 and 1000 °C are shown in Fig. 1. For the pure anatase titania (R0), XRD peaks of the anatase phase of titania at 25° (major), 37°, 48°, 55°, 56°, 62°, 71°, and 75° were evident. After calcination of the pure anatase titania sample, it was observed that besides the XRD peaks of pure anatase titania as shown above XRD peaks at

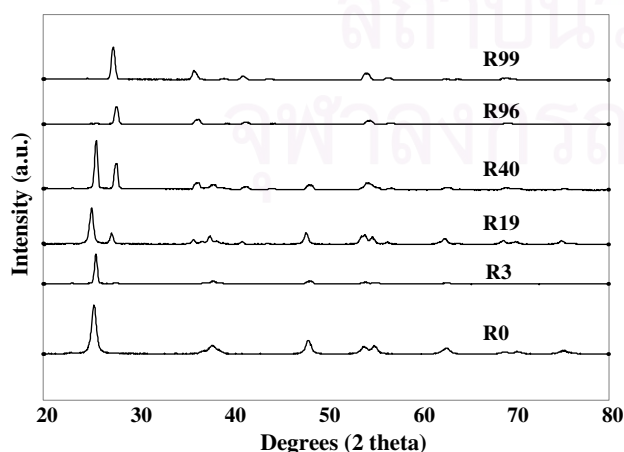


Fig. 1. XRD patterns for various ratios of rutile:anatase in titania supports.

28° (major), 36°, 42°, and 57° were gradually seen. These peaks were assigned to the rutile phase essentially formed after calcination of the pure anatase titania. Apparently, the major peak at 28° of the rutile phase gradually increased with increasing the calcination temperatures indicating a higher content of rutile phase in the titania. It was shown that the transformation from anatase to rutile phase (R99) was almost complete at a temperature of ca. 1000 °C, resulting in the disappearance of XRD peaks for the anatase phase of titania. After various titania supports were obtained, the preparation of Co/TiO₂ with various rutile:anatase ratios of titania was consequently conducted in order to investigate the effect of the rutile:anatase ratio on characteristics and catalytic properties of the Co/TiO₂ catalysts during CO hydrogenation.

3.2. Characteristics of Co/TiO₂

A 20 wt% of cobalt on titania supports containing various ratios of rutile:anatase phase was prepared by the conventional incipient wetness impregnation method. The XRD patterns for all calcined catalyst samples (Co/TiO₂) exhibited similar patterns as seen in Fig. 1. After calcination, all calcined samples exhibited XRD peaks, which were identical with those for the corresponding titania supports. This indicated that no further phase transformation from anatase to rutile occurred after calcination (at temperature ca. 500 °C for 4 h) of the catalyst samples. Besides the XRD peaks of the titania, all calcined samples also exhibited weak XRD peaks at 31°, 36°, and 65°, which were assigned to the presence of Co₃O₄. However, at high content of the rutile phase, the XRD peaks of Co₃O₄ were less apparent due to the strong intensity of XRD peaks for the rutile phase of titania. Based on the XRD results, it was clear that Co₃O₄ species were definitely present in a highly dispersed form.

SEM and EDX were also conducted in order to study the morphologies and elemental distribution of the catalyst samples, respectively. The typical SEM micrograph along with the EDX mapping (for Co, Ti, and O) are illustrated in Fig. 2 for the Co/R40 sample. The external surface of catalyst granule is shown in all figures and the light or white patches on the catalyst granule surface represent high concentration of cobalt oxides species on the surface. It can be seen that the cobalt oxide species were well dispersed and distributed (shown on mapping) all over the catalyst granule in all samples regardless of the ratio of rutile:anatase in the titania.

TPR was performed in order to identify the reduction behaviors and reducibility of catalysts. TPR profiles for all samples are shown in Fig. 3. TPR of the titania support samples used was also conducted at the same TPR conditions used for the catalyst samples (not shown) and no hydrogen consumption was detected.

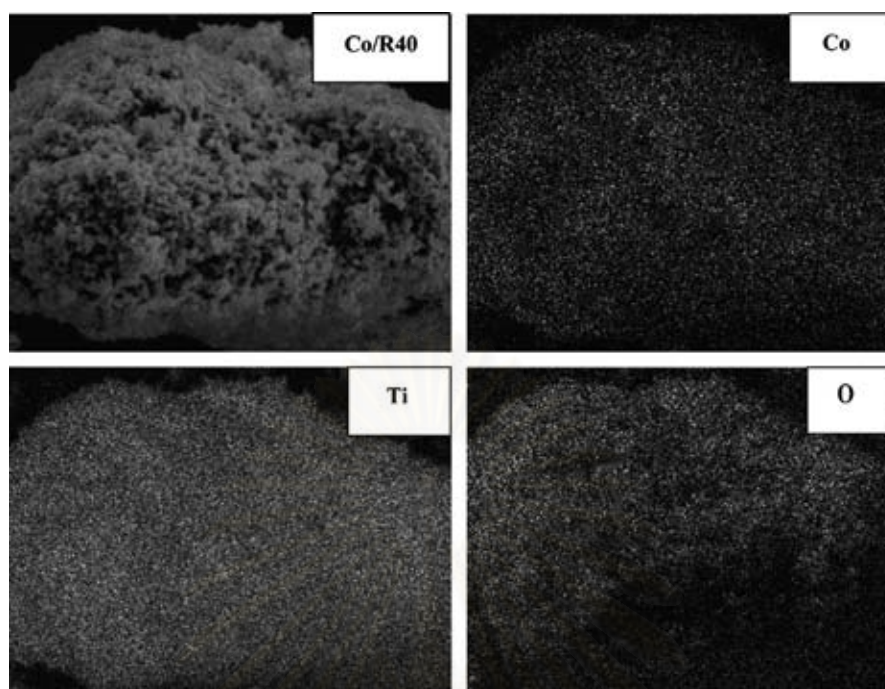


Fig. 2. A typical SEM micrograph for Co/R40 granule and EDX for Co, Ti, and O mapping.

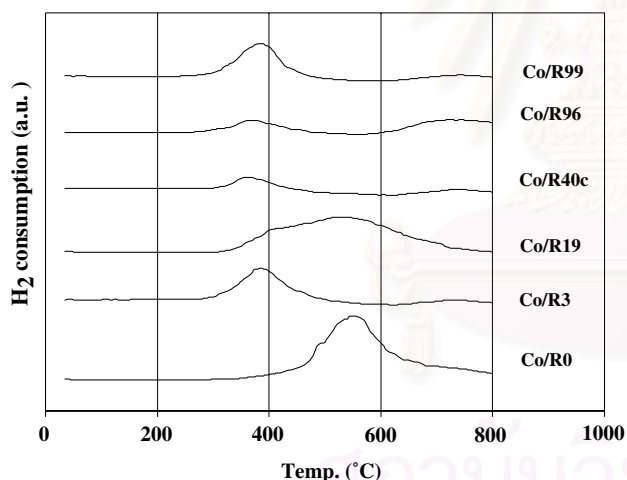


Fig. 3. TPR profiles for Co/TiO₂ catalysts with various ratios of rutile:anatase in titania supports used.

This indicated that the titania supports used themselves were not reducible at these TPR conditions. Apparently, TPR profiles of all calcined samples were similar exhibiting only one strong reduction peak as shown in Fig. 3. This peak can be assigned to the overlap of two-step reduction of Co₃O₄ to CoO and then to Co⁰ [25]. Under TPR conditions, the two reduction peaks based on the two-step reduction may or may not be observed. The presence of only one reduction peak during TPR for all catalyst samples indicated that no residual cobalt nitrates precursor remained on the samples under the calcination condition used in this study. It was found that a TPR peak located at ca.

380–700 °C (max. at 520 °C) was observed for the Co/R0 sample. However, this reduction peak was dramatically shifted about 50–80 °C lower when ca. 3–99% of rutile phase (Co/R3 to Co/R99) was present in the titania supports used. This suggests that the presence of rutile phase in titania can facilitate the reduction process of cobalt oxide species on the titania support leading to reduction at a lower temperature. Since TPR is more of a bulk technique, it should be noted that the number of reduced Co metal obtained from the TPR measurement might not be well representative of the number of reduced Co metal surface atoms available for catalyzing CO hydrogenation. Therefore, static H₂ chemisorption on the reduced cobalt catalyst samples was used to determine the number of reduced Co metal surface atoms. This is usually related to the overall activity of the catalyst during CO hydrogenation.

The resulting H₂ chemisorption results for all catalyst samples are shown in Fig. 4. It was found that the amounts of H₂ adsorbed increased with the presence of rutile phase in titania up to a maximum at 19% of rutile phase (Co/R19) before decreasing when greater amounts of the rutile phase were present. Since H₂ chemisorption is a surface technique that the reduced Co metal surface atoms can be measured directly. The amounts of H₂ adsorbed on Co/TiO₂ obtained were lower compared to those for Co/Al₂O₃ and Co/SiO₂ at similar loading [5,6,21,22]. However, based on the H₂ chemisorption results in this present study, different ratios of rutile: anatase phase in titania exhibited different amounts of H₂ chemisorbed on the catalyst samples.

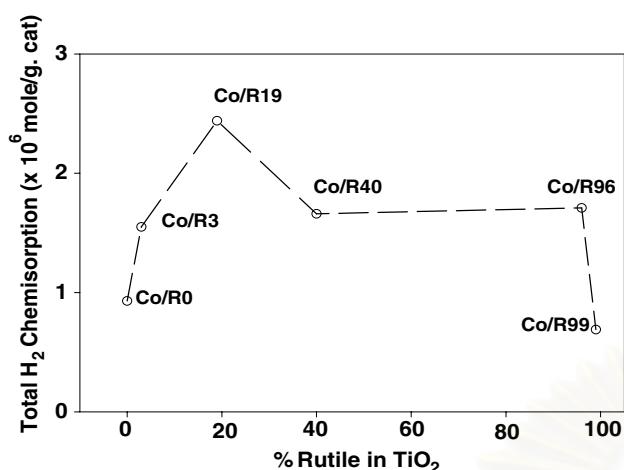


Fig. 4. H₂ chemisorption for Co/TiO₂ catalysts with various ratios of rutile:anatase in titania supports used.

3.3. Reactivity

In order to measure the catalytic properties of the catalyst samples with various ratios of rutile:anatase in titania, CO hydrogenation was performed in a fixed-bed flow reactor under differential condition. The results are shown in Fig. 5 and Table 1. It indicated that the reaction rate ranged between 0.3 and 6.6 $\mu\text{mole/g. cat. s}$ (initial) and between 0.2 and 5.2 $\mu\text{mole/g cat s}$ (steady state). This also showed that activities of the samples increased with the presence of rutile phase in titania up to a maximum at 19% of rutile phase (Co/R19) before decreasing when greater amounts of rutile phase were present, similar to the results obtained from H₂ chemisorption. Considering selectivity to methane, it was found that the presence of rutile phase in titania resulted in an increased selectivity to methane. After reaction, XRD of the spent catalyst samples was also

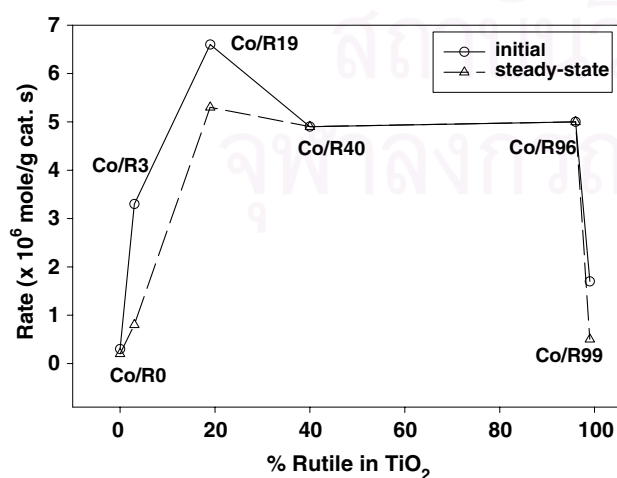


Fig. 5. Reaction rate during CO hydrogenation for Co/TiO₂ catalysts with various ratios of rutile:anatase in titania supports used.

Table 1

Activities and selectivity during CO hydrogenation of Co/TiO₂ via various rutile:anatase ratios of titania support

Catalyst samples	Rate ($\mu\text{mol/g cat s}$) ^a		Selectivity to CH ₄ (%)	
	Initial ^b	Steady state ^c	Initial ^b	Steady state ^c
Co/R0	0.3	0.2	71	68
Co/R3	3.3	0.8	99	99
Co/R19	6.6	5.3	98	98
Co/R40	4.9	4.9	97	96
Co/R96	5.0	5.0	99	99
Co/R99	1.7	0.5	94	94

^a CO hydrogenation was carried out at 220 °C, 1 atm, and H₂/CO/He = 20/2/8.

^b After 5 min of reaction.

^c After 5 h of reaction.

performed in order to identify the bulk crystalline phases of the spent catalyst samples. It showed that the XRD patterns of all spent catalyst samples were identical with those of the corresponding fresh ones suggesting no phase changes occurred during the reaction condition used.

Based on the reaction study, it can be concluded that the catalytic properties of Co/TiO₂ depend on the ratio of rutile/anatase. The results revealed that the presence of rutile phase of an optimum of the rutile phase (i.e., Co/R19) result in an increased catalytic activity during CO hydrogenation. It is proposed that the presence of rutile phase in titania can facilitate the reduction process of cobalt oxides species resulting in lower reduction temperatures. The presence of some rutile phase also resulted in an increased number of reduced cobalt metal surface atoms available for catalyzing the reaction. However, higher ratios (more than 19%) of rutile:anatase in titania decreased the catalyst activities. It should be mentioned that besides the ratios of rutile:anatase in titania, there are also other factors such as preparation methods, titania precursors, particle sizes, modes and types of reactions that would affect the characteristics and catalytic properties of titania used both as a catalyst support or a catalyst itself.

4. Conclusion

The present research showed a dependence of the characteristics and catalytic properties during CO hydrogenation on the ratio of rutile/anatase in titania for Co. The study revealed that the presence of 19% rutile phase in titania for Co/TiO₂ (Co/R19) exhibited the highest activity during CO hydrogenation. It appeared that the increase in activity was due to two reasons;(i) the presence of rutile phase in titania can facilitate the reduction process of cobalt oxide species into reduced cobalt metal and (ii) the presence of some rutile phase resulted in a larger number of reduced cobalt metal surface atoms, which is related to the activity during CO hydrogenation.

However, if the ratio of rutile:anatase was over 19%, the activity dramatically decreased. No further phase transformation of the supports occurred during calcination of the catalysis samples and reaction.

Acknowledgements

We gratefully acknowledge the financial support by the National Research Council of Thailand (NRCT), the Thailand Research Fund (TRF) and Thailand–Japan Technology Transfer Project (TJTTP-JBIC). We thank Prof. James G. Goodwin, Jr. at Clemson University for initiating this kind of project.

References

- [1] A.P. Steynberg, M.E. Dry, B.H. Davis, B.B. Breman, in: Fischer-Tropsch Technology Study, Surface Science and Catalysis 152 (2004) 64.
- [2] E. Iglesia, *Appl. Catal.* 161 (1997) 59.
- [3] R.C. Brady, R.J. Pettie, *J. Am. Chem. Soc.* 103 (1981) 1287.
- [4] A. Martinez, C. Lopez, F. Marquez, I. Duaz, *J. Catal.* 220 (2003) 486.
- [5] J. Panpranot, J.G. Goodwin Jr., A. Sayari, *Catal. Today* 77 (2002) 269.
- [6] J. Panpranot, J.G. Goodwin Jr., A. Sayari, *J. Catal.* 211 (2002) 530.
- [7] S.L. Sun, I. Isubaki, K. Fujimoto, *Appl. Catal.* 202 (2000) 121.
- [8] S. Ali, B. Chen, J.G. Goodwin Jr., *J. Catal.* 157 (1995) 35.
- [9] B. Jongsomjit, J. Panpranot, J.G. Goodwin Jr., *J. Catal.* 215 (2003) 66.
- [10] T. Das, G. Jacobs, P.M. Patterson, W.A. Conner, J.L. Li, B.H. Davis, *Fuel* 82 (2003) 805.
- [11] G. Jacobs, P.M. Patterson, Y.Q. Zhang, T. Das, J.L. Li, B.H. Davis, *Appl. Catal.* 233 (2002) 215.
- [12] M. Rothaemel, K.F. Hanssen, E.A. Blekkan, D. Schanke, A. Holmen, *Catal. Today* 38 (1997) 79.
- [13] V. Ragaini, R. Carli, C.L. Bianchi, D. Lorenzetti, G. Vergani, *Appl. Catal.* 139 (1996) 17.
- [14] V. Ragaini, R. Carli, C.L. Bianchi, D. Lorenzetti, G. Predieri, P. Moggi, *Appl. Catal.* 139 (1996) 31.
- [15] J.L. Li, G. Jacobs, T. Das, B.H. Davis, *Appl. Catal.* 233 (2002) 255.
- [16] G. Jacobs, T. Das, Y.Q. Zhang, J.L. Li, G. Racoillet, B.H. Davis, *Appl. Catal.* 233 (2002) 263.
- [17] J.L. Li, L.G. Xu, R. Keogh, B.H. Davis, *Catal. Lett.* 70 (2000) 127.
- [18] X.H. Li, K. Asami, M.F. Luo, K. Michiki, N. Tsubaki, K. Fujimoto, *Catal. Today* 84 (2003) 59.
- [19] K.Y. Jung, S.B. Park, *J. Photochem. Photobiol. A* 127 (1999) 117.
- [20] R.C. Reuel, C.H. Bartholomew, *J. Catal.* 85 (1984) 63.
- [21] B. Jongsomjit, J. Panpranot, J.G. Goodwin Jr., *J. Catal.* 204 (2001) 98.
- [22] B. Jongsomjit, J.G. Goodwin Jr., *Catal. Today* 77 (2002) 191.
- [23] A. Kogelbauer, J.C. Weber, J.G. Goodwin Jr., *Catal. Lett.* 34 (1995) 269.
- [24] Y. Zhang, D. Wei, S. Hammache, J.G. Goodwin Jr., *J. Catal.* 188 (1999) 281.
- [25] B. Jongsomjit, C. Sakdamnusun, J.G. Goodwin Jr., P. Prasertdam, *Catal. Lett.* 94 (2004) 209.

Available online at www.sciencedirect.com

SCIENCE @ DIRECT®

Materials Chemistry and Physics xxx (2005) xxx–xxx

MATERIALS
CHEMISTRY AND
PHYSICSwww.elsevier.com/locate/matchemphys

Catalytic behaviors of mixed TiO₂-SiO₂-supported cobalt Fischer–Tropsch catalysts for carbon monoxide hydrogenation

Bunjerd Jongsomjit*, Tipnapa Wongsalee, Piyasan Praserttham

*Center of Excellence on Catalysis and Catalytic Reaction Engineering, Department of Chemical Engineering,
Faculty of Engineering, Chulalongkorn University, Bangkok 10330, Thailand*

Received 11 April 2005; received in revised form 7 July 2005; accepted 9 August 2005

Abstract

In the present study, the catalytic behaviors of mixed TiO₂-SiO₂-supported cobalt (Co) Fischer–Tropsch (FT) catalysts via carbon monoxide (CO) hydrogenation were investigated. The various weight ratios of TiO₂/SiO₂ were prepared, then consequently impregnated with the cobalt precursor. After calcination, the various samples were characterized using XRD, Raman spectroscopy, scanning electron microscopy/energy dispersive X-ray (SEM/EDX), transmission electron microscopy (TEM), temperature-programmed reduction (TPR), and H₂ chemisorption. The characteristics of various samples were further discussed in more details. Based on the reaction study, it revealed that the presence of titania in the mixed supports resulted in decreased activities dramatically. However, longer chain hydrocarbons such as C₂–C₅ can be obtained substantially with increasing the amounts of titania in the mixed supports.

© 2005 Elsevier B.V. All rights reserved.

Keywords: Silica; Titania; Cobalt; Catalyst; CO hydrogenation

1. Introduction

It has been known that supported cobalt (Co) catalysts are preferred for Fischer–Tropsch (FT) synthesis because of their high activities during FT synthesis based on natural gas [1], high selectivity to linear long chain hydrocarbons and also low activities for the competitive water–gas shift (WGS) reaction [2,3]. Many inorganic supports such as SiO₂ [4–8], Al₂O₃ [9–14], TiO₂ [15–17] and zeolites [18] have been extensively studied for supported Co catalysts for years. It is known that in general, the catalytic properties depend on reaction conditions, catalyst compositions, metal dispersion, and types of inorganic supports used. Thus, changes the catalyst compositions and/or even though the compositions of supports used may lead to significantly enhance the catalytic properties as well.

The TiO₂-SiO₂ mixed oxide has been considered to be very attractive as catalysts and supports, which have brought much attention in recent years. It was reported that TiO₂-SiO₂

mixed materials have been used as catalysts and supports for various reactions [19]. However, the use of this mixed oxide support here with the cobalt catalyst has not been reported yet. This TiO₂-SiO₂ mixed oxide would lead to robust catalytic supports of cobalt catalyst for carbon monoxide (CO) hydrogenation reaction.

Therefore, the main objective of this present study was to investigate the catalytic behaviors of mixed TiO₂-SiO₂-supported cobalt Fischer–Tropsch catalyst via CO hydrogenation reaction. The ratios of TiO₂/SiO₂ used were varied. The mixed oxide supports and catalyst precursors were prepared, characterized and tested for CO hydrogenation. The role of titania in the mixed oxide supports on the catalytic behaviors was also further discussed.

2. Experimental

2.1. Material preparation

2.1.1. Preparation of TiO₂-SiO₂ mixed oxide support

TiO₂-SiO₂ mixed oxide supports [surface areas of SiO₂ = 300 m² g⁻¹ and TiO₂ = 70 m² g⁻¹ (anatase form)]

* Corresponding author. Tel.: +662 2186869; fax: +662 2186877.

E-mail address: bunjerd.j@chula.ac.th (B. Jongsomjit).

2

B. Jongsonjit et al. / Materials Chemistry and Physics xxx (2005) xxx–xxx

were prepared according to the method described by Conway et al. [20]. In particular, 1 g of TiO₂-SiO₂ mixed oxide support was physically mixed by dispersing in toluene (ca. 20 ml). The mixture was stirred for 30 min, filtered, and then dried under vacuum. The TiO₂/SiO₂ weight ratios were varied from 0/1, 2/8, 4/6, 6/4, 8/2, and 1/0. The mixed supports were calcined at 500 °C for 4 h.

2.1.2. Preparation of catalyst samples

A 20 wt.% of Co/TiO₂-SiO₂ mixed support was prepared by the incipient wetness impregnation. A designed amount of cobalt nitrate [Co(NO₃)₂·6H₂O] was dissolved in deionized water and then impregnated onto the mixed oxide supports obtained from Section 2.1.1. The catalyst precursor was dried at 110 °C for 12 h and calcined in air at 500 °C for 4 h.

2.2. Catalyst nomenclature

The nomenclature used for the catalyst samples in this study is following:

- Co-*a/b* refers to the cobalt catalyst on the TiO₂-SiO₂ mixed oxide support, where *a* is the weight ratio of TiO₂ and *b* the weight ratio of SiO₂

2.3. Catalyst characterization

2.3.1. X-ray diffraction

XRD was performed to determine the bulk crystalline phases of catalyst. It was conducted using a SIEMENS D-5000 X-ray diffractometer with Cu K α ($\lambda = 1.54439 \text{ \AA}$). The spectra were scanned at a rate of $2.4^\circ \text{ min}^{-1}$ in the range $2\theta = 20\text{--}80^\circ$.

2.3.2. Raman spectroscopy

The Raman spectra of the samples were collected by projecting a continuous wave laser of argon ion (Ar⁺) green

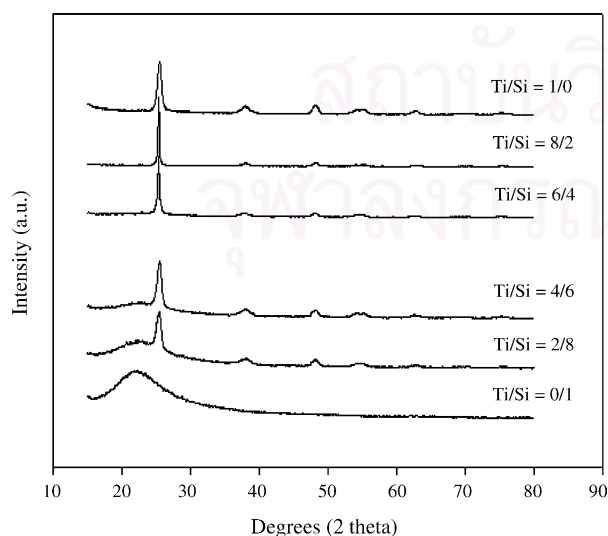


Fig. 1. XRD patterns for various ratios of TiO₂/SiO₂ mixed supports.

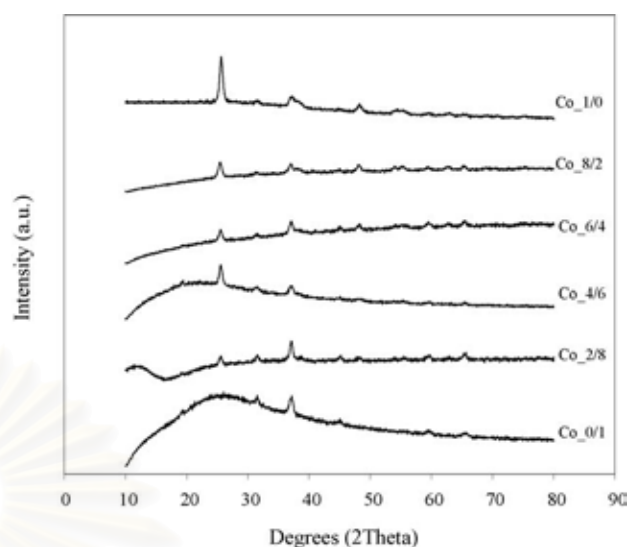


Fig. 2. XRD patterns for the various mixed TiO₂/SiO₂-supported cobalt catalysts after calcination.

(514.532 nm) through the samples exposed to air at room temperature. A scanning range of $100\text{--}1000 \text{ cm}^{-1}$ with a resolution of 2 cm^{-1} was applied. The data were analyzed using the Renishaw Windows-based Raman Environment (WiRE) software, which allows Raman spectra to be captured, calibrated, and analyzed using system 2000 functionality via Galactic GRAMS interface with global imaging capacity.

2.3.3. Scanning electron microscopy (SEM) and energy dispersive X-ray (EDX) spectroscopy

SEM and EDX were used to determine the catalyst morphologies and elemental distribution throughout the catalyst granules, respectively. The SEM of JEOL mode JSM-5800LV was applied. EDX was performed using Link Isis series 300 program.

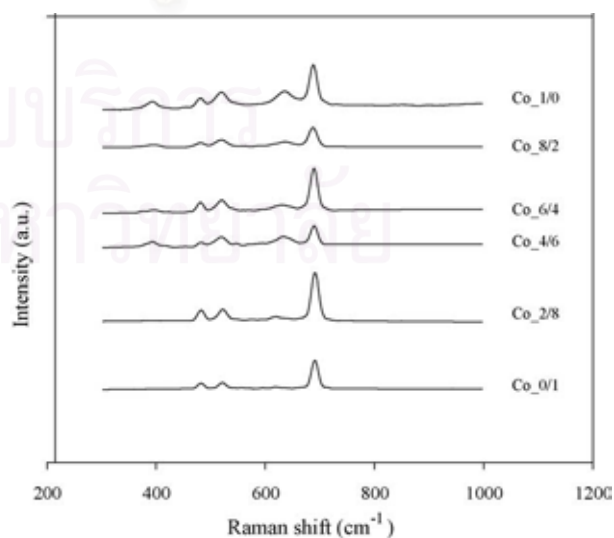


Fig. 3. Raman spectra for the various mixed TiO₂/SiO₂-supported cobalt catalysts after calcination.

2.3.4. Transmission electron microscopy (TEM)

The dispersion of cobalt oxide species on the various mixed oxide supports was determined using a JEOL-TEM 200CX transmission electron spectroscopy operated at 100 kV with 100k magnification.

2.3.5. Hydrogen chemisorption

Static H_2 chemisorption at $100^\circ C$ on the reduced cobalt catalysts was used to determine the number of reduced surface cobalt metal atoms. This is related to the overall activity of the catalysts during CO hydrogenation. Gas volumetric chemisorption at $100^\circ C$ was performed using the method described by Reuel and Bartholomew [21]. The experiment was performed in a Micromeritics ASAP 2010 using ASAP 2010C V3.00 software.

2.3.6. Temperature-programmed reduction (TPR)

TPR was used to determine the reduction behaviors and reducibilities of the samples. It was carried out using 50 mg of a sample and a temperature ramp from 35 to $800^\circ C$ at $5^\circ C min^{-1}$. The carrier gas was 5% H_2 in Ar. A cold trap was placed before the detector to remove water produced during the reaction. A thermal conductivity detector (TCD) was used to determine the amount of H_2 consumed during TPR. The H_2 consumption was calibrated using TPR of Ag_2O at the same conditions [9,22–26].

2.4. Reaction

CO hydrogenation ($H_2/CO=10/1$) was performed to determine the overall activity of the catalyst samples. Hydro-

genation of CO was carried out at $220^\circ C$ and 1 atm. A flow rate of $H_2/CO/He=20/2/8 cc min^{-1}$ in a fixed-bed flow reactor under differential condition was used. A relatively high H_2/CO ratio was used to minimize deactivation due to carbon deposition during reaction. Typically, 20 mg of a catalyst sample was reduced in situ in flowing H_2 ($30 cc min^{-1}$) at $350^\circ C$ for 10 h prior to the reaction. Reactor effluent samples were taken at 1-h intervals and analyzed by GC. In all cases, steady-state was reached within 5 h.

3. Results and discussion

3.1. Characteristics of Co/TiO_2-SiO_2

The XRD patterns of mixed TiO_2-SiO_2 supports before impregnation with the cobalt precursor are shown in Fig. 1. It was observed that the pure silica exhibited a broad XRD peak assigning to the conventional amorphous silica. Similar to the pure silica, the XRD patterns of pure titania indicated only the characteristic peaks of anatase titania at 25° (major), 37° , 48° , 55° , 56° , 62° , 71° , and 75° . XRD patterns of the mixed oxide supports containing various ratios of titania and silica revealed the combination of titania and silica supports based on their contents. It can be seen that the intensity of XRD characteristic peaks for both supports was changed based on the ratios of titania and silica. After impregnation with the cobalt precursor and calcination, all samples of Co/TiO_2-SiO_2 catalyst were again identified using XRD. The XRD patterns of all calcined samples are shown in Fig. 2. After calcination, all samples exhibited XRD peaks,

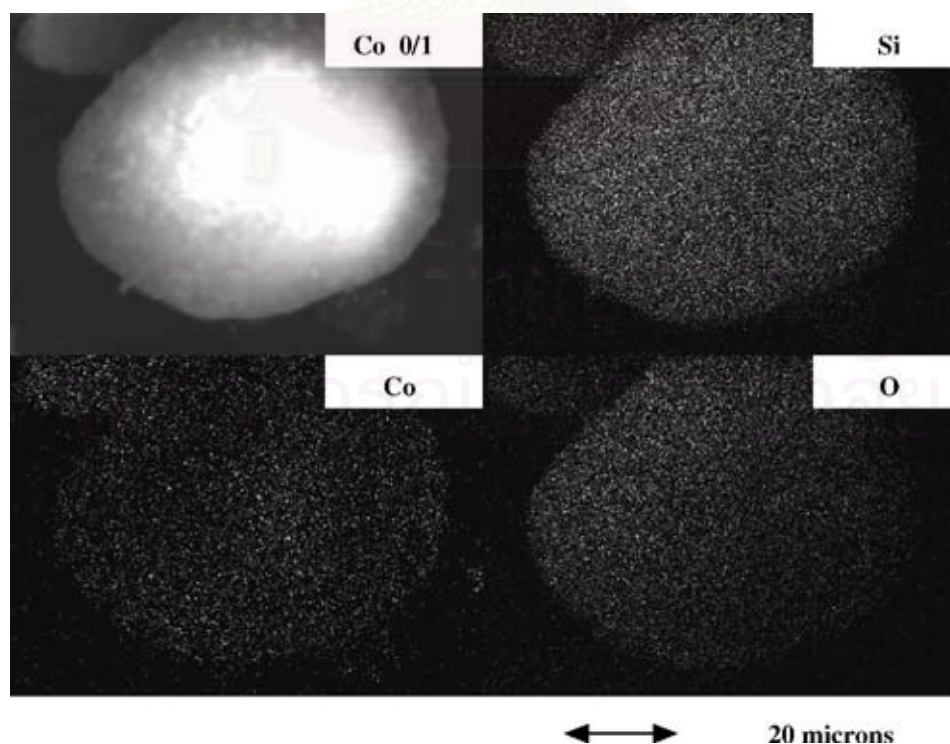


Fig. 4. SEM micrograph and EDX mapping of the calcined Co/SiO_2 catalyst.

4

B. Jongsojtit et al. / Materials Chemistry and Physics xxx (2005) xxx–xxx

which were identical with those for the corresponding mixed oxide supports used as seen in Fig. 1. This indicated that there was no further phase transformation from anatase to rutile occurred after calcination (at temperature ca. 500 °C for 4 h). The amorphous silica also exhibited good stability upon the same calcination process. Besides the corresponding mixed oxide supports detected, all calcined samples also exhibited weak XRD peaks at 31°, 36°, and 65°, which were assigned to the presence of Co_3O_4 . Based on XRD results, it indicated that the presence of Co_3O_4 was apparently in the highly dispersed form. Raman spectroscopy is one of the most powerful techniques used to identify the metal oxide species present. It was found that the titania support exhibited the Raman bands at 640, 514 and 397 cm^{-1} for TiO_2 in its anatase form as seen from our previous work [27] whereas silica was the Raman insensitive upon the scanning range

applied. The Raman spectra for all calcined samples as shown in Fig. 3 exhibited the Raman bands of the titania support as mentioned above with two shoulders at 690 and 480 cm^{-1} , assigned to Co_3O_4 [9,22,27] with corresponding to those with XRD.

SEM and EDX were also conducted in order to study the morphologies and elemental distribution of the samples, respectively. Apparently, SEM micrographs and EDX mapping exhibited similar trends of morphologies and elemental (Co, Si, Ti, and O) distributions. The typical SEM micrographs along with the EDX mapping (for Co, Si, and O) of Co/SiO_2 sample are illustrated in Fig. 4 indicating the external surface of the sample granule. It can be seen that the cobalt oxide species were well distributed (shown on EDX mapping) all over the sample granule. In order to determine the morphologies and elemental distributions of cobalt

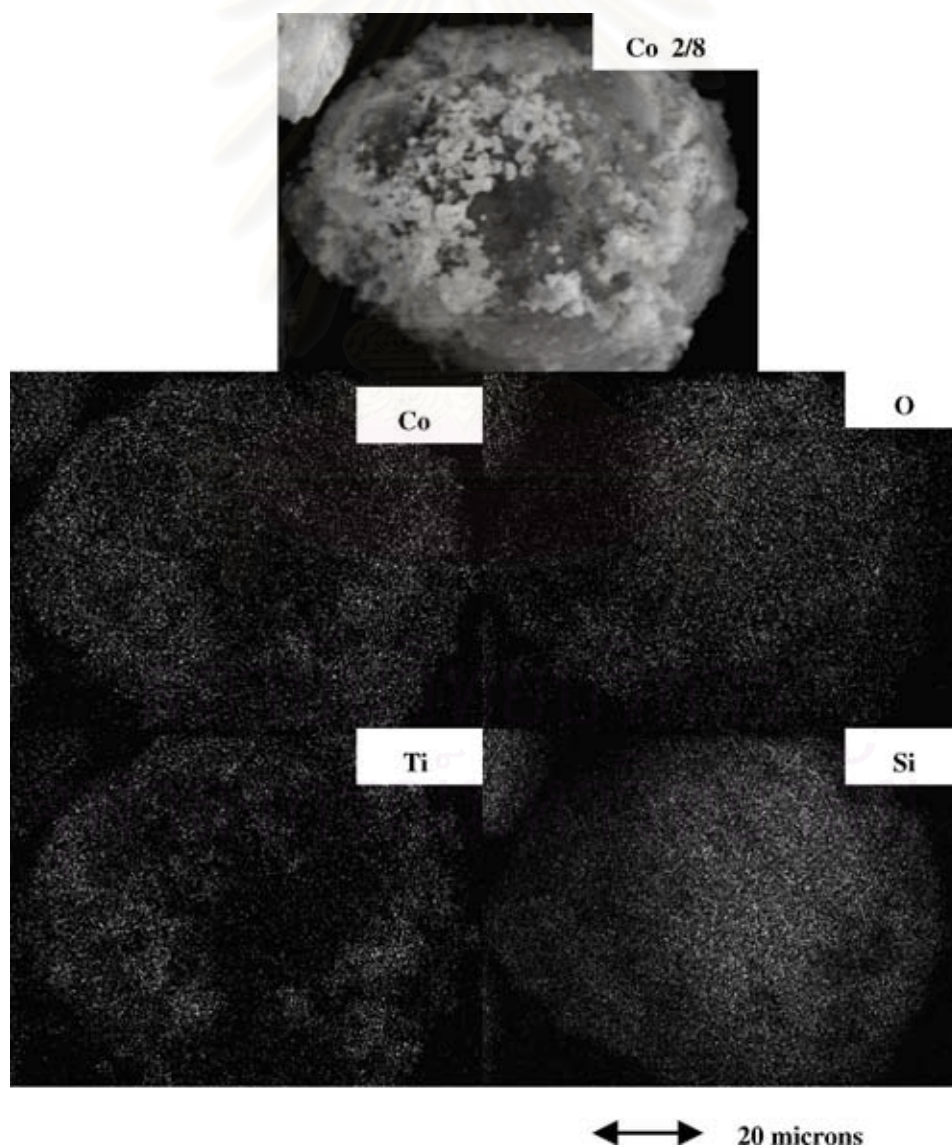


Fig. 5. SEM micrograph and EDX mapping of the calcined $\text{Co}/\text{TiO}_2\text{-SiO}_2$ (2/8) catalysts.

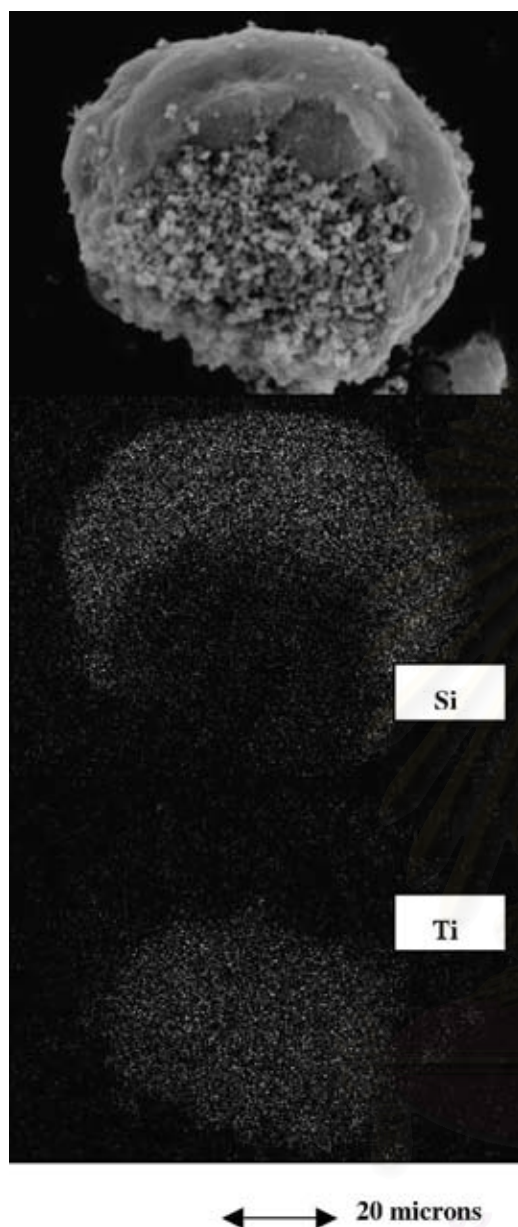


Fig. 6. A typical of SEM micrograph and EDX mapping of mixed TiO_2 - SiO_2 support.

oxides on the mixed TiO_2 - SiO_2 supports, the typical SEM micrographs along with the EDX mapping (for Co, Si, Ti, and O) are shown in Fig. 5, which is similar with those as seen in Fig. 4. However, an obvious charged surface under SEM electron bombarding is visible in Fig. 4. Besides the observation of well distribution for cobalt oxide species, it indicated that titania was apparently located on the outer surface of silica as shown in Fig. 6. The connectivity of Si–O–Ti can be confirmed by the IR spectroscopy indicating the IR bands at ca. 980 and 1100 cm^{-1} [28,29]. In order to determine the dispersion of cobalt oxide species on the various mixed oxide supports, a more powerful technique such as TEM was applied to all samples. The TEM micrographs

for all samples are shown in Fig. 7. The dark spots represented cobalt oxide species or patches dispersing on the various mixed TiO_2 - SiO_2 supports. It can be observed that a highly dispersed form of cobalt oxide species trended to be achieved with the presence of titania in the mixed oxide supports resulting in an appearance of smaller cobalt oxide patches. When combined the Raman spectroscopic results with those from TEM, it is likely that larger shoulders at 690 and 480 cm^{-1} would result in more dispersion of Co. It should be mentioned that although the more highly dispersed cobalt oxide patches with the presence of titania, their distributions seen by TEM were not as good as those seen in the pure silica support. On the other hand, the cobalt oxide patches present on the pure silica support exhibited better distribution, however, with lower degree of dispersion than any other samples. This can be attributed to higher surface areas of the silica support itself. It should be mentioned that high surface area of support could result in better distribution of Co, but somehow does not guarantee good dispersion (small Co patches). Besides, the highly dispersed form of cobalt oxide species could not guarantee the large number of reduced cobalt metal surface atoms, which is related to the overall activity of the catalyst. In addition, the highly dispersed form of cobalt oxide species, the interaction of those with the specified supports has to be essentially considered. Thus, temperature-programmed reduction on the calcined samples needs to be performed in order to give a better understanding according to such a reduction behavior. The TPR profiles for all samples are shown in Fig. 8. It was found that there was only one reduction peak, however, at different reduction temperatures for all calcined samples. The lowest reduction temperatures located at ca. 280 – $600\text{ }^\circ\text{C}$ (maximum at $450\text{ }^\circ\text{C}$) was observed on the Co/SiO_2 sample. However, the reduction temperatures were found to dramatically shift to higher temperatures with increasing the amounts of titania present in the mixed oxide supports. Thus, the highest reduction temperatures located at ca. 370 – $650\text{ }^\circ\text{C}$ (maximum at $550\text{ }^\circ\text{C}$) can be observed for the Co/TiO_2 sample. The pronounced shift of reduction temperatures to higher ones found with the presence of titania can be attributed to the strong support interaction between the cobalt oxides and titania [30]. This was suggested that with the presence of titania it was more difficult for the cobalt oxide species to be reduced at the specified condition than those in silica itself. However, since the catalyst samples were reduced at different temperatures, it may not be useful to compare the reducibility of samples at this condition. Besides, the number of reduced Co metal surface atoms can be calculated directly from the H_2 chemisorption results, which is more acceptable since all catalyst samples are reduced at the standard reduction condition.

It is known that the active form of supported cobalt FTS catalysts is cobalt metal (Co^0). Thus, reduction of cobalt oxide species is essentially performed in order to transform cobalt oxide species obtained after calcination process into the active cobalt metal atoms for catalyzing the reac-

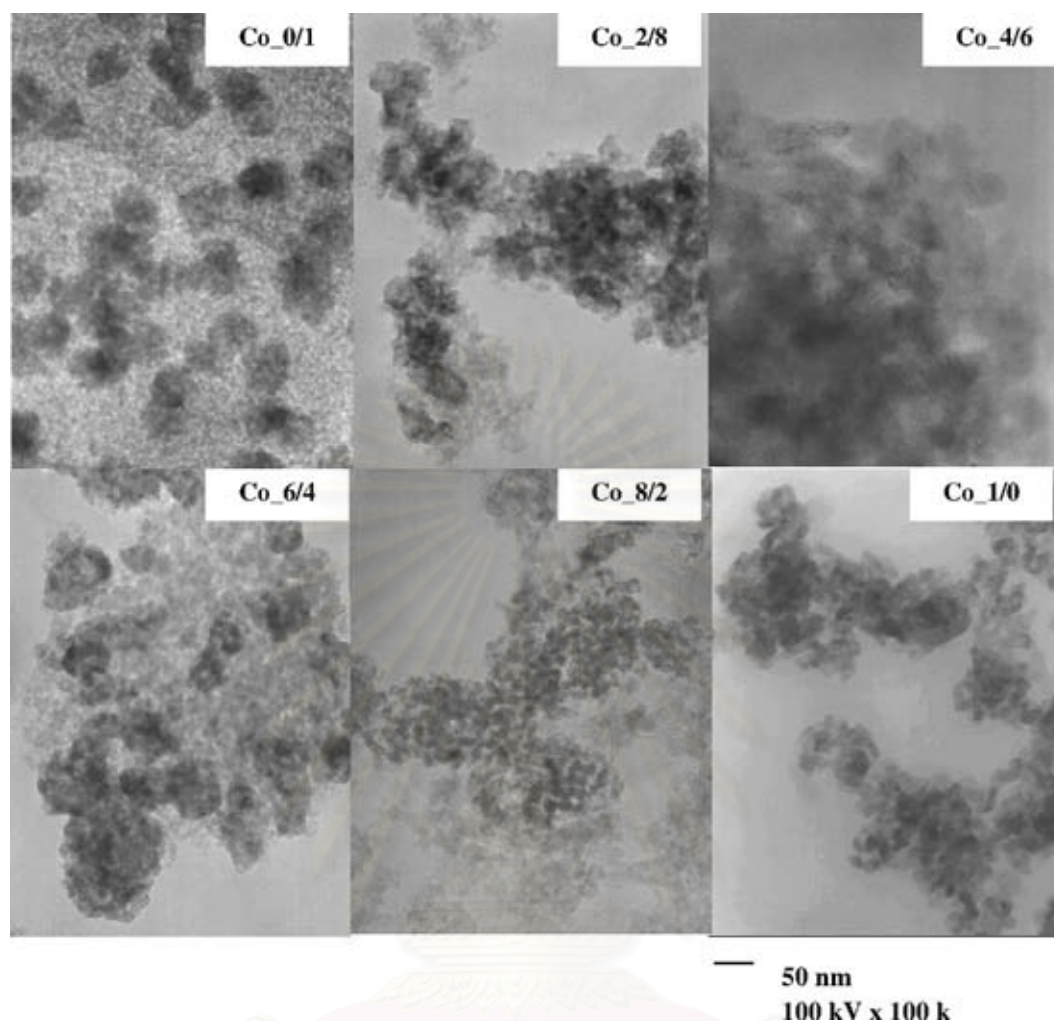


Fig. 7. TEM micrographs of the various mixed $\text{TiO}_2/\text{SiO}_2$ -supported cobalt catalysts after calcinations.

tion. Therefore, the static H_2 chemisorption on the reduced cobalt samples was used to determine the number of reduced cobalt metal surface atoms. This is usually related to the overall activity of the catalyst during carbon monoxide hydrogenation. The resulted H_2 chemisorption for all samples are shown in Table 1. It revealed that the number of reduced cobalt metal surface atoms decreased with the amounts of titania present in the mixed oxide supports. These results

were corresponding with those from the TPR as mentioned before.

3.2. Reaction study

In order to determine the catalytic behaviors of the cobalt catalyst on various mixed TiO_2 - SiO_2 supports, CO hydrogenation ($\text{H}_2/\text{CO} = 10/1$) was performed to determine the

Table 1

Show the H_2 chemisorption, reaction rates, and product selectivity of various samples

Catalyst samples	H_2 Chemisorption ($\mu\text{mol g}_{\text{cat}}^{-1}$)	Rate ($\times 10^2 \text{ g CH}_2 \text{ g}_{\text{cat}}^{-1} \text{ h}^{-1}$) ^a		Product selectivity ^b (%)	
		Initial ^b	SS ^c	CH_4	$\text{C}_2\text{--C}_5$
Co_0/1	11.11	38.9	34.3	99	1
Co_2/8	10.70	32.2	30.4	95	5
Co_4/6	1.85	14.2	10.0	87	13
Co_6/4	0.42	2.7	0.7	74	26
Co_1/0	0.22	1.4	0.8	68	32

^a CO hydrogenation was carried out at 220°C , 1 atm, and $\text{H}_2/\text{CO}/\text{He} = 20/2/8$.

^b After 5 h of reaction.

^c After 5 min of reaction.

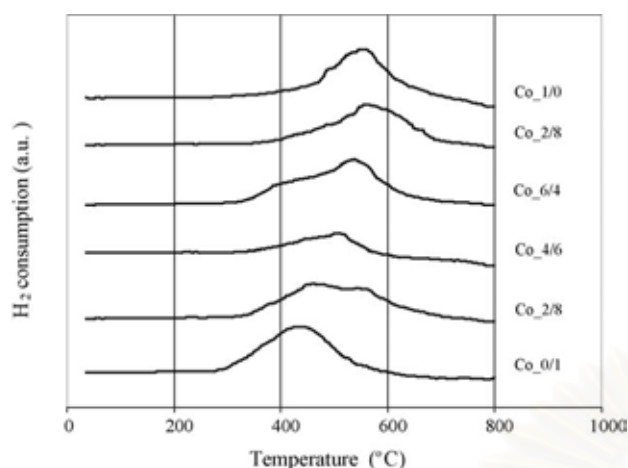


Fig. 8. TPR profiles of the various mixed $\text{TiO}_2/\text{SiO}_2$ -supported cobalt catalysts after calcination.

overall activity and selectivity of the catalyst samples. Hydrogenation of CO was carried out at 220°C and 1 atm. A flow rate of $\text{H}_2/\text{CO}/\text{He} = 20/2/8 \text{ cc min}^{-1}$ in a fixed-bed flow reactor under differential condition was used. In fact, a relatively high H_2/CO ratio was used to minimize deactivation due to carbon deposition during reaction. The resulted reaction study is also shown in Table 1. As expected, based on the H_2 chemisorption results, the overall activities for both initial and steady-state rates dramatically decreased with the amounts of titania present on the mixed oxide supports. This was basically due to the less number of reduced cobalt metal surface atoms with the presence of titania as seen by the H_2 chemisorption results along with higher surface area of silica as mentioned earlier. However, with some consideration on the product selectivity obtained, an interesting discovery can be observed in this present study. Considering the selectivity of product, it showed that the selectivity to methane essentially decreased with the amounts of titania in the supports. On the other hand, more amounts of longer chain hydrocarbons ($\text{C}_2\text{--C}_5$) can be obtained with the presence of titania in the mixed supports. It is known that CO hydrogenation is a kind of polymerization reactions where insertion of the $-\text{CH}_2-$ (methylene group) occurs through the active center. Thus, the product distribution strongly depends on the nature of active centers, rate of propagation, and rate of termination. Obviously, the termination of chain growth occurs and is recognized as the chain growth probability. Based on product selectivity found here, it can be concluded that the presence of titania in the mixed supports apparently inhibited the chain growth probability resulting in the observation of longer chain hydrocarbons even at the specified methanation condition. In order to study this effect in more details, the reaction intermediates at specified conditions must be further investigated with more powerful techniques such as the steady-state isotropic transient kinetic analysis (SSITKA) which has been successfully done by Goodwin and coworkers [5,6,8,9,31,32].

4. Summary

The present study showed impact of various mixed $\text{TiO}_2\text{--SiO}_2$ -supported cobalt catalysts on their catalytic behaviors. It was found that both initial and steady-state rates during CO hydrogenation dramatically decreased with the amounts of titania present in the mixed supports. The decreased activities had to be attributed to the less number of reduced cobalt metal surface atoms for catalyzing the reaction. At the specified conditions, the selectivity of the longer chain hydrocarbons ($\text{C}_2\text{--C}_5$) was more pronounced with the presence of titania in the mixed supports. It can be concluded that the presence of titania apparently inhibited the chain growth probability during CO hydrogenation.

Acknowledgements

We gratefully acknowledge the financial support by the National Research Council of Thailand (NRCT), the Thailand Research Fund (TRF) and Thailand–Japan Technology Transfer Project (TJTTP-JBIC). We would like to thank Prof. James G. Goodwin Jr. at Clemson University for initiating this kind of project. We would like to extend our thanks to the National Metal and Materials Technology Center (MTECH) for Raman spectroscopy analysis.

References

- [1] H.P. Wither Jr., K.F. Eliezer, J.W. Mechell, *Ind. Eng. Chem. Res.* 29 (1990) 1807.
- [2] E. Iglesia, *Appl. Catal. A* 161 (1997) 59.
- [3] R.C. Brady, R.J. Pettie, *J. Am. Chem. Soc.* 103 (1981) 1287.
- [4] A. Martinez, C. Lopez, F. Marquez, I. Duaz, *J. Catal.* 220 (2003) 486.
- [5] J. Panpranot, J.G. Goodwin Jr., A. Sayari, *Catal. Today* 77 (2002) 269.
- [6] J. Panpranot, J.G. Goodwin Jr., A. Sayari, *J. Catal.* 211 (2002) 530.
- [7] S.L. Sun, I. Isubaki, K. Fujimoto, *Appl. Catal. A* 202 (2000) 121.
- [8] S. Ali, B. Chen, J.G. Goodwin Jr., *J. Catal.* 157 (1995) 35.
- [9] B. Jongsomjit, J. Panpranot, J.G. Goodwin Jr., *J. Catal.* 215 (2003) 66.
- [10] T. Das, G. Jacobs, P.M. Patterson, W.A. Conner, J.L. Li, B.H. Davis, *Fuel* 82 (2003) 805.
- [11] G. Jacobs, P.M. Patterson, Y.Q. Zhang, T. Das, J.L. Li, B.H. Davis, *Appl. Catal. A* 233 (2002) 215.
- [12] M. Rothaemel, K.F. Hanssen, E.A. Blekkan, D. Schanke, A. Holmen, *Catal. Today* 38 (1997) 79.
- [13] V. Ragaini, R. Carli, C.L. Bianchi, D. Lorenzetti, G. Vergani, *Appl. Catal. A* 139 (1996) 17.
- [14] V. Ragaini, R. Carli, C.L. Bianchi, D. Lorenzetti, G. Predieri, P. Moggi, *Appl. Catal. A* 139 (1996) 31.
- [15] J.L. Li, G. Jacobs, T. Das, B.H. Davis, *Appl. Catal. A* 233 (2002) 255.
- [16] G. Jacobs, T. Das, Y.Q. Zhang, J.L. Li, G. Racoillet, B.H. Davis, *Appl. Catal. A* 233 (2002) 263.
- [17] J.L. Li, L.G. Xu, R. Keogh, B.H. Davis, *Catal. Lett.* 70 (2000) 127.
- [18] X.H. Li, K. Asami, M.F. Luo, K. Michiki, N. Tsubaki, K. Fujimoto, *Catal. Today* 84 (2003) 59.

- [19] X. Gao, I.E. Wachs, *Catal. Today* 51 (1999) 233.
- [20] S.J. Conway, J.W. Falconer, C.H. Rochester, *J. Chem. Soc., Faraday Trans.* 185 (1989) 71.
- [21] R.C. Reuel, C.H. Bartholomew, *J. Catal.* 85 (1984) 63.
- [22] B. Jongsomjit, J. Panpranot, J.G. Goodwin Jr., *J. Catal.* 204 (2001) 98.
- [23] B. Jongsomjit, J.G. Goodwin Jr., *Catal. Today* 77 (2002) 191.
- [24] A. Kogelbauer, J.C. Weber, J.G. Goodwin Jr., *Catal. Lett.* 34 (1995) 269.
- [25] Y. Zhang, D. Wei, S. Hammache, J.G. Goodwin Jr., *J. Catal.* 188 (1999) 281.
- [26] B. Jongsomjit, C. Sakdamnusun, J.G. Goodwin Jr., P. Praserthdam, *Catal. Lett.* 94 (2004) 209.
- [27] B. Jongsomjit, C. Sakdamnusun, P. Praserthdam, *Mater. Chem. Phys.* 89 (2005) 395.
- [28] D.C.M. Dutoit, M. Schneider, J. Baiker, *J. Catal.* 153 (1995) 165.
- [29] B. Jongsomjit, S. Ngamposri, P. Praserthdam, *Catal. Lett.* 100 (2005) 139.
- [30] R. Riva, H. Miessner, R. Vitali, G. Del Piero, *Appl. Catal. A* 196 (2000) 111.
- [31] S. Vada, B. Chen, J.G. Goodwin Jr., *J. Catal.* 153 (1995) 224.
- [32] S.H. Ali, J.G. Goodwin Jr., *J. Catal.* 176 (1998) 3.



สถาบันวิทยบริการ
จุฬาลงกรณ์มหาวิทยาลัย

VITAE

Miss Tipnapa Wongsalee was born on June 6th, 1981 in Bangkok, Thailand. She finished high school from Lampangkunlayanee School, Lampang in 1999, and received the Bachelor degree of Science with a major in Industrial Chemistry from Chiangmai University in May 2003. She continued her Master's study at the department of Chemical Engineering, Chulalongkorn University in June 2003.



สถาบันวิทยบริการ
จุฬาลงกรณ์มหาวิทยาลัย